AN EXPERIMENTAL INVESTIGATION OF REACTIVITY-CONTROLLED COMPRESSION IGNITION COMBUSTION IN DIESEL ENGINES USING HYDROUS ETHANOL

A DISSERTATION
SUBMITTED TO THE FACULTY OF THE GRADUATE SCHOOL OF THE UNIVERSITY OF MINNESOTA
BY

WEI FANG

IN PARTIAL FULFILLMENT OF THE REQUIREMENTS
FOR THE DEGREE OF
DOCTOR OF PHILOSOPHY

ADVISORS:
DAVID B. KITTELSON
WILLIAM F. NORTHROP

JUNE, 2016

Acknowledgments

I would like to sincerely thank my advisors, Prof. David B. Kittelson and Prof. William F. Northrop, for all the continuous support, guidance and mentoring on my study, research and career development throughout these years. They have set great examples for me and inspired me to diligently pursue knowledge and become a better researcher. I would also like to express my gratitude to my committee members, Prof. Zongxuan Sun and Prof. Jonathan Chaplin, for their insightful advice and help on my work.

My appreciation also goes to the members of the TE Murphy Engine Research Laboratory at the University of Minnesota for their kind and generous help on my research and life. I would always remember the happy and meaningful time spent in the engine lab with all these great colleagues and classmates.

I would also like to acknowledge the support I received from the National Energy Technology Laboratory (NETL), the University of Minnesota Initiative for Renewable Energy and the Environment (IREE), the Minnesota Corn Growers Association, and the Agricultural Utilization Research Institute of Minnesota under grant number AIC194.

Last but not least, I would like to thank my parents and my wife for their support and understanding all along the way.

Abstract

This thesis presents a systematic investigation of advanced dual-fuel low temperature combustion (LTC) strategy, reactivity-controlled compression ignition (RCCI), on a modified diesel engine to obtain high thermal efficiency and low engine-out emissions using hydrous ethanol as the primary fuel. Direct use of hydrous ethanol in internal combustion engines has been shown to provide significant energy savings in the bio-ethanol production process, substantially improving life-cycle energy use and economics compared to commercially available anhydrous ethanol. While many studies have reported high thermal efficiency and extremely low soot and NO_X emissions without exhaust aftertreatment systems in RCCI engines fueled with petroleum-based fuels, limited work has been done regarding the characteristics of performance and emissions of RCCI operation using hydrous ethanol. In this work, a systematic experimental investigation has been conducted to explore the operability region, characterize the performance and emissions, and optimize the key operating parameters of RCCI operation using hydrous ethanol as the primary fuel. It has been shown that hydrous ethanol with water content of up to 25% by volume can be effectively used in RCCI operation with ethanol energy fraction up to 75% over a wide engine load range. However, intake charge heating is needed at low loads and exhaust gas recirculation (EGR) is required under high load conditions. Response surface methodology (RSM) has been shown to be an efficient approach of identifying and optimizing the key engine operating parameters of RCCI operation with reduced experimentation. The performance and emissions characteristics of RCCI combustion have been shown to be different and subject to the influence of different engine operating parameters under different engine

operating conditions. NO_X and soot emissions have been considerably reduced with the optimal settings of operating parameters generated from the RSM models. The fumigated low reactivity fuel has been shown to primarily contribute to the relatively high hydrocarbon emissions from the RCCI combustion. The particulate matter (PM) emissions from RCCI combustion have been shown to be primarily composed of semi-volatile organic compounds and a smaller fraction of solid carbonaceous particles. The characteristics of RCCI PM emissions vary when using different low reactivity fuels and they are highly sensitive to dilution conditions such as dilution ratio and sampling system temperature.

Table of Contents

List of Tables

List of Figures

Nomenclature

γ	Ratio of specific heats
η_{comb}	Combustion Efficiency
η_i	Indicated Thermal Efficiency
ANOVA	Analysis of Variance
AKI	Anti-Knock Index
ATDC	After Top Dead Center
CA˚	Crank Angle Degree
CA5	Crank Angle location of 5% Gross Heat Release
CA50	Crank Angle location of 50% Gross Heat Release
CA95	Crank Angle location of 95% Gross Heat Release
CCD	Central Composite Design
CDC	Conventional Diesel Combustion
CI	Compression Ignition
COV	Coefficient of Variation
CS	Catalytic Stripper
DoE	Design of Experiments
Dwell	Time Interval between Two Diesel Injections
EC	Elemental Carbon
EGR	Exhaust Gas Recirculation

FEF	Fumigant Energy Fraction
FSN	Filter Smoke Number
FTIR	Fourier Transform Infrared
GA	Genetic Algorithm
GCMS	Gas Chromatography Mass Spectrometry
HC	Hydrocarbon
HCCI	Homogeneous Charge Compression Ignition
HDR	High Dilution Ratio
HDT	High Dilution Temperature
IMEP	Indicated Mean Effective Pressure
Inj1Fr	Fraction of First Diesel Injection
LDR	Low Dilution Ratio
LDT	Low Dilution Temperature
LTC	Low Temperature Combustion
LTHR	Low Temperature Heat Release
OC	Organic Carbon
PFI	Port Fuel Injection
P_{int}	Intake Air Pressure
PM	Particulate Matter
PPCI	Partially Premixed Compression Ignition
PPRR	Peak Pressure Rise Rate

P_{rail}	Diesel Fuel Rail Pressure
PRF	Primary Reference Fuel
RCCI	Reactivity-Controlled Compression Ignition
RoHR	Rate of Heat Release
RoPR	Rate of Pressure Rise
RSM	Response Surface Methodology
SOC	Start of Combustion
SI	Spark Ignition
SMPS	Scanning Mobility Particle Sizer
SOIC1	Start of Injection Command for the 1st Injection
SOIC2	Start of Injection Command for the 2nd Injection
TDC	Top Dead Center
TDMA	Tandem Differential Mobility Analyzer
T_{int}	Intake Air Temperature
TWI	Two-Way Interaction
ULSD	Ultra-Low-Sulfur Diesel
VGT	Variable Geometry Turbocharger

Chapter 1 Introduction

1.1. **Motivation**

Internal combustion engines have played an indispensable role in human society in a wide range of applications due to their high reliability, low manufacturing cost and high power density. The two most common types of internal combustion engines are four-stroke spark ignition (SI) and compression ignition (CI) engines. The thermal efficiency of CI engines is generally higher than that of SI engines due to the capability to operate with higher compression ratio, leaner fuel-air charge and lower throttling losses. However, the main challenges for CI engines are relatively high levels of soot and oxides of nitrogen (NO_X) emissions. Reactivity-controlled compression ignition (RCCI) is a newly developed low temperature combustion (LTC) strategy for use in CI engines that has been shown to yield high thermal efficiency and simultaneously low soot and NO_X emissions. The RCCI approach employs in-cylinder blending of two fuels with distinct auto-ignition properties such as gasoline and diesel fuel to create an optimal fuel reactivity distribution in the combustion chamber.

Increasing the use of biomass-based fuels will benefit society by mitigating our dependence on fossil fuels for energy, reducing greenhouse gas emissions and stimulating rural economies. Ethanol is an important type of biofuel that can be made from common crops such as sugar cane, potatoes or corn using fermentation and distillation. Fuel ethanol currently used in IC engines is mostly anhydrous (>99% ethanol), requiring very energy-intensive distillation processes and drying to remove water. Direct use of hydrous

ethanol in IC engines has the potential to significantly improve the economics and life-cycle energy balance of bio-ethanol.

RCCI operation with petroleum-based fuels has been thoroughly investigated in literature, but comprehensive experimental investigations of RCCI operation using hydrous ethanol are scarce. Various issues have challenged the use of hydrous ethanol in conventional SI and CI engines; however, the RCCI approach provides a new efficient and clean solution for utilizing hydrous ethanol in IC engines. This work represents a systematic investigation of the diesel-hydrous ethanol RCCI operation with hydrous ethanol providing most of the fuel energy. Due to the complex interactions of many engine parameters associated with fueling and air management, their combined impacts on RCCI combustion are not currently fully understood. Response surface methodology (RSM) is an effective and efficient tool for engine optimization and used to optimize a selection of operating parameters for optimal performance and emissions output. This work explores the use of RSM for optimizing RCCI with hydrous ethanol and also indicates the strengths of RSM for simplifying engine testing more generally where multiple active operating parameters often lead to cumbersome experimental studies. Further, detailed particulate matter emissions measurements conducted in this work will offer some insight into the characteristics of particle emissions from the low-emissions RCCI strategy.

1.2. **Project Objective Statement**

The first objective of this study was to explore the operability region of the diesel-hydrous ethanol RCCI strategy. The engine was operated in single-cylinder mode from low to high-load conditions to obtain high thermal efficiency and low NO_X and soot

emissions, with hydrous ethanol providing over 70% of total fuel energy. At each load, the second diesel injection timing was swept and the baseline settings of operating parameters were determined for further optimization.

The second objective of this study was to optimize operating parameters to obtain optimal overall performance and emissions output under selected engine operating conditions using RSM techniques. RSM has been shown to be an effective and efficient approach for optimizing engine operating parameters where comprehensive physical understanding of their interactions have not been identified. In this work, RSM was used to determine the effects and interactions of intake air conditioning and fuel delivery parameters on emissions and to generate parameter settings for optimal overall performance and emissions outputs. A series of Design of Experiments (DoE) tests were conducted under each operating conditions to build statistical RSM models and derive optimal combinations of key engine parameters with reduced experimental time and resource costs.

The third objective of the work was to characterize the particulate matter (PM) emissions from RCCI using hydrous ethanol as the secondary, low reactivity fuel. Particle number and volume concentration, size distribution, volatile fraction and effects of fuel properties on the PM emissions were examined when using different low reactivity fuels in RCCI.

1.3. **Significance of Work**

This work shows that diesel-hydrous ethanol RCCI can yield high thermal efficiency along with low engine-out emissions over a wide operability region. More broadly, it offers a bright prospect for alleviating environmental degradation and fossil fuel

depletion caused by diesel engine operation. The RSM optimization process performed in this study not only produces optimal performance and emissions output for this specific test engine under selected operating conditions, but also provides a more systematic and thorough understanding of the RCCI combustion and serve as an example for the optimization of other complex systems with multiple active factors. Additionally, this work contributes to a deeper understanding of the nature of particulate matter emissions from the low-emissions and high efficiency RCCI strategy and provides recommendations for practical applications that would benefit by implementing this promising new engine strategy.

Chapter 2 Background

2.1. **Premixed Low Temperature Combustion**

With increasing concern about fossil fuel depletion and environmental degradation, research in internal combustion engines has been directed towards improving thermal efficiency, lowering engine-out emission levels, and effectively using alternative fuels to reduce our dependency on non-renewable fuels. Due to their capability to operate with higher compression ratio, leaner fuel-air charge and lower throttling losses, CI engines are more efficient than spark-ignited engines. However, the main challenge for CI engines is to meet increasingly stringent emissions legislation at an affordable cost while maintaining or improving their efficiency advantages.

In recent years, advanced combustion strategies for CI engines have drawn great interest from the engine research community for simultaneous reduction in NO_X and soot emissions to potentially avoid the complexity and expense of exhaust aftertreatment systems. Most of the published effort falls into the area of premixed LTC. In premixed LTC engines, the fuel-air charge is well-mixed and highly diluted, decreasing peak combustion temperature and fuel-rich zones, hence leading to simultaneously low NO_X and soot emissions. Thermal efficiency of premixed LTC engines is generally comparable to conventional diesel engines with lower combustion efficiency offset by improved thermodynamic cycle efficiency due to shorter combustion duration, lower heat loss and higher ratio of specific heats [1].

There have been various strategies proposed to achieve premixed LTC depending on the fuel used. For fuels with high volatility and high resistance to auto-ignition such as

gasoline or ethanol, homogeneous charge compression ignition (HCCI) strategy has been studied; for fuels with lower volatility but higher propensity for auto-ignition such as diesel, partially premixed compression ignition (PPCI) strategy is commonly used [2].

2.1.1. **Homogeneous Charge Compression Ignition**

In an HCCI engine, a homogeneous mixture of fuel and air is introduced into the cylinder during the intake stroke in a similar way as in a conventional PFI gasoline engine. The upward movement of the piston then compresses the fully premixed fuel and air charge during the compression stroke, rapidly raising the in-cylinder pressure and temperature to a critical point where auto-ignition of the mixture occurs as the piston approaches TDC. Like in a conventional diesel engine, the ignition of the fuel and air charge is initiated by the compression movement of the piston without the assistance of a spark plug. Unlike in a diesel engine where the combustion process consists of a premixed combustion phase and a mixing controlled combustion phase due to the direct injection of fuel near TDC, the combustion process in an HCCI engine proceeds with the entire fuel and air mixture releasing its energy in a set of nearly simultaneous reactions; hence no stationary or propagating flame front is present and the combustion duration is very short in HCCI combustion. HCCI yields ultra-low levels of NO_X and soot emissions because the fuel and air mixture is highly dilute and well mixed. It also has the potential to achieve high thermal efficiency due to the capability of operating with high compression ratio, low heat loss and near constant-volume heat-release manner.

Considerable research effort has been dedicated to exploring the operability region of HCCI combustion using different fuels and engine configurations. Christensen et al. [3] investigated HCCI combustion on a single-cylinder engine with variable compression

ratio enabled by a hydraulically controlled secondary piston. Mixtures of different fuels such as iso-octane, normal heptane, gasoline and diesel fuel were used to examine the effect of fuel properties on HCCI combustion and emissions characteristics. The results showed that liquid fuel with different auto-ignition propensity could be used in HCCI combustion with an appropriate compression ratio. The thermal efficiency was not significantly improved with the increase of compression ratio however due to reduced combustion efficiency. They also found that NO_X emissions were very low under different conditions and were not dependent on compression ratio. The same group of researchers [4] also explored the feasibility of extending the load operability region of HCCI operation by employing supercharging. They demonstrated that 14 bar indicated mean effective pressure (IMEP) was achievable using natural gas and a compression ratio of 17:1. Higher loads were primarily limited by the high rate of heat release peak cylinder pressure. Olsson et al. [5] developed a closed-loop control strategy for a turbo-charged HCCI engine using two fuels, iso-octane and n-heptane. They achieved HCCI operation under a speed range from 700 rpm to 2000rpm and load range up to 6.5 bar IMEP with this dual fuel approach.

One important focus of HCCI research is the control of the auto-ignition timing or start of combustion (SOC). Two of the most common control methods are thermal conditioning of the intake charge and modulated exhaust gas recirculation (EGR). Martinez-Frias et al. [6] developed a purely thermal control system for HCCI engines which consisted of a preheater, a supercharger, and an intercooler to utilize the thermal energy from EGR and supercharger compression work in an adjustable manner for optimal intake charge temperature and density. This system demonstrated capability to

achieve highly efficient HCCI operation over a wide range of operating conditions. Koopmans et al. [7] conducted a gasoline fueled HCCI study using a single-cylinder engine with variable valve timing control capability. They showed that HCCI combustion could be initiated by increased internal EGR enabled by negative valve overlap. The work also found reduced fuel consumption, CO and NO_X emissions and similar HC emissions compared to SI combustion. Chen et al. [8] explored the effect of EGR on HCCI combustion characteristics using modeling techniques. They found that trapped EGR could initiate HCCI combustion and advance ignition timing by raising the intake charge temperature. Some chemical effects were also revealed that the N_2 in EGR had an effect on heat release rate, while CO_2 and H_2O had a tendency to retard the ignition timing. Shi et al. [9] compared the effect of internal EGR enabled by negative valve overlap and cooled external EGR on HCCI combustion. They demonstrated that internal EGR produced less smoke emissions compared to external EGR, while cooled external EGR could effectively retard the SOC, which was beneficial for high cetane number fuel such as diesel.

Theoretically, HCCI is an ideal combustion strategy since it has the potential to produce extremely low levels of NO_X and soot emissions as well as diesel-like thermal efficiencies. However, several technical challenges must be overcome before the concept can be widely implemented in practical applications. One drawback associated with HCCI is low combustion efficiency under low load conditions. Hwang et al. [10] demonstrated that as the equivalence ratio was decreased below 0.2, the combustion efficiency was remarkably reduced and CO and HC emissions were significantly increased since some bulk-gas reactions such as CO-to-CO_2 conversion were inhibited

due to the excessively low combustion temperatures. Another challenge for HCCI combustion is the control of combustion phasing and pressure rise rate at high loads since the ignition timing is solely determined by chemical reaction rates. In an experimental study, Dec et al. [11] showed that as the equivalence ratio exceeded 0.3, excessively high peak pressure rise rates and knocking noise were observed.

2.1.2. **Partially Premixed Compression Ignition**

HCCI is less feasible for fuels with low volatility and high cetane number such as diesel fuel, as it is difficult to obtain fully premixed fuel and air mixture with either PFI or DI fuel injection systems, and compression ratio needs to be reduced to avoid knocking. Accordingly, partially premixed compression ignition (PPCI) combustion is more commonly used for simultaneous reduction in NO_X and soot emissions for diesel fuel.

PPCI is realized using different approaches, but a common goal of these methods is to promote fuel and air mixing and to reduce in-cylinder temperatures compared to conventional diffusive diesel combustion. Some researchers have studied altering fuel injection timing and using high levels of cooled EGR to extend the mixing time of fuel and air. Hasegawa et al. [12] utilized double injection strategy to realize PPCI and named the concept as Uniform Bulky Combustion System (UNIBUS). They demonstrated that the first injection with very advanced timing led to suppressed high temperature reactions and simultaneously low NO_X and soot emissions.

Kimura et al. [13] developed a combustion strategy named Modulated Kinetics (MK), which combined high EGR levels and late diesel injection timing to obtain low in-cylinder combustion temperature and extended ignition delay. Significant reduction in

both NO_X and PM emissions were achieved compared to conventional diesel operation. However, deterioration of fuel economy was observed with this strategy due to low combustion efficiency.

Walter et al. [14] developed an engine operating in conventional diesel mode at high loads and in PPCI mode at partial load conditions. Injectors with narrow included angles were used to limit fuel wall impingement for the PPCI operation, and near-zero NO_X and PM emissions along with high fuel efficiency were achieved.

Kook et al. [15] investigated the effect of charge dilution level and injection timing on PPCI combustion and emissions characteristics and postulated a progress path of combustion process on the equivalence ratio and temperature plane. They found that emissions formation processes were dominated by the mixing-controlled phase rather than the premixed phase despite the increased ignition delay due to the high dilution level. They also demonstrated that CO emissions increased under high dilution conditions but can be alleviated with earlier injection timings.

Neely et al. [16] used up to three early pilot injections to enable PPCI combustion and investigated the effect of the injection timing, quantity and number of pilot injections. They concluded that the best potential for reducing NO_X emissions with PPCI combustion existed at low load conditions, and that PPCI combustion control was more feasible with lower in-cylinder pressures and temperatures obtained by modifications of compression ratio, piston bowl and injector nozzle geometry.

Akihama et al. [17] compared the soot formation processes between conventional diesel combustion and diesel LTC enabled by high EGR rates using various engine modeling tools, and demonstrated that soot formation in LTC was significantly

suppressed as the conversion from PAH to soot was inhibited via operating in the low temperature regions.

Jacob et al. [18] compared PPCI combustion enabled by high level EGR with two different approaches; one used intake throttle and the other used variable geometry turbocharger (VGT) for EGR rate control. They found that PM emissions from the VGT method were lower than those from the throttling method due to the significantly higher air fuel ratio, while the higher air fuel ratio associated with the VGT method contributed to higher CO and HC emissions relative to the throttling method.

Investigations have also been conducted to modify diesel injectors for reduced spray wall impingement and improved fuel vaporization within the limited mixing time available in high speed engines. Iwabuchi et al. [19] investigated PPCI combustion on a diesel engine with low penetration injections and early fuel injection timing. They demonstrated that NO_X and smoke emissions were significantly lower in PPCI operation than in conventional diesel operation, while the PPCI operability region was limited to partial load conditions with lower fuel efficiency and higher HC emissions. Akagawa et al. [20] adopted a pintle-type injector and a reduced top-land-crevice piston along with early injection timing to reduce HC and CO emissions in PPCI operation. They also concluded that fuel consumption could be improved with use of EGR or addition of an oxygenated component to the diesel fuel.

Challenges associated with diesel PPCI combustion include high CO and unburned hydrocarbon (HC) emissions [21], poor controllability during transient operation, decreased maximum power output due to reduced charge flow [22] and limited load range due to onset of diffusion combustion at high injection duration.

2.2. **Reactivity-Controlled Compression Ignition (RCCI)**

Dual-fuel premixed LTC strategies offer more flexibility to control the combustion process and extend engine operating range compared to single-fuel operation. Olsson et al. [23] originally developed a strategy for HCCI combustion phasing and load control through variation of the relative ratio and total fueling rate of two fuels with distinct auto-ignition properties. They found that although combustion phasing could be better controlled with dual-fueling, the rates of pressure rise and heat release were still excessively high at high loads due to the nearly constant-volume heat release event. Dual-fuel PPCI strategies with direct injection of diesel fuel and port injection of less reactive fuels like iso-octane [22] or methane [25] were also shown to offer good controllability and ease the need for high EGR rate. Inagaki et al. [22] observed very low levels of NO_X and soot emissions, moderate combustion rates and high thermal efficiency at loads up to 12 bar IMEP with diesel fuel injected at 40 ºBTDC.

RCCI is a newly developed dual-fuel PPCI strategy that employs early direct split-injection of a high reactivity fuel such as diesel fuel into a well-mixed charge of air and a low reactivity fuel such as gasoline. Two fuels of differing reactivity create an optimal fuel reactivity distribution to precisely manage the combustion process and achieve high thermal efficiency and simultaneously low NO_X and soot emissions [26–30].

Diesel-gasoline RCCI has been extensively studied in the literature over a wide range of operating conditions on various types of engines. Modeling and experimental work by Kokjohn et al. on a heavy-duty single-cylinder diesel engine [24,31,32] showed that the fuel reactivity stratification generated by early direct split-injection of diesel fuel led to staged consumption of the two fuels, reducing rate of pressure rise and extending

combustion duration as compared with HCCI operation; thus, the operability range could be extended to higher loads while HCCI-like NO_X and soot emissions are retained.

Hanson et al. [26] investigated effects of the diesel fuel injection parameters on RCCI combustion and emissions, revealing that increasing diesel fuel in the second injection or retarding diesel fuel injection timing resulted in greater fuel reactivity and equivalence ratio gradients in the combustion chamber, leading to more advanced combustion phasing, higher rate of pressure rise and increased NO_X and soot emissions.

Kokjohn et al. [27] compared RCCI operation between light-duty and heavy-duty engines. They reported comparably low NO_X and soot emissions but lower thermal efficiency on the light-duty engine compared to the heavy-duty engine operation. The lower thermal efficiency in the smaller engine was caused by higher relative heat loss due to surface-to-volume effects. Splitter et al. [33] examined the effects of the high reactivity fuel injection strategy on RCCI combustion at low loads, demonstrating significant reductions in HC and CO emissions and an increase of thermal efficiency with split-injection strategy compared to single-injection. Walker et al. [34] investigated effects of the diesel fuel injection pressure on RCCI combustion. They presented comparable performance and emissions results with lower injection pressure enabled by a GDI fueling system compared to operation with high injection pressure using a common-rail injection system. However, combustion efficiency was found to be slightly reduced due to poorer mixing.

To address issues related to storing two different kinds of fuel at the point of use, some researchers have investigated single-fuel RCCI using fuel additives. Gasoline-fueled RCCI were demonstrated by dosing gasoline with a small quantity of cetane

number improver such as di-tert butyl peroxide [35] or 2-ethylhexyl nitrate [30]. Comparable performance and emissions output could be obtained with lower direct injection pressure compared to diesel-gasoline RCCI due to the higher volatility of gasoline. Further, compression work was reduced as low temperature heat release was diminished due to the absence of diesel fuel, resulting in improved thermal efficiency.

Increasing research effort has been devoted to RCCI operation using alternative fuel combinations to take advantage of inherent synergies as well as increased fuel renewability. Splitter et al. [28] compared diesel-E85 RCCI and diesel-gasoline RCCI at different loads, finding that the combustion duration in diesel-85% ethanol in gasoline blend (E85) RCCI was longer than in diesel-gasoline RCCI, possibly due to the combustion-inhibiting effect of ethanol and the greater reactivity gradient between ethanol and diesel fuel. Further, diesel-E85 RCCI required lower EGR level than diesel-gasoline RCCI, leading to increased thermal efficiency.

Hanson et al. [36] examined effects of replacing gasoline and diesel fuel with 20% ethanol in gasoline (E20) and 20% soy methyl biodiesel blend (B20) on a multi-cylinder RCCI engine. They found that using E20 reduced pressure rise rate and heat release rate, extended the operability range and improved thermal efficiency due to decreased heat and pumping losses; however, there was a slight reduction in combustion efficiency. Nieman et al. [37] investigated RCCI operation using natural gas as the low reactivity fuel at various operating conditions. They demonstrated efficient and clean RCCI combustion without using EGR at loads up to 13.5 bar IMEP. However, thermal efficiency was shown to be lower using natural gas as compared to gasoline.

2.3. **Use of Hydrous Ethanol in IC Engines**

Bio-ethanol can be produced from a variety of renewable agricultural feedstocks such as potatoes, sugar cane, starch and corn. It has gained wide acceptance in some automobile markets like Brazil due to good compatibility with current SI engine infrastructure, high octane number and other favorable properties [38]. In the United States, most fuel ethanol is anhydrous (>99% water), requiring highly energy-intensive water removal processes during production. Flowers et al. [39] showed that remarkable improvement of ethanol lifecycle energy balance and economics could be achieved if hydrous ethanol could be directly used in IC engines due to production energy savings in the distillation and dehydration processes. More recently, Saffy et al. [40] investigated the effect of ethanol concentration on energy use, water consumption and greenhouse gas emissions in corn ethanol production from a dry-mill, natural gas fired corn ethanol refinery. They demonstrated that the optimal ethanol concentration was 86% by weight in corn ethanol production as this grade of hydrous ethanol offered approximately 8% of energy cost savings, 8% of refinery emissions reduction as well as 3-6% of water consumption reduction.

Hydrous ethanol with low water content can be readily utilized in SI engines without major modification of the fuel supply system. Costa et al. [41] compared operations with hydrous ethanol containing 6.8% water by mass and a fuel blend of 78% gasoline and 22% anhydrous ethanol by mass on an SI engine. They reported higher thermal efficiency, lower CO and HC emissions and higher NO_X with use of hydrous ethanol compared with the fuel blend. Clemente et al. [42] developed a hydrous ethanol (7% of

water by mass) fueled SI engine and demonstrated enhanced peak torque and power compared to operation using a fuel blend of 78% gasoline and 22% anhydrous ethanol.

Another important use of utilizing hydrous ethanol in IC engines is intake air fumigation of hydrous ethanol with direct-injection of diesel fuel as the ignition source. Like RCCI, dual fuel combustion uses a low reactivity fuel premixed with the intake air and diesel direct injection for ignition. However unlike RCCI, dual fuel fumigation modes do not use early diesel injection timing and result in a mixed diffusion and flame propagation combustion mode that does not have the same NO_X and soot reduction potential.

Chaplin et al. [43] investigated the effect of 190 proof hydrous ethanol fumigation in a modified diesel engine with varied diesel injection timing and fumigant flow rates. They demonstrated that the brake thermal efficiency of hydrous ethanol fumigation operation was comparable with diesel only operation at high load conditions but lower at low loads. It was also found that diesel injection timing needed to be advanced with higher hydrous ethanol flow rates due to the effect of longer ignition delay associated with the high heat of vaporization of ethanol.

Olson et al. [44] investigated fumigation of 100 proof hydrous ethanol to replace up to 40% of diesel fuel by volume on a 1.9L diesel engine. They showed reduced NO_X and soot emissions along with lower thermal efficiency and increased HC emissions compared to diesel only operation.

Some researchers have investigated LTC strategies with hydrous ethanol as the primary fuel. Flowers et al. [39] used modeling techniques to assess operation of an HCCI engine fueled with hydrous ethanol. They showed that HCCI operation with

relatively high thermal efficiency and low NO_X emissions could be achieved using 70 proof hydrous ethanol.

Dempsey et al. [45] investigated diesel-hydrous ethanol RCCI operation using computational models and experimental testing. Their modeling results demonstrated low NO_X and soot emissions along with a gross indicated thermal efficiency of 55% at loads ranging from 5 to 17 bar IMEP using 150 proof hydrous ethanol. They also found that the significant charge cooling effect of water and ethanol retarded ignition and combustion, leading to increased premixed combustion control over diesel-gasoline RCCI. The same group also conducted an experimental investigation to validate their modeling results [46], reporting diesel-like thermal efficiencies and near zero levels of NO_X and soot emissions on heavy-duty and light-duty engines with use of two different grades of hydrous ethanol. This prior work sets the stage for the work described here.

In summary, RCCI has been shown to be a promising premixed LTC strategy to yield high thermal efficiency and simultaneously low NO_X and soot emissions. Although directly using hydrous ethanol in conventional SI or CI engines has been challenged by various issues like misfire, phase separation and high octane number, some researchers have demonstrated the feasibility to efficiently and extensively use hydrous ethanol in RCCI engines. To gain a more comprehensive understanding of the combustion and emissions characteristics and fully exploit the potential of diesel-hydrous ethanol RCCI operation, a systematic experimental investigation was conducted in this work.

2.4. **PM Emissions from Premixed LTC combustion**

Concerns about the adverse impact of particulate matter (PM) emissions on the environment and human health have motivated a large body of investigation focusing on characterizing and improving PM emissions from compression ignition (CI) engines. PM from conventional mixing controlled diesel combustion has been thoroughly studied over the past decades [47,48]. A typical particle size distribution consists of a nucleation mode and an accumulation mode. Nucleation mode particles are those with a mobility diameter less than 50 nm and are normally composed of sulfur compounds and volatile or semi-volatile material, formed during exhaust cooling and dilution processes. Accumulation mode particles are primarily carbonaceous soot agglomerates with a mobility diameter ranging from 50 to 500 nm formed by rich combustion of diesel fuel.

2.4.1. **Characteristics of Premixed LTC PM Emissions**

The characteristics of PM emissions from RCCI engines have been shown to be different from those from conventional diesel combustion (CDC). Prikhodko et al. [49] showed that RCCI combustion produced lower mass and number concentrations of PM, but a significantly higher fraction of nucleation mode particles compared to CDC. Kolodziej et al. [50] observed bimodal particle size distributions on a RCCI engine with both diesel and gasoline directly injected in the cylinder, and demonstrated that RCCI PM emissions were sensitive to diesel fuel proportion. Storey et al. [51] investigated the effect of lubricant oil on RCCI PM emissions and showed that the organic carbon fraction likely stemmed from partial oxidation of the fuel hydrocarbons rather than from the lubricant oil.

2.4.2. **Effect of Dilution Conditions on PM Emissions**

Semi-volatile PM emissions from CDC have been shown to be highly sensitive to the exhaust cooling and dilution conditions. Abdul-Khalek et al. [52] showed that dilution ratio, temperature and residence time had a large effect on the nucleation mode particles, while the accumulation mode particles were not as strongly influenced by these parameters. The same group of researchers developed methods to estimate nanoparticles growth rates [53], and observed that growth rates were strongly dependent on exhaust sampling and dilution conditions. Their model showed that soot agglomerates had an effect of depleting sulfuric acid and hydrocarbon materials. In low-soot engines operating in premixed LTC combustion modes, these species could form a large number of nanoparticles through heteromolecular nucleation process.

Franklin [54] investigated the effect of dilution air temperature on nucleation mode PM emissions from an ethanol-fueled HCCI engine. The PM sampling system consisted of two dilution stages. It was shown that the number and size of nanoparticles decreased significantly with increased primary dilution air temperature in the range of 25 ℃ to 35 ℃ and stabilized at higher temperatures. The secondary dilution air temperature had minimal effect on nucleation mode particle formation.

Montajir et al. [55] investigated the effect of exhaust gas quality, dilution ratio and temperature and thermal conditioning temperature on the measurement stability of diesel engine PM emissions. They concluded that nucleation mode particles with the size range of 15 nm to 30 nm were highly sensitive to thermal conditioning temperature, while the accumulation mode particles with a diameter about 100 nm were more stable under changes of dilution conditions.

As for LTC strategies like RCCI with dominating nucleation mode particles and high level of unburned HC, it is expected that sampling and dilution conditions have a larger impact on PM concentrations and size distributions compared to CDC. Kolodziej et al. [50] showed that both the nucleation and the accumulation mode particles were reduced with increased dilution ratio. Zhang et al. [56] compared the PM emissions from RCCI, HCCI and CDC and found that size of the nucleation mode was reduced and peak was shifted to smaller particle diameters with increased dilution ratio for all the three combustion strategies.

This research investigated the effects of dilution conditions and fuel properties on RCCI PM emissions to provide a more comprehensive and thorough understanding of the characteristics of RCCI PM emissions.

2.5. **Optimization of Engine Operating Parameters**

With the rapid development of internal combustion engine technology, the complexity of the optimization process of engine operation is enormously increased. Considerable research efforts have been devoted into different engine optimization approaches.

2.5.1. **Genetic Algorithm Optimization Approach**

Genetic algorithm (GA) is an algorithm that simulates the natural evolution processes of creatures. The algorithm starts with a population of individuals representing different combinations of the operating parameters settings. An objective function is used to evaluate the quality of each individual and those with high qualities are selected as good

solution with their attributes randomly combined to generate the next generation of individuals. Iterations of this process proceed until an optimal solution is found.

Wickman et al. [57] utilized GA and engine modeling techniques to optimize the engine combustion chamber geometry and air/fuel system related operating parameters for two different sized engines. With this method they obtained remarkable reduction in both engine-out emissions and fuel consumptions without manufacturing a large number of different designs.

Hiroyasu et al. [58] combined a sophisticated phenomenological spray-combustion model with GA to optimize EGR rates and multiple injections in a diesel engine. Fuel consumption, NO_X and soot emissions were minimized with Pareto optimum solutions.

Aldawood et al. [59] investigated the optimization of the cylinder pressure history, pressure rise rate and gross IMEP of a dual-fuel HCCI engine using GA and a highly reduced primary reference fuel (PRF) mechanism. The optimized model was compared with experimental data and good agreement was observed over a wide range of operating conditions.

Nieman et al. [37] used GA coupled with KIVA3V CFD codes and CHEMKIN chemistry tool to improve the performance and emissions from a diesel-methane RCCI engine under different speed and load conditions. By optimizing variables such as fraction of methane, diesel injection timing and quantity, they found that very low NO_X and soot emissions were achievable at loads up to 13.5 bar IMEP without the use of EGR.

Although GA and engine modeling approaches have proven to be effective in optimization of engine operating parameters, their computational resource requirement is

high and an insight into the effects and interactions of different operating parameters is not guaranteed.

2.5.2. **Response Surface Methodology (RSM) Optimization Approach**

Another method for optimization of engine operating parameters is RSM. RSM is a set of mathematical and statistical techniques seeking to optimize an objective function (or response) that is affected by multiple factors using design of experiments (DoE) methods and statistical analysis [60]. Instead of seeking the optimal solution within a large number of randomly generated candidates, RSM utilizes reduced and simplified experimental designs to gain a thorough understanding of the system as well as obtain the optimal combinations of operating parameters. It has been shown to be an effective and efficient tool for engine optimization that avoids extensive experimental testing and the need for a complicated CFD modeling process.

Montgomery et al. [61] used RSM for optimization of the dual-injection conventional diesel operation, demonstrating remarkable improvements of fuel economy and emissions over the baseline conditions with optimized injection parameters, boost and EGR levels.

Lee et al. [62] conducted RSM optimization of a high-speed direct-injection diesel engine and achieved simultaneous reductions in NO_X and PM emissions without compromising fuel economy.

Amann et al. [63] applied RSM to optimize operating parameters such as EGR rate, intake air pressure and temperature and compression ratio for optimal fuel economy on an HCCI engine with variable compression ratio capability. They built a RSM model

with quadratic, linear and interaction terms and achieved extremely low NO_X and soot emissions as well as comparable fuel economy as in conventional SI and DI engines.

Pandian et al. [64] used RSM to optimize the performance and emissions of a diesel engine fueled with diesel and biodiesel blend. The RSM models were shown to be capable of predicting brake specific energy consumption, brake thermal efficiency, CO, HC, NO_X and smoke opacity and revealing the interactions between operating parameters such as injection pressure, injection timing and nozzle tip protrusion.

An advantage of RSM over other optimization methods such as GA is the capability of providing insights into the effects and interactions of different operating parameters while generating optimal outcome with a minimal number of experiments. The RSM approach was used in this research to optimize combustion and emissions in a diesel-hydrous ethanol RCCI engine as well as investigate the effects and interactions of key engine operating parameters.

Chapter 3 Experimental Apparatus

3.1. **Test Engine**

Experiments in this study were conducted using a modified Isuzu 4HK1-TC direct-injection medium-duty diesel engine with specifications listed in Table 1. The engine test stand was initially built by Franklin et al. for multi-cylinder hydrogen- and ethanol-fueled HCCI work [54] and modified afterwards for single-cylinder RCCI investigations as performed in this study. A schematic of the experimental setup is shown in Figure 1. The engine was coupled to a DC dynamometer capable of either engine motoring or power absorbing modes. Since the effect of cylinder balancing is not a focus of this research, the intake and exhaust lines of engine cylinder number 1 were isolated so that the originally four-cylinder engine could be operated in single-cylinder mode to reduce test setup complexity and fuel consumption. A laboratory compressed air supply was connected to the engine intake system, with intake air pressure adjusted by a pressure regulator. Intake air temperature was controlled using an in-line resistive air heater coupled with a PID temperature controller. As the power for intake air heating was not measured, it was not included in the efficiency calculations. A hot-wire type gas flow meter was used to measure intake air mass flow rate with a surge tank downstream to dampen oscillatory flow resulting from single-cylinder operation. A customized EGR supply system was used to deliver adjustable and cooled EGR flow. The stock compression ratio, valve timing, piston bowl and combustion chamber geometry were retained.

The stock common-rail direct-injection diesel fuel supply system was used for diesel fuel delivery, and fuel injections were controlled by a National Instruments/Drivven

stand-alone injector driver system. This system was able to carry out up to five injection events in a single engine cycle, with adjustable fuel rail pressure, injection timings and durations. Liquid low-reactivity fuel such as gasoline or ethanol was introduced into the intake port with an automotive-style port fuel injection (PFI) injector. The fuel was preheated to approximately 70 ℃ in a concentric hose with engine coolant flowing in the outer layer to improve the combustion stability. Liquid fuel flow rates were monitored continuously via mass change in the fuel supply tanks using electronic balances. Gaseous low-reactivity fuel such as hydrogen was delivered through a separate PFI injector, and the fuel flow rates were measured with a Sierra gas mass flow meter.

Table 1: Specifications of the engine used in the experimental study

Engine Type	4-stroke DI Diesel
Manufacturer/Model	Isuzu 4HK1-TC
Number of Cylinders	4, in-line
Bore x Stroke (mm)	115 x 125
Conn. Rod Length (mm)	198
Crank Length (mm)	62.5
Clearance Volume (liter)	0.0742
Displacement (liter)	1.298
Number of Cylinders	4, in-line
Total Displacement (liter)	5.192
Compression Ratio	18.5
Diesel Injection System	Common Rail, Solenoid
Gasoline/Ethanol/Hydrogen Injection System	Port Fuel Injection
Rated Power	157 kW @ 2550 rpm
Rated Torque	597 N-m @ 1850 rpm

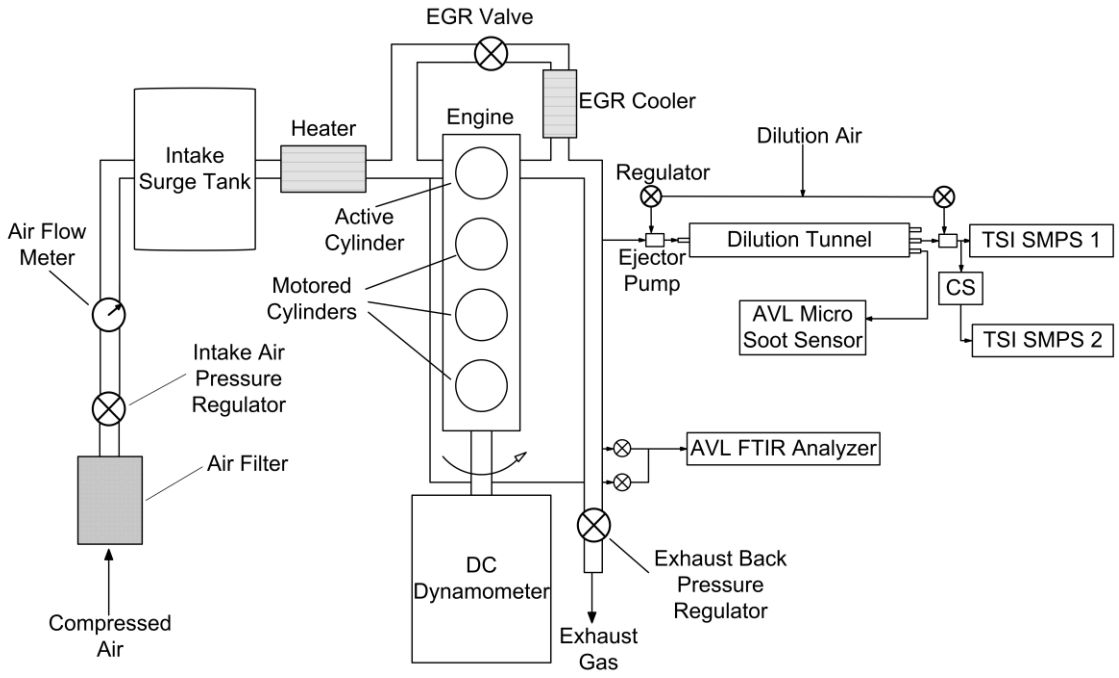

Figure 1: Schematic of experimental system

3.2. **Emissions Instrumentation**

3.2.1. **Gaseous Emissions Measurement**

Engine gaseous emissions such as NO, NO_2, CO and total HC were measured using an AVL Fourier Transform Infrared (FTIR) analyzer on a wet basis with a hot sample line maintained to 190˚C. Since different FTIR species recipes were used to measure the HC for different combustion modes, the total HC volumetric concentrations for the diesel-gasoline RCCI, diesel-hydrogen RCCI and conventional diesel combustion modes were calculated using Equation (1), and the total HC emissions for the diesel-hydrous ethanol RCCI mode were calculated using Equation (2).

$$(1) x_{HC} = x_{CH_4} + 2 \cdot x_{C_2H_2} + 2 \cdot x_{C_2H_4} + 2 \cdot x_{C_2H_6} + 3 \cdot x_{C_3H_6} + 5 \cdot x_{IC_5} + 5 \cdot x_{NC_5} + 7.5 \cdot AHC$$

$$(2) x_{HC} = x_{CH_4} + 2 \cdot x_{C_2H_2} + 2 \cdot x_{C_2H_4} + 2 \cdot x_{C_2H_6} + 3 \cdot x_{C_3H_6} + x_{HCHO} + 2 \cdot x_{MECHO} + 2 \cdot x_{ETOH}$$

Here, x_i is the wet volumetric concentration of a species *i* in the exhaust gas where IC_5 denotes isopentane, NC_5 denotes normal pentane, AHC denotes total aromatics, HCHO denotes formaldehyde, MECHO denotes acetaldehyde, and ETOH denotes ethanol. The molecular weight of hydrocarbons was assumed to be 14 g/mol for calculation of gross-indicated specific HC. A Raman Laser Gas Analyzer was used to measure hydrogen in the exhaust gas.

3.2.2. **PM Emissions Measurement**

Mass concentrations of soot emissions were measured by an AVL Micro-Soot photo-acoustic analyzer. A two-stage micro-dilution system similar to the one developed by Abdul-Khalek [52] was used to simulate the process of exhaust gas mixing with ambient air and cooling. To investigate the effect of dilution conditions on the PM emissions from different combustion modes, two levels of primary dilution temperature and primary dilution ratio settings were selected. The primary dilution temperature was measured downstream of the primary ejector pump where the exhaust sample and dilution air were well mixed. The low dilution temperature (LDT) and high dilution temperature (HDT) conditions represent the primary dilution temperatures of 25 ˚C and 47 ˚C, respectively. Two different size orifices were used in the primary ejector pump to set the primary dilution ratios. The low dilution ratio (LDR) and high dilution ratio (HDR) conditions represent the primary dilution ratios of 6:1 and 18:1, respectively. The outer wall of the dilution tunnel was water jacketed and held at a constant temperature equal to the primary dilution temperature for each condition. The secondary dilution temperature was kept at 25˚C and dilution ratio was fixed at 14:1 for all tested conditions. A TSI Scanning Mobility Particle Sizer (SMPS) was used to measure the PM number concentrations and

size distributions downstream of the secondary dilution stage. A sample of diluted exhaust was sent through a catalytic stripper (CS) similar to the device developed by Abdul-Khalek et al. [66] to remove sulfur compounds and soluble organic materials, and a second SMPS was used to acquire the PM measurement downstream of the CS. It has been demonstrated that an operating temperature of 300 ℃ leads to essentially complete removal of volatile sulfate and hydrocarbon particles with the CS [66].

3.3. **In-Cylinder Combustion Analysis**

High-speed in-cylinder pressure measurement was accomplished using a Kistler 6056A piezoelectric pressure transducer at a resolution of 0.36 crank angle degrees (CA˚). In combustion analysis, the gross indicated mean effective pressure (IMEP) was calculated over the power portion of the cycle from -180 to 180 CA˚. The apparent rate of heat release (RoHR) was calculated based on a first law analysis given in [67]. A constant ratio of specific heats $\gamma = 1.3$ was assumed for the compression and expansion processes as opposed to derived polytropic exponents since the absolute value of heat released was not as critical to this study as the bulk shape of the RoHR curve with respect to crank angle. CA05 and CA50 denote the calculated crank angle locations of 5% and 50% cumulative heat release and were used to represent the ignition timing and combustion phasing, respectively.

3.4. **Fuel Properties**

Table 2 presents the physical fuel properties used in this study. The hydrous ethanol tested contained 25% water by volume (150 proof) and was splash blended. Non-oxygenated gasoline fuel was obtained from a local fuel station with an Anti-Knock

Index (AKI) of 91. Commercially available #2 ultra-low sulfur diesel (ULSD) was used in this research, and the properties were obtained from an independent lab analysis. Fuel properties of hydrogen, ethanol and gasoline were derived from Reference [67].

Table 2: Physical fuel properties used in this study

Fuel	ULSD	200 Proof Ethanol	150 Proof Ethanol	Gasoline	Hydrogen
Density (kg/m^3)	852	782	867	720-780	0.090
Heat of Vaporization (kJ/kg)	270	840	1262	305	—
Lower Heating Value (MJ/kg)	42.8	26.9	18.9	44.0	120.0
Research Octane Number	—	107	—	92-98	130
Cetane Number	41.1	—	—	—	—
H/C Ratio	1.79	3.00	3.33	1.87	—

Chapter 4 Dual-Fuel Combustion using Different Fumigants[1]

The purpose of this section was to present the comparison of hydrogen, ethanol and gasoline as fumigants in RCCI and to compare the performance and emissions characteristics of gasoline-diesel RCCI at different levels of fumigant energy fraction (FEF). A naturally-aspirated single-cylinder diesel engine was used for the experimental study. The first part of this section discussed combustion and emissions using hydrogen, gasoline, and ethanol at a constant FEF over a large direct diesel injection timing range. In the second part, the effect of FEF on the operable diesel injection timing range with gasoline as a fumigant was examined in more detail.

4.1. **Experimental Procedure**

The constant engine operating conditions used in the experiments are listed in Table 3. For each of the five conditions, diesel injection timing was varied over the widest possible range without encountering unstable combustion as detected by a coefficient of variation (COV) of IMEP greater than 4%. For each condition, a nominal IMEP was set to 450 kPa at a baseline timing setting. Fueling was then held constant for the injection timing sweep by maintaining the same injection duration and pressure, resulting in an IMEP variance of approximately ± 20 kPa. In the first set of experiments, gasoline, hydrogen and ethanol were used as fumigants, and the FEF was fixed to $80 \pm 1\%$. These cases are denoted by G-1, H-1 and E-1. For the H-1 case, hydrogen was diluted with 60% nitrogen in part to simulate its typical concentration in syngas produced by biomass gasification [68] as well as to prevent excessively high cylinder pressure rise rate. In the

[1] This chapter is based on paper "Dual-fuel diesel engine combustion with hydrogen, gasoline and ethanol as fumigants: effects of diesel injection timing" (Fang et al., 2014), ***J. Eng. for Gas Turbines and Power***, 136(8), 081502.

second set of experiments, only gasoline was used as fumigant. The energy fractions of gasoline in total energy input were set to 70%, 80% and 90%, while the total energy input was kept constant. These three different gasoline fraction cases were denoted by G-2, G-1, and G-3.

Table 3: Constant parameters for the investigated engine operating conditions

Condition	H-1	E-1	G-1	G-2	G-3
Fumigant	H_2	Ethanol	Gasoline	Gasoline	Gasoline
Engine Speed (rpm)	1500	1500	1500	1500	1500
Nominal IMEP (kPa)	450	450	450	450	450
EGR (%)	0	0	0	0	0
Fumigant Energy Fraction (%)	80	80	80	70	90
Intake Temperature (˚C)	35	35	35	35	35
Intake Pressure (kPa)	98	98	98	98	98
Diesel Injection Pressure (bar)	400	400	400	400	400

4.2. **Results and Discussion**

4.2.1. **Comparison of Fumigant Type**

This section discusses the experimental results of changing direct diesel injection timing with gasoline, ethanol and hydrogen as fumigants with 80% FEF. Figure 2 shows how ignition delay, CA50 and indicated gross cycle efficiency ($\eta_{i,g}$) varied with diesel injection timing for the three different fumigants. The range of diesel injection timing

over which stable combustion could be maintained was widest for G-1 while the range for E-1 was much narrower than the other two cases. One explanation for this narrow timing range is the very high heat of vaporization of ethanol, which cooled the incoming charge and caused lower in-cylinder temperature prior to the onset of combustion for E-1. A second consideration is ethanol's inhibition effect on low temperature combustion during the first-stage of heat release as demonstrated by Splitter et al. [28]. They found that a lower FEF was required when using E85 as the fumigant compared to a 95.6 RON gasoline to achieve similar engine performance. Hashimoto [69] also showed the inhibition effect of ethanol on homogeneous ignition of n-heptane in a rapid compression machine using varying ethanol concentrations.

A minimum point of CA50 as a function of injection timing existed for all three cases. Either advancing or retarding the diesel injection from this point resulted in retarded combustion phasing. This trend has been seen in other studies of premixed CI combustion in engines [70]. With more advanced diesel injection, mixing time for diesel and the surrounding charge was extended, leading to longer ignition delay and a more retarded and premixed combustion event. As the diesel injection timing was retarded, combustion became more coupled with the injection event due to higher local reactivity in the piston bowl thereby resulting in delayed ignition and combustion. The divergence of timing and combustion phasing with early diesel injection indicates primarily premixed combustion, i.e. the RCCI regime. In this region, the ignition delay and combustion phasing varied with fumigant types, with ethanol having the longest delay and the most retarded combustion phasing followed by hydrogen and gasoline. At a diesel SOI of -48˚C ATDC, the ignition delay of the H-1 case was approximately 10˚

longer and CA50 was nearly 15˚ more retarded compared to the G-1 case. At retarded diesel injection timing, ignition delay and CA50 converged for the three fuels, suggesting that the directly-injected diesel fuel might have dominated ignition timing and combustion phasing like in traditional dual-fuel fumigation combustion.

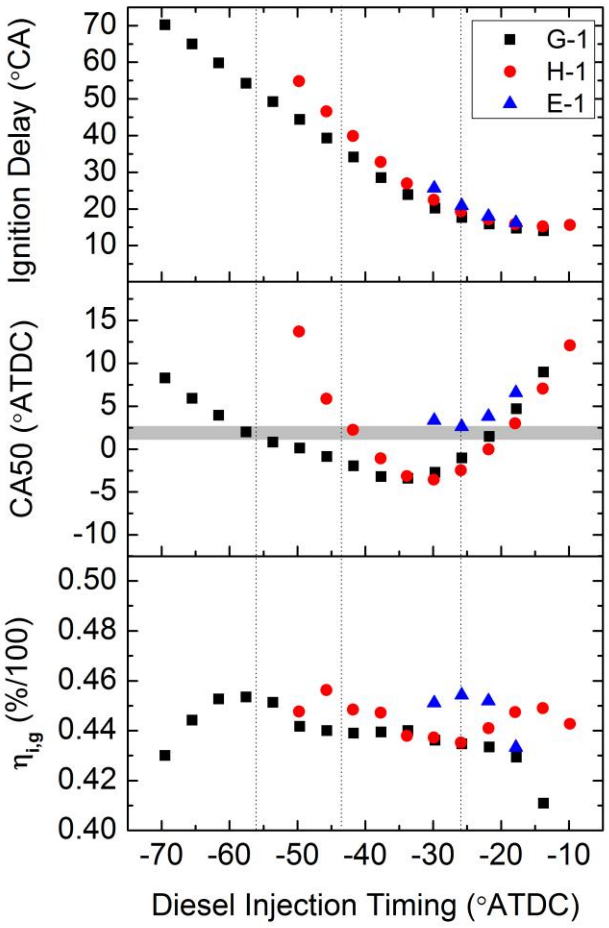

Figure 2: Ignition delay, CA50 and gross indicated cycle efficiency versus diesel injection timing for G-1, H-1and E-1 cases

The peak $\eta_{i,g}$ was nearly the same for all three fumigants but occurred at different diesel injection timings. For H-1 and G-1, peak efficiency occurred in the region of more advanced diesel injection timing and corresponded well with CA50 located just after TDC as indicated by the shaded horizontal line in Figure 2. In our previous work [70], we showed that primarily premixed fumigation operation led to peak thermal efficiency with

combustion phasing near TDC since the compression and expansion strokes of the cycle more closely approximated the ideal constant-volume Otto Cycle. For the E-1 case, peak $\eta_{i,g}$ occurred at more retarded diesel timing but also corresponded to CA50 near TDC.

A more detailed look at combustion resulting from varying diesel injection timing for the three fumigants is shown in Figure 3 where the apparent gross RoHR is plotted versus crank angle at three timing settings. With early diesel injection at SOI=48˚ BTDC, the degree of diesel premixing was very high, and combustion of diesel and fumigant appeared to occur simultaneously, resulting in Gaussian-shaped RoHR curves. The H-1 case had a more delayed heat release event than G-1 but with a sharper shape of RoHR. Another interesting comparison between the two fumigants at early timing is that gasoline clearly had an early low temperature heat release event commonly seen in premixed CI combustion whereas the H-1 case did not. Both cases used the same quantity of diesel but the absence of low temperature heat release when using hydrogen as a fumigant is further evidence that the fumigant plays a key role in the ignition process.

Similar observations have been shown and discussed by Guo et al. [71]. In a study of a diesel HCCI engine with hydrogen enrichment, it was shown that the participation of hydrogen in some reactions during low temperature heat release stage led to delayed combustion phasing as well as diminished low temperature heat release. Also, it was deduced by Westbrook et al. [72] that hydrogen enhanced the rate of the reaction, $H + O_2 = O + OH$ which controlled the high temperature heat release event and thus shortened the combustion duration.

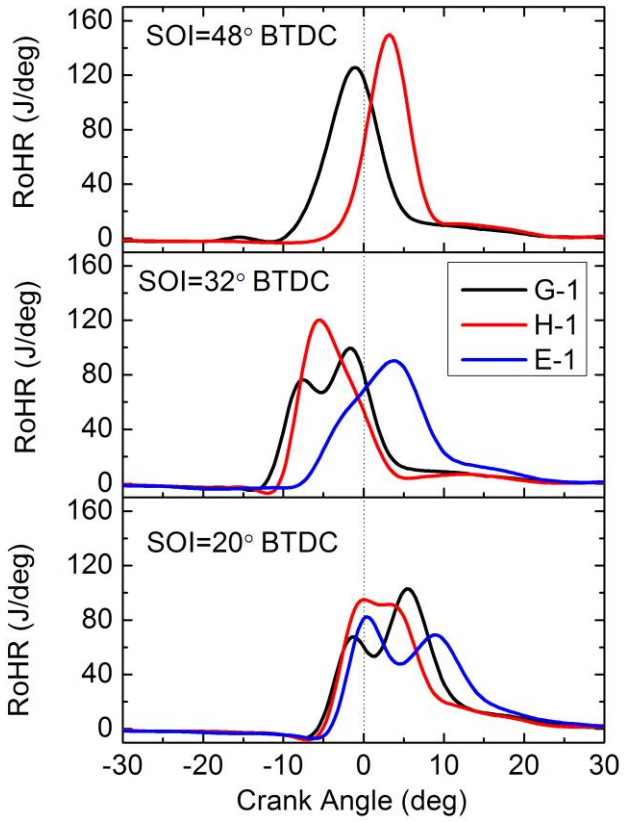

Figure 3: Gross apparent rate of heat release for G-1, H-1 and E-1 cases at 48˚, 32˚, 20˚ diesel injection timing

At SOI=32˚ BTDC, the H-1 case still exhibited a largely Gaussian RoHR curve indicative of premixed combustion but the G-1 case had two distinct heat release peaks. This dual heat release is typically explained by combustion of the directly-injected diesel fuel providing ignition energy for premixed combustion of the fumigant [70]. Note from Figure 2 that at SOI=32˚ BTDC, the ignition delay for H-1 was larger than G-1 while the CA50 locations for the two cases were almost the same. This was most likely caused by the combination of inhibited low temperature heat release and promoted reaction rates during high temperature heat release by hydrogen as previously discussed. These effects also led to the observation that although hydrogen did not allow as large of a diesel

timing range as illustrated in Figure 2, it did result in a shorter premixed combustion event. The E-1 case had very late combustion without a distinct diesel ignition curve, which is indicative of ethanol's inhibition effect as previously discussed.

With late diesel injection timing at SOI=20˚ BTDC, two distinct peaks in RoHR were observed for all three fuels. Ignition occurred at nearly the same crank angle indicating that the injected diesel fuel played a more dominant role in determining ignition. Hydrogen had the shortest combustion duration, again due to enhanced reaction rates during high temperature heat release. The E-1 case had the longest combustion duration due to the inhibition effect of ethanol extending the second heat release peak into the expansion stroke.

The emissions of NO_X, soot, CO and H_2 are given in Figure 4 for the three fumigant fuels on a gross-indicated specific basis plotted versus CA50 to examine their dependence on combustion phasing over the directly-injected diesel timing range. NO_X emissions were lower in the region of more advanced diesel injection timing and increase for the same combustion phasing as timing was retarded. This is most likely due to more heterogeneous combustion with later diesel injection. Although early injection timing lowered NO_X similarly for the three tested fuels, the H-1 case showed discernibly lower NO_X with retarded diesel timing. Here, it is possible that hydrogen had the effect of reducing diffusion burning by accelerating the combustion of injected diesel as observed by shorter combustion duration shown in Figure 3; however, more detailed conclusions about the nature of this trend is beyond the scope of this work.

Soot emissions were low and for all three fuels over the tested timing range. This indicates that combustion was primarily premixed throughout the tested range with

minimal high temperature fuel-rich regions in the cylinder. The H-1 condition exhibited the highest soot emissions with retarded diesel injection timing, possibly resulting from the high temperature burning of hydrogen combined with a late diesel injection.

Emissions of CO were extremely low for the H-1 condition indicating that the directly-injected diesel fuel might not have contributed strongly to CO emissions in fumigation combustion. This corresponds well to other published studies that showed CO mostly resulting from incomplete combustion in the squish volume for premixed modes of diesel combustion [73]. CO was nearly the same for E-1 and G-1 at retarded diesel timing settings. For G-1, retarded timing resulted in much higher CO compared to advanced timing. Within the range of advanced timing for G-1, a minimum for CO was found at approximately the CA50 corresponding to the highest $\eta_{i,g}$ point in Figure 2 linking the overall thermal efficiency to combustion efficiency.

Hydrogen emissions were nearly constant over the timing range for the H-1 case. This independence from diesel injection timing and combustion phasing is evidence that hydrogen within the piston bowl region was always consumed but fumigated hydrogen in the squish and crevice regions remained. The short combustion duration for the H-1 case even with retarded combustion phasing shown in Figure 3 reinforces this idea and strengthens the argument that hydrogen enables enhanced premixed burning of both fumigant and the directly injected diesel fuel.

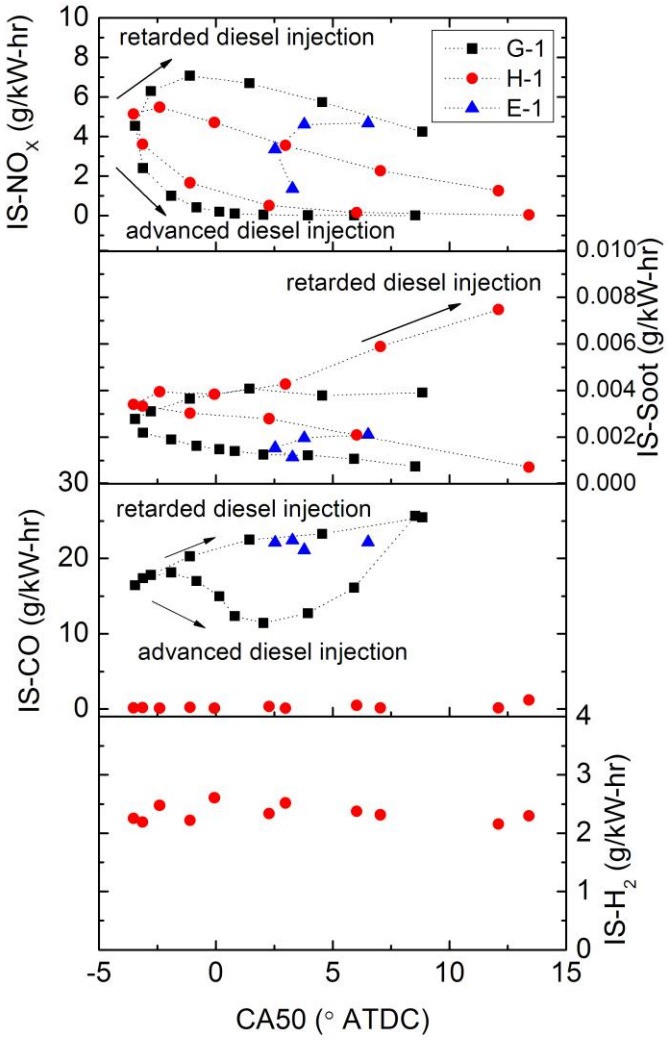

Figure 4: Gross indicated specific NO_X, soot, CO and H_2 emissions for G-1, H-1 and E-1 cases

Figure 5 shows a plot of detailed hydrocarbon emissions data measured using the FTIR analyzer as a function of CA50. The indicated specific emissions of HC, the sum of species specified in Section 3.2.1, had a nearly monotonic dependence on combustion phasing regardless of early or late diesel injection timing. HC emissions for the H-1 and E-1 cases were extremely low because ethanol was not considered as part of the HC

calculation and because the directly injected diesel fuel was mostly consumed throughout the timing range.

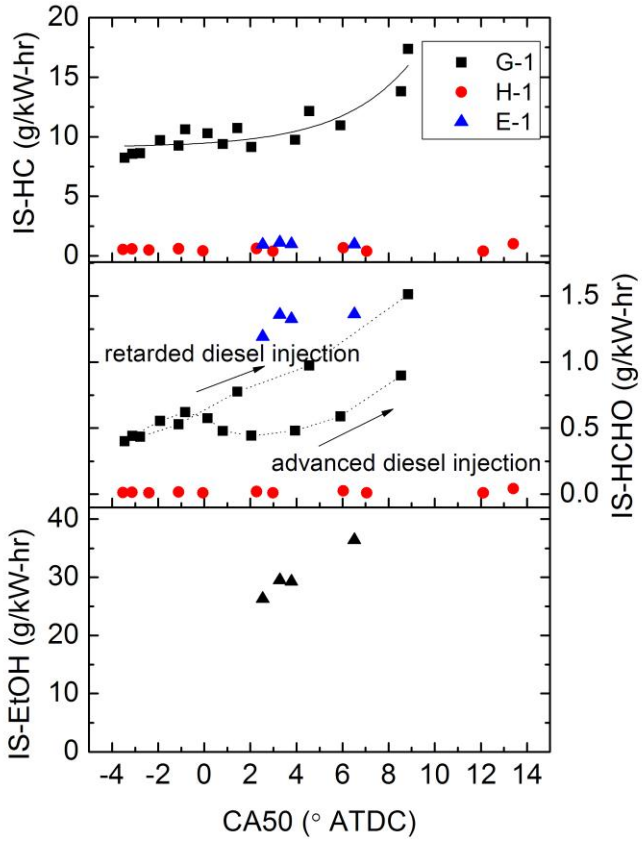

Figure 5: Gross indicated specific HC, HCHO, EtOH emissions for G-1, H-1 andE-1 cases

The illustrative trend line shown for the G-1 case in the HC plot in Figure 5 indicates that there was an asymptote in emissions as combustion phasing was advanced. This is evidence of the highest combustion efficiency occurring with phasing close to TDC. Overall, the HC emissions for H-1 and E-1 were more than ten times less than the G-1 case; therefore it is likely that the remaining hydrocarbons mostly consisted of partially burned gasoline located in the squish and crevice regions. As combustion phasing was retarded, unburned HC occurred from late burning resulting in poorer combustion

quality, a phenomenon shown in an optical study of premixed diesel combustion performed by Ekoto et al. [74].

Formaldehyde was also found in the exhaust emissions and shown to occur mostly from over-lean areas in the combustion chamber [75]. The trend shown for the G-1 case closely resembled the CO curve shown in Figure 4 where retarded injection resulted in higher formaldehyde emissions at retarded combustion phasing. A minimum in formaldehyde for G-1 was also seen in the advanced region establishing a linkage between formaldehyde and CO emissions for premixed CI combustion. Formaldehyde emissions for the E-1 case were the highest in the retarded diesel injection timing region and may have been due to the well-known linkage between alcohol fuels and aldehyde emissions for spark-ignited engines [76].

Ethanol emissions for the E-1 case were higher on an indicated specific basis than the overall HC emissions for the G-1 case. This is most likely due to the inhibition effect of the fumigated ethanol and later burning previously described resulting in poorer late cycle oxidation. The oxygen mass in the unburned ethanol could be a minor contributor.

Comparing hydrogen with ethanol and gasoline as fumigants over a large range of diesel injection timing at constant FEF illuminates some interesting features of dual-fueled diesel modes in general. First, by using hydrogen as a fumigant, relatively low CO and HC emissions were found; therefore, the high HC and CO emissions shown in Figure 3 and Figure 4 for the G-1 case could be assumed to originate from the fumigated gasoline. Also, based on the emissions of hydrogen for the H-1 case, the unburned fumigant in the squish and crevice regions where cold over-lean conditions existed were

essentially constant, a trend further evidenced by the shape of the HC versus CA50 curve for the G-1 case in Figure 5.

4.2.2. **Comparison of Fumigant Energy Fraction**

The previous section showed how combustion proceeded differently when the reactivity of the fumigant mixture was changed. The charge reactivity prior to diesel injection can also be altered by changing the quantity of fumigant injected. Here to elucidate the differences between fuel and fumigant mixture, three FEF levels of 70, 80 and 90 % were examined at the same nominal IMEP over a large range of diesel injection timing. The amount of diesel fuel injected was adjusted accordingly to keep the total fuel energy input constant for these three cases. Figure 6 shows the variation of ignition delay, CA50 and $\eta_{i,g}$ with diesel injection timing. As the FEF reduced, the operational timing window became wider due to increased overall reactivity of the fuel-air mixture. At early diesel injection, the ignition delay increased for higher FEF levels, similar to reducing fumigant reactivity. At late diesel injection, nearly no difference was seen in ignition delay for all the three cases because ignition was controlled by the injection event of diesel fuel as previously discussed.

As in the variation of fumigant type, the peak $\eta_{i,g}$ corresponded well with an overall CA50 occurring just after TDC in the advanced diesel injection region for changing gasoline energy fraction as shown in Figure 6. However, the magnitude was different as FEF was altered; higher diesel fuel content led to higher peak $\eta_{i,g}$. One possible explanation is that combustion duration was shortened as the overall reactivity of fuels was increased at the same combustion phasing, leading to more constant volume-like combustion.

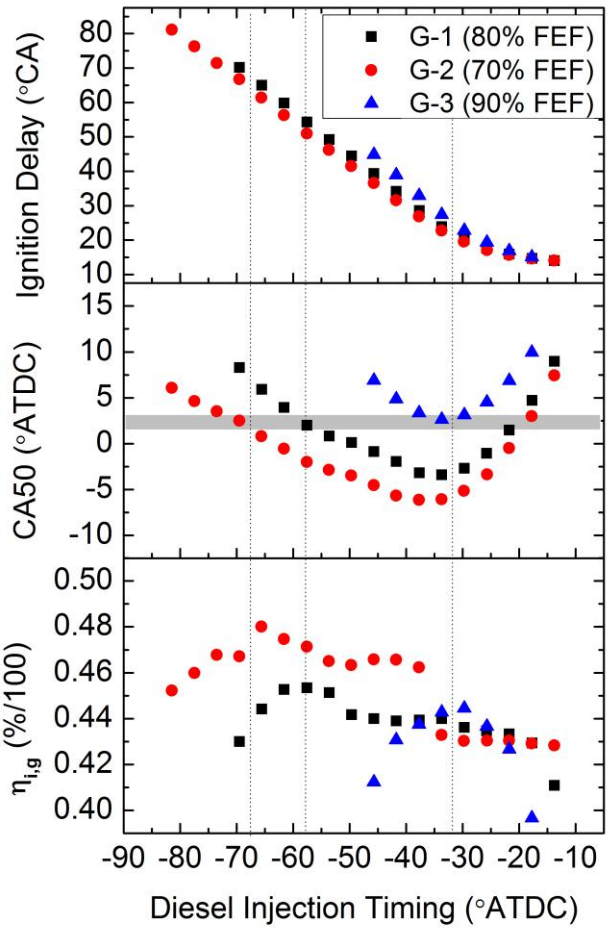

Figure 6: Ignition delay, CA50 and gross indicated cycle efficiency versus diesel injection timing for G-1, G-2 and G-3 cases

To further examine combustion trends, Figure 7 shows RoHR curves at three diesel injection timing settings for the three tested FEF levels. At early injection timing of SOI=48˚ BTDC, combustion proceeded in a primarily premixed fashion for each case with higher gasoline fraction leading to later peak RoHR and overall longer combustion duration. It can also be observed from the RoHR at later injection timing shown in Figure 7 that the level of FEF had a predictable effect on the relative magnitude of the first and second stages of high temperature heat release. As more diesel fuel was added, the first stage of heat release became more dominant due to the increased reactivity of the injected

charge near the location of injection. It can be seen that the second peak of heat release trace was largely prolonged at higher FEF and more delayed diesel SOI, suggesting that the combustion of premixed gasoline resembled the flame propagation in a conventional SI engine.

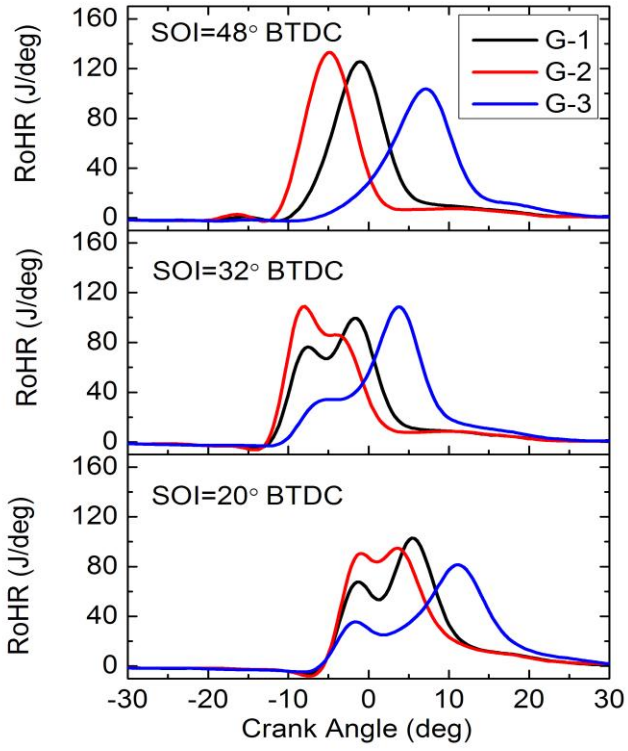

Figure 7: Gross apparent rate of heat release for G-1, G-2 and G-3 cases at 48˚, 32˚, 20˚ diesel injection timing

Figure 8 shows the gross indicated specific emissions of NO_X, soot, HC, CO for at the three FEF levels. Like in Figure 4, two regions of NO_X emissions existed, one for advanced and one for retarded diesel injection timing. The NO_X emissions in the latter region were reduced with more gasoline, which strengthens the argument that the diesel injection played the key role in creating inhomogeneous regions in the combustion chamber where temperatures and mixture were sufficient for NO_X production. Soot

emissions were near lower detectable measurement limits for the entire tested FEF and diesel injection timing range indicating lean, premixed conditions throughout.

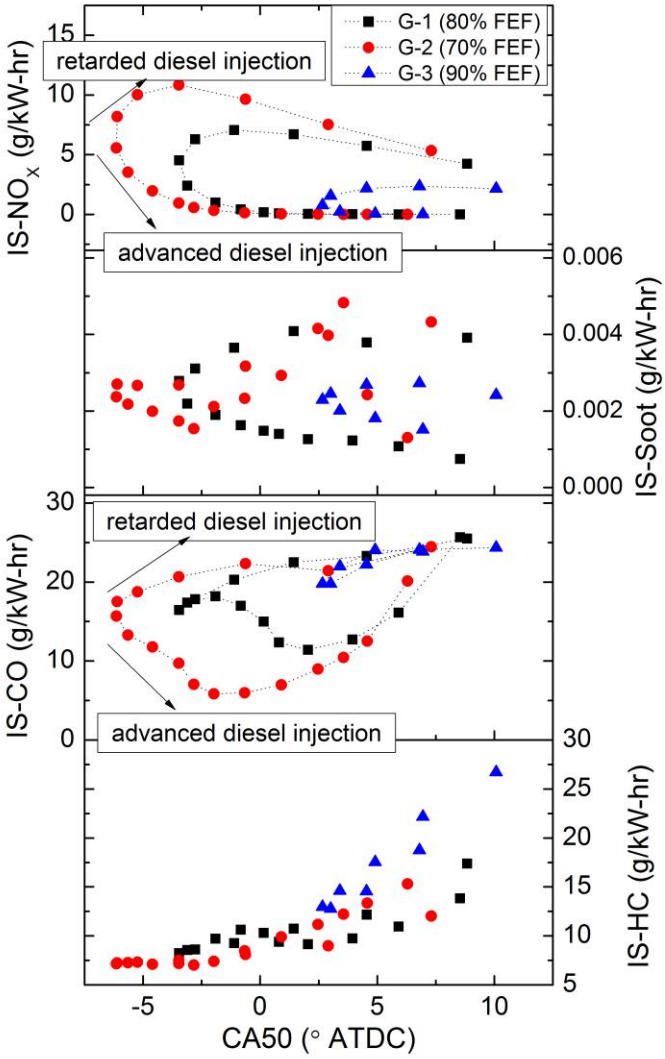

Figure 8: Gross indicated specific NO_X, soot, CO and HC, for G-1, G-2 and G-3 cases

Emissions of CO for the three FEF cases shown in Figure 8 had similar trends to the fumigant variation from Figure 4. In the advanced timing region, the combustion phasing of minimum CO coincided with the CA50 of best efficiency shown in Figure 6. Again, this establishes a link between overall thermal efficiency and combustion efficiency. HC

emissions had a strong dependence on combustion phasing independent of FEF, especially with CA50 near TDC. This confirms the earlier conclusion that HC resulting from dual-fuel combustion was mostly linked to the fumigated fuel but also indicates that the quantity of fumigated fuel was not as important. Hanson et al. [77], in recent work with an optimized piston bowl with a shallow bowl for RCCI found that HC emissions might be more linked to crevice flows than squish volume. With combustion phasing occurring later in the expansion stroke, conditions were not favorable for oxidation of these crevice flows when they emerged, thus accounting for the strong dependence of HC emissions on CA50.

4.3. **Conclusions**

This work experimentally examined dual-fuel combustion in a single cylinder diesel engine at an engine load of 450 kPa IMEP. Three fumigant types; gasoline, ethanol and hydrogen and three FEF levels; 70, 80 and 90% with gasoline as a fumigant were investigated over a wide range of direct diesel injection timing. Very advanced timing led to primarily premixed CI combustion whereas more retarded timing resulted in more traditional fumigation combustion with increased diffusion burning.

One conclusion of the work is that a fumigant's propensity for autoignition has a discernible effect on ignition delay especially with early diesel injection. For example, ethanol delayed ignition and combustion phasing, severely limited the operable diesel injection timing range and resulted in high unburned ethanol concentration in the exhaust. Hydrogen retarded the ignition but shortened the combustion duration compared with gasoline. Increasing FEF with the same fumigant delayed the ignition timing and

combustion phasing as well as increased the combustion duration at early diesel injection timings.

The use of hydrogen as a fumigant allowed some interesting insights about the nature of HC and CO emissions in dual-fuel combustion. With hydrogen fumigation, CO and HC emissions were very low compared with ethanol and gasoline, establishing that they mainly result from incomplete combustion of the fumigated fuel. Hydrogen emissions were independent of diesel injection timing and HC emissions were strongly linked to combustion phasing, further indicating that squish and crevice flows are mostly responsible for partially burned species from fumigation combustion.

Chapter 5 Diesel-Hydrous Ethanol RCCI under Different Loads[2]

In the United States, the primary feedstock for bio-ethanol fuel production is corn starch. In corn ethanol production, the most energy consuming processes are those for water removal (distillation and dehydration) [39]. A large portion of energy can be saved and the ethanol life cycle efficiency and economics will be remarkably improved if hydrous ethanol can be directly used in IC engines. Saffy et al. [40] demonstrated that hydrous ethanol with ethanol concentration of 86% by weight offered approximately 8% of energy cost savings, 8% of refinery emissions reduction as well as 3-6% of water consumption reduction in corn ethanol production. Scania produced hydrous ethanol fueled heavy-duty diesel engines with water content limited to 6.2% [78]. Up to 5% of ignition improver was used for igniting the fuel and compression ratio is higher than normal diesel engines. Costa et al. [41] observed higher thermal efficiency, lower CO and HC but higher NO_X emissions with the use of hydrous ethanol with water content of 6.8% by mass than gasoline-anhydrous ethanol blend in an SI engine. Dempsey et al. [45] investigated RCCI operation using hydrous ethanol as the low reactivity fuel and diesel as the high reactivity fuel using computational models. Low NO_X and soot emissions with a gross indicated thermal efficiency of 55% were predicted at loads ranging from 5 to 17 bar IMEP using hydrous ethanol with water content of 30% by mass. It was also seen that combustion was retarded due to the significant charge cooling effect of water and ethanol. The same group also conducted an experimental study on RCCI operation using diesel fuel and hydrous ethanol [46], demonstrating diesel-like thermal efficiencies

[2] This chapter is based on paper "An Experimental Investigation of Reactivity-Controlled Compression Ignition Combustion in a Single-Cylinder Diesel Engine Using Hydrous Ethanol" (Fang et al., 2015), ***J. Energy Resour. Technol.***, 137(3), 031101.

and near zero levels of NO_X and soot emissions in both heavy-duty and light-duty engines with the use of two different grades of hydrous ethanol.

The purpose of this part of the research was to experimentally verify the modeling and experimental results of Dempsey et al. [45,46] and to investigate the effect of the second diesel injection timing on combustion and emissions of diesel-hydrous ethanol RCCI at different load conditions in a modified diesel engine operated in single-cylinder mode.

5.1. **Experimental Procedure**

Table 4 gives the engine operating conditions used in the experiments. For each of the four conditions, the first start of injection command (SOIC1) for diesel fuel was fixed at -60 ^{o} ATDC with the fraction of total diesel fuel in the first injection fixed at 60%. The second start of injection command (SOIC2) was varied over the widest possible range without encountering unstable combustion as detected by a coefficient of variation (COV) of indicated mean effective pressure (IMEP) greater than 5%. Figure 9 gives the normalized injection current and in-cylinder pressure traces of one operating point as an example to illustrate the diesel injection scheme. The mass fraction and timing of the first diesel injection were set according to the modeling work by Dempsey et al. [45]. For each load condition, nominal loads of 4.3 bar, 6.1 bar, 7.7 bar and 8.6 bar IMEP were set at a baseline timing setting. Fueling was then held constant for the SOIC2 sweep by maintaining the same injection durations and pressures, resulting in an IMEP variance within the range of ± 0.5 bar. Intake air heating was employed for each case to maintain

stable combustion, with higher intake air temperature required for lower load conditions. A similar trend was shown by Dempsey et al. [45].

Table 4: Parameters for the investigated engine operating conditions

Condition	4.3 bar IMEP w/o EGR	6.1 bar IMEP w/o EGR	7.7 bar IMEP w/o EGR	8.6 bar IMEP w/ EGR
Engine Speed (rpm)	1500	1500	1500	1500
Nominal IMEP (bar)	4.3	6.1	7.7	8.6
EGR (%)	0	0	0	29
Hydrous Ethanol Energy Fraction (%)	75	76	76	76
Intake Temperature (˚C)	102	99	79	84
Intake Pressure (bar)	1.6	1.7	1.6	1.8
Diesel Injection Pressure (bar)	400	800	800	800
SOIC 1 (°ATDC)	-60	-60	-60	-60
SOIC 2 (°ATDC)	-34 ~ -28	-32 ~ -20	-26 ~ -18	-24 ~ -14
Fraction of Total Diesel Fuel in 1st Injection (%)	60	60	60	60
Fuel/Air Equivalence Ratio	0.31	0.38	0.45	0.69

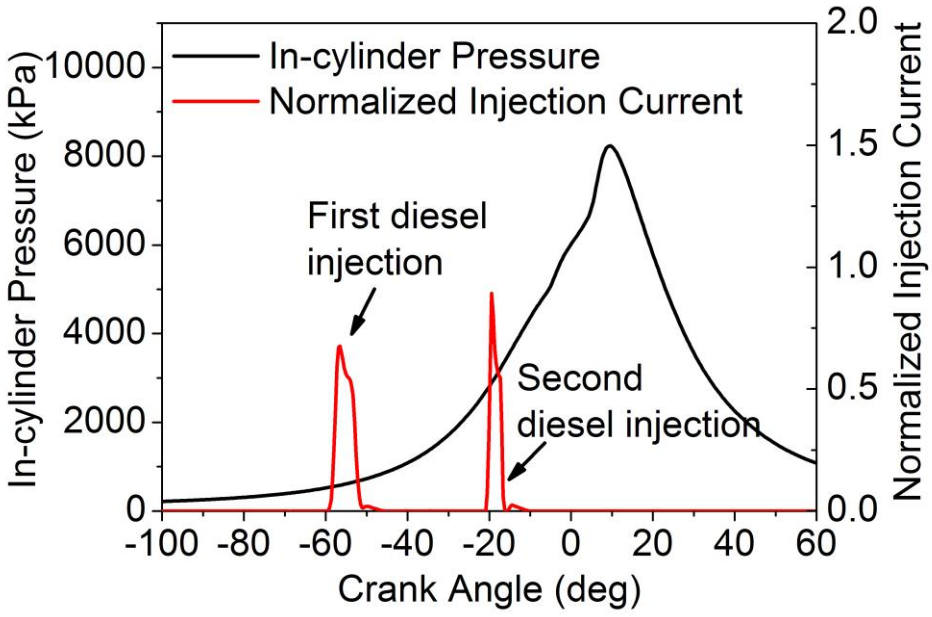

Figure 9: In-cylinder pressure and normalized injection pressure traces for SOIC1= -60 ° ATDC, SOIC2= -22 ° ATDC at 6.1 bar IMEP

Hydrous ethanol with water content of 25% by volume (150 proof) was used as the low reactivity fuel, and the energy fraction of the ethanol in the total energy input was fixed at 75 ± 1%. Commercially available #2 ultra-low sulfur diesel (ULSD) was used in the study.

5.2. **Results and Discussion**

In this section, the experimental results are presented and discussed regarding the effect of the second diesel injection timing on the performance and emissions characteristics of diesel-hydrous ethanol RCCI combustion. Figure 10 presents CA05, CA50 and indicated gross cycle efficiency ($\eta_{i,g}$) as a function of SOIC2 for the four cases listed in Table 4. It can be seen that the position and width of the SOIC2 window where stable operation could be maintained varied significantly for the loads tested. The 4.3 bar

IMEP case had a narrower SOIC2 window located farther away from TDC than the 6.1 bar IMEP case, possibly due to the lower global equivalence ratio and lower diesel injection pressure leading to longer required mixing time for diesel fuel and air. Due to greater charge cooling and combustion inhibition effects with increasing hydrous ethanol [28,45,69], the two highest loads had narrower SOIC2 operating windows than the 6.1 bar IMEP case. Further, the operability ranges were shifted closer to TDC, increasing the reactivity stratification and offsetting the aforementioned inhibition of ignition. EGR was necessary for the 8.6 bar IMEP case to achieve low levels of NO_X emissions typical of RCCI combustion. This runs counter to the modeling results of [45] where no EGR was required up to 17 bar IMEP. Both the ignition timing and combustion phasing were remarkably retarded for the highest load case and the SOIC2 window was further shifted towards TDC creating higher local reactivity and equivalence ratio in the piston bowl.

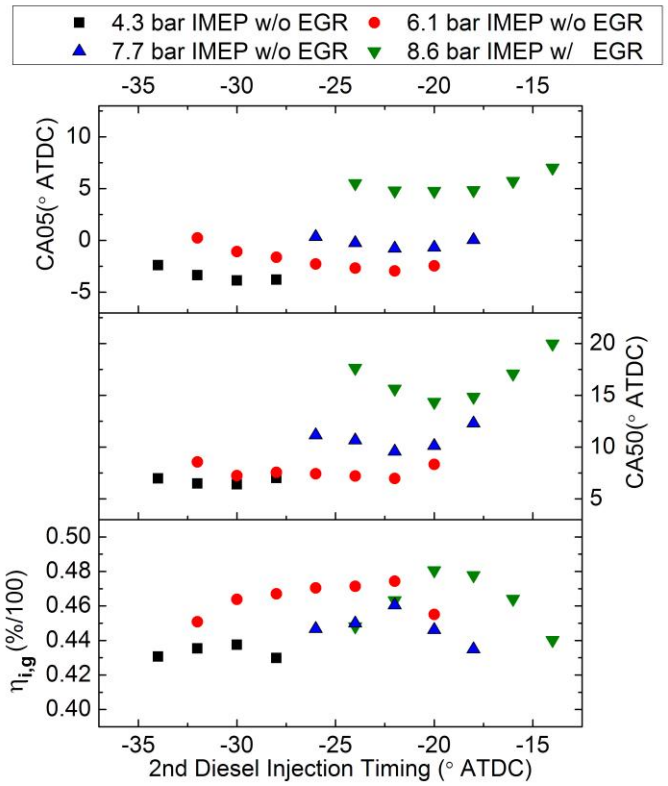

Figure 10: CA05, CA50 and gross indicated cycle efficiency versus second diesel injection timing

All four tested loads had a minimum of CA05 and CA50 with respect to SOIC2. Either more advanced or more delayed SOIC2 led to delayed ignition timing and combustion phasing as measured by CA05 and CA50 respectively. Similar phenomenon has been observed in previous studies with single injection of diesel fuel [70,79]. As the SOIC2 was advanced from the minimum point, the mixing time for diesel fuel and surrounding charge was extended, leading to more premixed combustion. Meanwhile, a portion of the diesel fuel spray missed the piston bowl and targeted at the squish area, causing over-mixing and wall impingement; therefore, a more delayed heat release event. As the SOIC2 was retarded from the minimum point, the local reactivity and equivalence ratio in piston bowl became higher, resulting in ignition and combustion more coupled

with the second diesel injection events, and hence more delayed CA05 and CA50. It can also be observed that for each case, the peak cycle efficiency was achieved at the SOIC2 timing of minimum CA50. This is consistent with previous findings [70,79] that cycle efficiency was enhanced as combustion phasing was located closer to TDC in dual-fuel PPCI combustion strategies. Although the combustion phasing was significantly delayed for the 8.6 bar IMEP case compared to other cases, relatively high peak cycle efficiency was obtained, possibly due to reduced heat loss and improved combustion efficiency associated with the use of EGR.

To further examine the combustion characteristics associated with the diesel-hydrous ethanol RCCI, RoHR traces with respect to varying SOIC2 are given in Figure 11. With SOIC2 closer to TDC, a two-stage heat release curve was observed, with the first peak representing combustion of the more reactive diesel fuel in piston bowl, followed by a higher spike indicating the premixed combustion of the remaining well-mixed fuel-air charge. As SOIC2 was advanced, the first peak was reduced in magnitude due to lower local reactivity and equivalence ratio in piston bowl. Since mixing time for the diesel fuel introduced during the second injection and its surrounding charge was extended, the reactivity gradient between piston bowl and squish area was reduced, and the two heat release peaks gradually merged to form a single-peak Gaussian-shaped RoHR curve. Further advancing SOIC2 led to earlier ignition timing and sharper RoHR curve until the minimum point of CA50 was reached. Beyond this point, ignition timing was retarded and combustion duration was elongated with more advanced SOIC2. At the same SOIC2, the ignition timing was retarded and combustion duration was extended as the load was increased due to the larger charge cooling and combustion inhibition effects. The first-

stage heat release event was much less prominent in the 8.6 bar IMEP case in contrast with other cases because the EGR further inhibited early-stage heat release reactions.

Figure 12 presents the emissions of NO_X and soot on a gross-indicated specific basis with respect to SOIC2 for the four cases. The peak NO_X emissions were observed where the SOIC2 was slightly later than the minimum point of CA50, possibly caused by the combined effects of high in-cylinder temperature associated with the relatively early combustion phasing and the occurrence of near-stoichiometric regions created by the late SOIC2. Advancing the SOIC2 allowed more premixed and leaner combustion, largely reducing the in-cylinder temperature and the near-stoichiometric spots, and hence decreasing the NO_X emissions. The higher NO_X emissions for the 4.3 bar IMEP case as compared to the 6.1 bar IMEP case at the same SOIC2 are likely to be caused by the lower diesel injection pressure which resulted in worse mixing of the diesel fuel and air. The use of EGR significantly reduced NO_X emissions due to the decreased in-cylinder temperature for the 8.6 bar IMEP case as comparing the two highest load cases.

Soot emissions were consistently low throughout the range of SOIC2 for each case, indicating primarily premixed combustion with minimal high temperature fuel-rich regions in the cylinder. The 4.3 bar IMEP case exhibited the highest soot emissions, potentially associated with poorer mixing resulting from lower diesel injection pressure. Soot emissions were significantly reduced with the use of EGR at the 8.6 bar condition. This may have been caused by retarding ignition timing and combustion phasing, allowing extended mixing time for diesel fuel and surrounding charge as is typical with PPCI combustion modes.

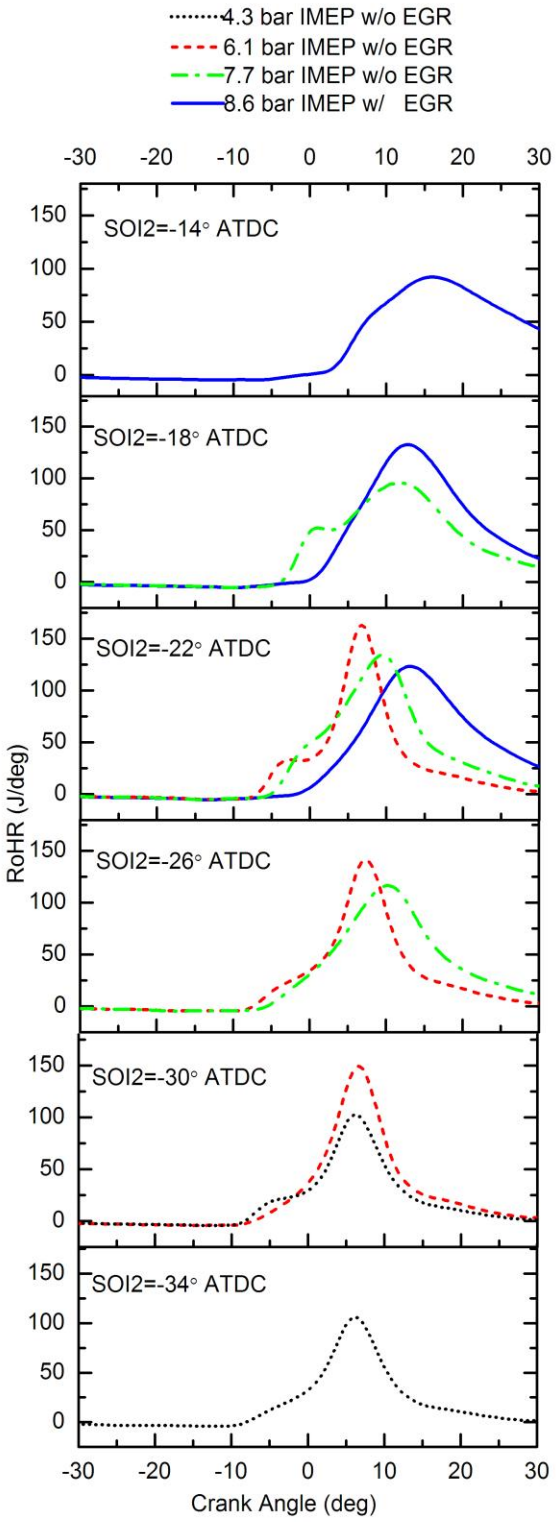

Figure 11: Gross apparent rate of heat release at varying second diesel injection timing

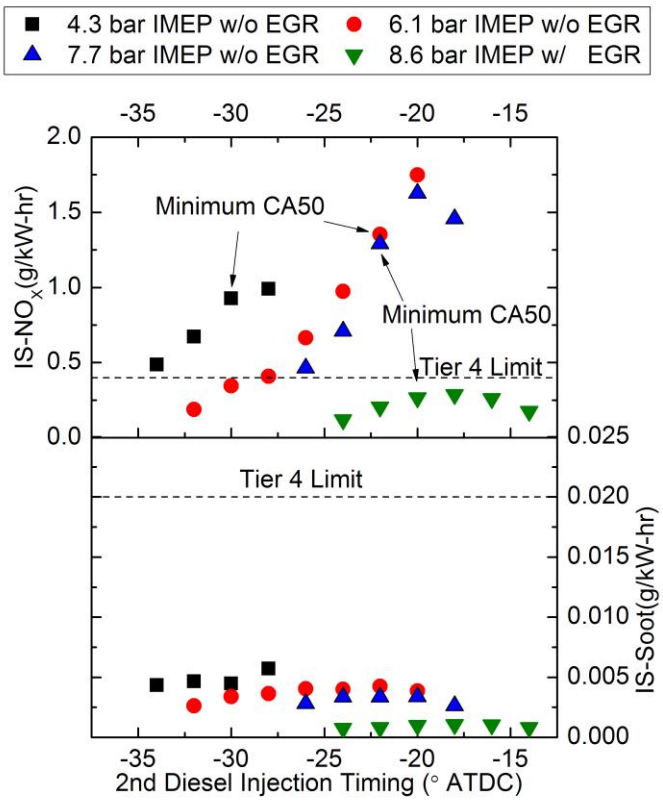

Figure 12: Gross indicated specific NO_X, soot versus second diesel injection timing

For PPCI modes like the one studied here, emissions from partially burned fuel are significantly higher than for conventional diesel combustion. The CO, HC, aldehydes and ethanol emissions varied similarly as a function of SOIC2 for each load case as shown in Figure 13. A minimum point of CO and HC emissions was observed at the minimum CA50 timing point for each case. When the second diesel injection timing was more retarded than the minimum CA50 point, a relatively fuel-rich region was formed in the piston bowl, with insufficient oxygen to oxidize the CO or HC produced in the bowl. When the second diesel injection timing was advanced relative to the minimum CA50 point and a larger portion of fuel jet targeted at the squish region and cylinder wall, over-mixing occurred and CO or HC could not be fully oxidized due to low temperature in the

cylinder. When the second diesel injection was well timed, the diesel fuel could be optimally distributed in both the piston bowl and squish region. As a result, fuel-rich spots and over-mixing could be avoided, reducing the CO and HC emissions, thus improving combustion efficiency. It can also be seen that the CO and HC emissions were the highest for the lowest load case, indicating that the fuel-air mixture is overly lean.

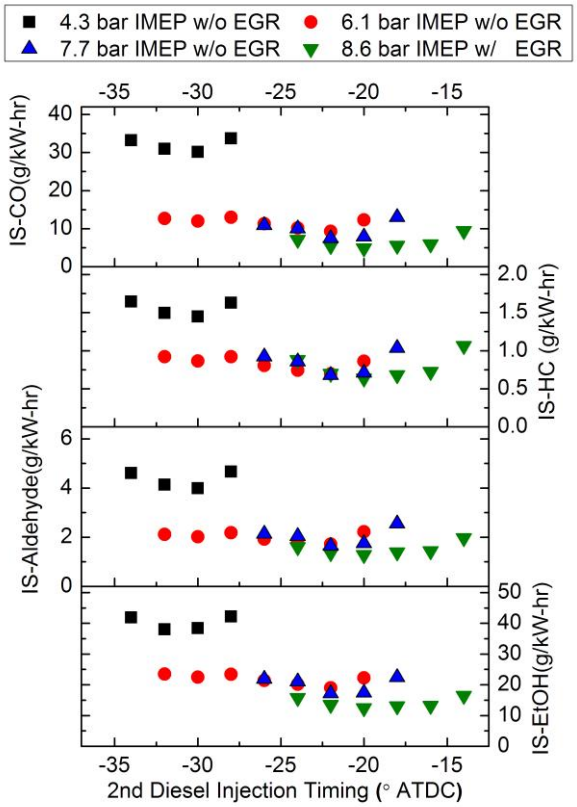

Figure 13: Gross indicated specific CO, HC, aldehydes, ethanol emissions versus second diesel injection timing

In an experimental study by Dempsey et al. [46] on a heavy-duty engine, the same grade of hydrous ethanol as in this study (150 proof) was used, and the engine was operated at a load of approximately 8 bar IMEP. Engine operating parameters and experimental results of the peak thermal efficiency points in the 7.7 bar and 8.6 bar IMEP cases are listed in Table 5, along with the two operating points given in [46] for detailed

comparison. As can be seen in the table, our experiments required more retarded diesel injection timing and higher degree of intake heating for stable combustion than in [46]. These discrepancies might have been related to differences in air intake system configuration, combustion chamber geometry, characteristics of the DI and PFI injectors and the intake charge motion. The higher intake air temperature and higher compression ratio used in our work compared to [46] contributed to higher peak in-cylinder temperature, leading to an increase in thermal NO_X production. Additionally, a more delayed second diesel injection timing led to more heterogeneous mixture of fuel and air, and hence more near-stoichiometric zones in the cylinder, favoring the formation of NO_X. With the use of EGR, the NO_X in this study was lowered to about 1/5 of that without EGR. Indicated thermal efficiencies were lower in this study, possibly due to the retarded combustion phasing as compared to that in [46] leading to reduced thermodynamic cycle efficiency. Combustion phasing was delayed even more with the use of EGR; however, the indicated thermal efficiency was increased. This might have been due to improved combustion efficiency and reduced heat loss. The unburned HC emissions listed in Table 5 were a sum of the HC species specified in Section 3.2.1, with the unit converted to g/kg-fuel for comparison purposes. As consistent with in [46], relatively high unburned HC and CO emissions were observed in this study, commonly seen for a premixed strategy such as RCCI. Another finding similar with in [46] is that although acceptably low levels of COV of IMEP were obtained, relatively high levels of COV of PPRR were observed. This is potentially caused by cycle-to-cycle variation in the bulk gas temperature at the start of compression stroke, resulting from variation in the degree of

vaporization of hydrous ethanol. With the use of EGR, the COV of both IMEP and PPRR are lowered, indicating more stable combustion as well as lower PPRR.

Table 5: Comparisons of operating parameters and experimental results between selected operating points in this study and in Reference [46]

Operating Points	Point_1 (Dempsey et al.)	Point_2 (Dempsey et al.)	7.7 bar IMEP w/o EGR	8.6 bar IMEP w/ EGR
Operating Parameters				
Single-Cylinder Displacement (L)	2.44	2.44	1.30	1.30
Compression Ratio	16.1	16.1	18.5	18.5
Total Fuel (PFI+DI) (mg/cycle)	163	177	103	113
Load (Gross IMEP) (bar)	~8	~8	7.7	8.6
Engine Speed (rpm)	1300	1300	1500	1500
Hydrous Ethanol Mass Fraction (%)	82	89	88	88
Grade of Hydrous Ethanol (proof)	150	150	150	150
Diesel SOI #1 (˚ATDC)	-59	-59	-60	-60
Diesel SOI #2 (˚ATDC)	-35	-35	-22	-20
Fraction of Total Diesel Fuel in First Injection (%)	55%	57%	60%	60%
Diesel Injection Pressure (bar)	800	800	800	800
EGR (%)	0%	0%	0%	29%
Intake Pressure (bar)	1.57	1.61	1.6	1.8
Intake Temperature (˚C)	36	60	79	84
Global Equivalence Ratio	0.34	0.38	0.45	0.69
Experimental Results				
CA50 (˚ATDC)	4.6	4.7	9.6	14.4
NO_X (g/kW-hr)	0.10	0.09	1.29	0.27
Soot (g/kW-hr)	0.007	0.005	0.003	0.001
Unburned HC (g/kg-fuel)	58.46	52.60	73.75	56.64
CO (g/kg-fuel)	78.86	35.50	28.22	19.16
Combustion Efficiency (%)	89.0	91.3	92.8	94.7
Gross Indicated Efficiency (%)	50.7	51.3	46.0	48.1
PPRR (bar/deg)	3.3	6.4	3.8	2.3
COV of IMEP (%)	2.3	1.8	2.7	1.7
COV of PPRR (%)	13.5	18.9	34.7	19.7

5.3. **Conclusions**

In this section, the effects of the second diesel injection timing on performance and emissions characteristics of diesel-hydrous ethanol RCCI combustion mode were experimentally investigated. With the mass fraction and timing of the first diesel injection kept constant, a sweep of the second diesel injection timing was performed at various load conditions. The effects of using EGR in RCCI combustion were also explored in comparing the two higher load cases.

It can be concluded from this study that 150 proof hydrous ethanol can be used as the low reactivity fuel in RCCI up to 8.6 bar IMEP and with 75% or higher ethanol energy fraction while achieving simultaneously low levels of NO_X and soot emissions. The second diesel injection timing can be adjusted to achieve a maximum in thermal efficiency and minimum in CO and HC emissions while setting a constant first diesel injection. This study in part confirms the feasibility of using hydrous ethanol as the low reactivity fuel in RCCI as was previously suggested in modeling and experimental studies [45,46] and opens the opportunity for further exploration of hydrous ethanol use in diesel engines to improve the renewability of ethanol, increase engine efficiency and reduce harmful engine exhaust emissions.

Chapter 6 Optimization of Diesel-Hydrous Ethanol RCCI Combustion using Response Surface Methodology[3]

The purpose of this section was to apply RSM to RCCI operation of a single-cylinder research engine using diesel as the high-reactivity fuel, and hydrous ethanol as the low-reactivity fuel with the primary goal to lower engine-out pollutant emissions. Critical operating parameters associated with engine fueling and air-handling systems were identified and their effects on engine performance and emissions were evaluated and optimized.

6.1. Experimental Procedure

6.1.1. RSM Optimization Methods

At the beginning of the RSM optimization, a mathematical expression of the optimization objective was established. Montgomery et al. [61] proposed an equation to represent combination of multiple objectives. In this study, a similar equation was used as the objective function for the RSM optimization, describing the objectives as to obtain an overall minimum of weighted CO_2, HC, CO, NO_X and soot emissions, as shown in Equation (3).

$$(3) \qquad f(X) = RESPONSE = \frac{1000}{\left(\frac{IS-CO_2}{IS-CO_{2_t}}\right)^2 + \left(\frac{IS-HC}{IS-HC_t}\right)^2 + \left(\frac{IS-CO}{IS-CO_t}\right)^2 + \left(\frac{IS-NOx}{IS-NOx_t}\right)^2 + \frac{IS-Soot}{IS-Soot_t}}$$

In the equation: $\mathbf{X}=\{x_1, x_2 \ldots x_n\}$ denotes the vector of operating parameters to be optimized; IS-CO_2, IS-HC, IS-CO, IS-NO_X and IS-Soot denote measured emissions on an

[3] This chapter is based on paper "Optimization of Reactivity-Controlled Compression Ignition Combustion Fueled with Diesel and Hydrous Ethanol Using Response Surface Methodology" (Fang et al., 2015), ***Fuel***, 160(2015) 446-457.

indicated specific basis; IS-CO_{2t}, IS-HC_t, IS-CO_t, IS-NO_{Xt} and IS-$Soot_t$ denote target values for the indicated specific emissions.

Emission terms in the objective function were expressed on an indicated specific basis because engine was operated in single-cylinder mode. Soot emissions were generally much lower than the target value throughout the RCCI operating region according to preliminary experimental results. Therefore a smaller weighting exponent was applied to the soot term implying that soot emissions are of lower priority when the other emissions are above their target levels, and a reduction in soot emissions is more attractive when the other emissions are reduced below the target levels [62]. All terms of interest were placed in denominator so that the optimization objective is intuitively to search for the highest response value rather than the lowest; the integer 1000 in the numerator is a scaling factor to avoid the inconvenience of working with non-integer values as suggested by Montgomery et al. [61].

Table 6: Target CO_2, HC, CO, NO_X and soot emissions values for use in the RSM optimization study

IS-CO_2 (g/kW-hr)	IS-HC (g/kW-hr)	IS-CO (g/kW-hr)	IS-NO_X (g/kW-hr)	IS-Soot (g/kW-hr)
536.8	17.34	11.70	0.32	0.008

Table 6 gives the target values of the emission terms on a gross indicated specific basis. The target values for NO_X and soot emissions were calculated based on the US EPA Tier 4-Final standard for non-road diesel engines, assuming a conversion factor of 0.5 from PM to soot based on the results from [49] and a mechanical efficiency of 80% for conversion from brake to indicated specific basis. Kokjohn et al. [27] showed that

indicated thermal efficiency was generally higher than 50% in RCCI operation in both heavy-duty and light-duty engine experiments. Accordingly, the calculation of the target value for CO_2 emission term was based on the assumption that the engine is operated using neat diesel fuel with a 50% indicated thermal efficiency and 100% combustion efficiency. The lowest values of the CO and HC emissions from the heavy-duty diesel-hydrous ethanol RCCI experiments conducted by Dempsey et al. [46] were chosen as the target values for the CO and HC emission terms in this work.

Table 7: Selected operating parameters in the factor-screening experiments

Symbol	**T_{int}**	**P_{int}**	**EGR**	**Dwell**
Operating Parameter	Intake Temperature	Intake Pressure	EGR Rate	Interval between Two Injections
Symbol	**SOIC 2**	**P_{rail}**	**Inj1Fr**	**FEF**
Operating Parameter	Second Diesel Injection Timing	Diesel Fuel Rail Pressure	Fraction of First Diesel Injection	Fumigant Energy Fraction

Engine speed was held constant at 1500 rpm at all testing conditions, which is the manufacturer specified speed for peak rated torque. The RSM optimization process was independently conducted for two engine loads, 4.5 and 10 bar nominal indicated mean effective pressure (IMEP), representing low- and medium-load conditions, respectively. Table 7 lists the eight operating parameters that are directly related to engine fueling and intake air handling systems, and they consist of the vector X in Equation (3). To determine the starting point for each optimization process, a set of preliminary experiments were conducted. The fumigant energy fraction (FEF), defined as the lower

heating value of hydrous ethanol times its mass flow divided by the total fuel energy input based on lower heating value, was kept at ~75%, with the remainder provided by diesel fuel. Fueling strategy of diesel fuel has been shown to be critical in generating an optimal fuel reactivity distribution in the cylinder in a paper by Kokjohn et al. [31]. They used CFD modeling to propose a diesel fuel injection scheme that results in minimal cylinder wall film level and avoids fuel-rich regions in the cylinder. The scheme included two injections at about 60 and 30 ºBTDC, with the first injection delivering ~60% of the total diesel fuel input. In the current work, the first diesel injection timing was fixed at ~60 ºBTDC, with the ratio of first and second injection durations set to be 3:2. Since the second diesel injection timing has been shown to largely affect the RCCI combustion [26], it was chosen as a variable in the preliminary experiments and swept over the widest possible range where stable combustion can be maintained. The injection timing that resulted in the highest response in each sweep was selected as the timing for the starting points. The diesel fuel injector rail pressure was fixed at 800 bar at the high load as consistent with studies by Kokjohn et al. [24,26,28,35]. At the low load, the rail pressure was reduced to 400 bar to allow reasonably long injection durations. As shown in a previous study [65], intake air heating was required to overcome the charge cooling effect of hydrous ethanol. The required intake air temperature was much higher for the lower load case due to leaner fuel-air charge in the cylinder. At the high-load condition, EGR was needed for reducing NO_X emissions and the peak rate of pressure rise (RoPR). Operating parameters for the starting points are summarized in Table 8.

Table 8: Operating parameters of the starting points

	Low Load	High Load
Engine Load (bar IMEP nominal)	4.5	10
Engine Speed (rev/min)	1500	1500
Diesel SOIC 1 (ºATDC)	-60	-60
Diesel SOIC 2 (ºATDC)	-32	-22
DI Injection Pressure (bar)	400	800
Fraction of 1st Diesel Injection (%)	60	60
Ethanol Energy Fraction (%)	75	75
Intake Temperature (ºC)	102	43
Intake Pressure (bar)	1.6	1.9
EGR rate (% vol.)	0	29
Fuel/Air Equivalence Ratio	0.31	0.60

6.1.2. **Optimization Process under the Low Engine Load Condition**

For each load condition, a set of two-level fractional factorial experiments was conducted in the vicinity of the starting points to evaluate the effect of each factor. Analysis of variance (ANOVA) was performed on the experimental results. The factors with a p-value greater than 0.05 were considered to be active, while the factors with a p-value less than 0.05 were held constant in the following experiments. Subsequently, another set of two-level fractional factorial experiments combined with certain number of

center and axial runs was conducted to construct a second-order regression model of the response as a function of the active factors. An optimization path was generated from the model and a set of experiments was conducted along the path to obtain the optimal response.

At the beginning of the optimization process, a set of factor screening experiments was conducted to identify factors that significantly affect the responses. Table 9 gives the factor level settings and the corresponding response values of the factor screening experimental design. This is a two-level fractional factorial design consisting of 16 corner runs and 3 center runs with a resolution of IV. Table 10 presents the regression coefficients and P values of the 8 factors based on the ANOVA of the factor screening results. Effect was considered to be significant if the P value was less than 0.05. Accordingly, SOIC2, Inj1Fr, P_{rail}, P_{int} were the five factors that had significant impact on the response for the 4.5 bar IMEP condition. They were subject to further optimization while the remaining three factors were kept constant in the following experiments. To fit a first-order regression model to the response, another set of two-level fractional factorial experiments were conducted, with the inactive factors held constant.

Table 11 gives the factor level settings and response values for this design. The design is of resolution V and all main effects and two-way interactions (TWI) can be independently estimated. ANOVA results of the fitted first-order models with and without TWI terms are presented in Table 12 and Table 13, respectively. The P values for both models were smaller than 0.05, indicating that a second-order model was needed to better describe the response.

Table 9: Factor level settings and response values of the factor screening design under the low load condition

Test Order	Dwell	SOIC2	Inj1Fr	FEF	P_{rail}	T_{int}	P_{int}	EGR	Response
1	0	0	0	0	0	0	0	0	60
2	-1	1	-1	1	1	-1	1	-1	102
3	-1	-1	-1	-1	-1	-1	-1	-1	4
4	-1	-1	1	1	1	1	-1	-1	101
5	-1	1	-1	-1	1	1	-1	1	70
6	1	1	-1	-1	-1	-1	1	1	21
7	1	1	1	1	1	1	1	1	151
8	1	-1	1	-1	-1	1	-1	1	15
9	1	-1	-1	1	1	-1	-1	1	80
10	0	0	0	0	0	0	0	0	63
11	-1	-1	1	-1	1	-1	1	1	43
12	1	1	-1	1	-1	1	-1	-1	106
13	-1	-1	-1	1	-1	1	1	1	7
14	-1	1	1	-1	-1	1	1	-1	86
15	-1	1	1	1	-1	-1	-1	1	112
16	1	1	1	-1	1	-1	-1	-1	144
17	1	-1	1	1	-1	-1	1	-1	52
18	1	-1	-1	-1	1	1	1	-1	6
19	0	0	0	0	0	0	0	0	49

Table 10: Regression coefficients and P values of the factors from ANOVA of the factor screening results under the low load condition

Term	Regression Coefficient	P Value
Intercept	66.6	—
Dwell	3.1	0.371
SOIC2	30.0	4.0E-06
Inj1Fr	19.2	1.8E-04
FEF	20.1	1.2E-04
P_{rail}	18.3	2.6E-04
T_{int}	-0.9	0.784
P_{int}	-10.2	0.012
EGR	-6.4	0.084

Table 11: Factor level settings and response values of the first-order model design under the low load condition

Test Order	SOI2	Inj1Fr	FEF	P_{rail}	P_{int}	Response
1	0	0	0	0	0	38
2	-1	-1	1	-1	-1	15
3	-1	-1	-1	-1	1	4
4	1	1	1	-1	-1	85
5	0	0	0	0	0	41
6	-1	-1	-1	1	-1	9
7	-1	-1	1	1	1	30
8	1	1	-1	-1	1	35
9	0	0	0	0	0	40
10	1	-1	1	-1	1	24
11	-1	1	-1	-1	-1	36
12	-1	1	1	1	-1	107
13	1	-1	1	1	-1	84
14	0	0	0	0	0	36
15	-1	1	1	-1	1	24
16	1	-1	-1	1	1	10
17	1	1	1	1	1	69
18	0	0	0	0	0	34
19	-1	1	-1	1	1	36
20	1	-1	-1	-1	-1	9
21	1	1	-1	1	-1	80
22	0	0	0	0	0	33

Table 12: ANOVA of the first-order model without TWI under the low load condition

	Degree of Freedom	Sum Square	Mean Square	F Value	P Value
First Order Terms	5	13904.3	2780.9	18.3	4.1E-06
Residuals	16	2425.6	151.6	—	—
Lack of Fit	11	2381.1	216.5	24.3	0.001
Pure Error	5	44.5	8.9	—	—

Table 13: ANOVA of the first-order model with TWI under the low load condition

	Degree of Freedom	Sum Square	Mean Square	F Value	P Value
First Order Terms	5	13904.3	2780.9	136.9	4.3E-06
TWI	10	2303.7	230.4	11.3	0.004
Residuals	6	121.8	20.3	—	—
Lack of Fit	1	77.3	77.3	8.7	0.032
Pure Error	5	44.5	8.9	—	—

A central composite design (CCD) that consists of corner runs from the previous design, a set of axial runs and center runs was used to build a second-order model. The factor level settings and corresponding response values are given in Table 14. Table 15 and Table 16 show the regression coefficients and P values of the factors in the second-order models for the response and the five emission terms that constitute the response. Ridge analysis was conducted to obtain the optimization path for the response according to the second-order model.

Table 17 gives the factor level settings and predicted response values of operating points along the optimization path. A set of experiments was conducted along the optimization path, but some level settings were deviated from the designed values either due to measurement error or the necessity of maintaining stable operation. For instance, FEF deviated the most remarkably from its designed values, because higher fraction of diesel fuel was needed to avoid unstable combustion. The actual factor level settings and corresponding response values are shown in Table 18. It can be seen that the actual response monotonically increased along the optimization path, demonstrating that the RSM optimization process is effective. Only three steps along the path were feasible because further advancement led to unstable combustion.

Table 14: Factor level settings and response values of the additional center and axial points of the CCD under the low load condition

Test Order	SOI2	Inj1Fr	FEF	P_{rail}	P_{int}	Response
1	-2	0	0	0	0	14
2	0	0	0	0	0	27
3	0	0	0	0	2	18
4	0	0	0	0	-2	49
5	2	0	0	0	0	65
6	0	0	2	0	0	63
7	0	0	-2	0	0	11
8	0	-2	0	0	0	9
9	0	0	0	-2	0	19
10	0	0	0	2	0	58
11	0	2	0	0	0	108

Table 15: Regression coefficients and P values of the active factors in the second-order models of the response, CO_2 and HC emissions under the low load condition

	Response		CO_2		HC	
	Coeff.	P Val.	Coeff.	P Val.	Coeff.	P Val.
Intercept	35.811	1.5E-8	456.848	2.2E-16	28.191	8.7E-8
SOIC2	9.784	2.5E-5	-2.194	0.111	1.082	0.443
Inj1Fr	20.206	1.1E-8	1.761	0.193	-0.416	0.766
FEF	13.478	9.8E-7	-6.228	3.8E-4	7.638	1.2E-4
P_{rail}	11.318	6.0E-6	3.515	0.018	-2.106	0.149
P_{int}	-10.652	1.1E-5	2.736	0.053	-1.828	0.205
SOIC2:Inj1Fr	-0.156	0.933	-4.233	0.019	1.693	0.331
SOIC2:FEF	2.213	0.246	-2.887	0.090	0.753	0.660
SOIC2:P_{rail}	-0.896	0.630	-1.553	0.340	0.754	0.660
SOIC2:P_{int}	-3.008	0.123	7.029	7.3E-4	-1.864	0.287
Inj1Fr:FEF	-1.380	0.461	8.298	1.9E-4	-3.740	0.045
Inj1Fr:P_{rail}	1.979	0.297	-6.208	0.002	1.501	0.387
Inj1Fr:P_{int}	-5.921	0.007	-0.022	0.989	-1.906	0.276
FEF:P_{rail}	5.592	0.009	-0.984	0.541	1.567	0.367
FEF:P_{int}	-5.783	0.008	-6.478	0.001	1.210	0.483
P_{rail}:P_{int}	-4.859	0.020	-1.995	0.226	-0.142	0.934
$SOIC2^2$	0.674	0.619	1.400	0.242	-0.875	0.485
$Inj1Fr^2$	5.419	0.001	2.036	0.099	-0.634	0.611
FEF^2	0.128	0.924	4.495	0.002	0.230	0.853
P_{rail}^2	0.494	0.715	-0.986	0.403	3.046	0.028
P_{int}^2	-0.917	0.500	2.750	0.033	-1.121	0.375

Table 16: Regression coefficients and P values of the active factors in the second-order models of CO, NO_X and soot emissions under the low load condition

	CO		NO_X		Soot	
	Coeff.	P Val.	Coeff.	P Val.	Coeff.	P Val.
Intercept	30.402	5.5E-9	1.554	1.5E-9	0.006	2.1E-6
SOIC2	0.510	0.666	-0.440	2.3E-6	-6.3E-4	0.138
Inj1Fr	-0.082	0.944	-0.876	1.1E-9	-3.3E-4	0.416
FEF	0.937	0.432	-0.644	3.7E-8	-6.3E-4	0.137
P_{rail}	-2.013	0.106	-0.403	5.6E-6	-0.002	1.8E-4
P_{int}	4.583	0.002	0.270	2.4E-4	0.001	0.007
SOIC2:Inj1Fr	2.370	0.118	0.072	0.284	2.8E-5	0.955
SOIC2:FEF	1.483	0.313	-0.013	0.840	-4.0E-4	0.428
SOIC2:P_{rail}	-0.046	0.975	0.108	0.118	3.7E-4	0.457
SOIC2:P_{int}	-2.733	0.076	0.021	0.754	-1.7E-4	0.730
Inj1Fr:FEF	-4.373	0.009	0.536	2.4E-6	5.4E-4	0.291
Inj1Fr:P_{rail}	3.654	0.024	0.080	0.237	-2.1E-4	0.676
Inj1Fr:P_{int}	-1.139	0.435	0.008	0.903	1.6E-4	0.746
FEF:P_{rail}	2.103	0.161	-0.046	0.489	4.0E-4	0.424
FEF:P_{int}	1.488	0.312	-0.111	0.109	-1.6E-4	0.741
P_{rail}:P_{int}	-0.205	0.887	-0.046	0.486	-1.2E-4	0.813
$SOIC2^2$	-1.302	0.228	0.085	0.093	-4.0E-5	0.913
$Inj1Fr^2$	-0.331	0.753	0.128	0.018	1.5E-5	0.966
FEF^2	-0.958	0.368	0.126	0.020	3.2E-4	0.386
P_{rail}^2	2.148	0.058	-0.007	0.876	8.7E-4	0.029
P_{int}^2	-1.547	0.157	0.100	0.054	-1.2E-4	0.740

Table 17: Designed factor level settings of the optimization path under the low load condition

SOIC2	Inj1Fr	FEF	P_{rail}	P_{int}	Predicted Response
-2.28	-0.97	-0.45	0.22	1.88	3
-2.11	0.14	-0.04	0.78	1.17	20
-1.93	1.25	0.37	1.33	0.45	71
-1.76	2.36	0.78	1.88	-0.27	156

Table 18: Actual factor level settings of the optimization path under the low load condition

SOIC2	Inj1Fr	FEF	P_{rail}	P_{int}	Actual Response
-2.30	-0.95	-0.40	0.22	1.92	4
-2.10	0.16	0.08	0.78	1.22	13
-1.95	1.30	0.26	1.33	0.43	88
-1.75	2.17	0.16	1.88	-0.34	178

Table 19 gives the performance and emissions results of the operating points along the optimization path and at the starting point. Table 20 presents the comparison between the emissions results and the corresponding target values.

Table 19: Performance and emissions results at the starting point and operating points along the optimization path under the low load condition

	CO_2	NO_X	Soot	HC	CO	η_{comb}	CA50	η_i	Response
	g/kW-hr					%	°ATDC	%	—
Starting Point	455	1.48	0.0057	29.6	31.3	86.1	2.8	45.1	37
Stationary Point	478	5.40	0.0095	19.2	29.9	86.9	-0.8	49.0	4
Step 1	479	2.98	0.0051	20.7	27.1	87.8	0.5	46.7	13
Step 2	477	0.86	0.0039	24.5	20.0	88.7	4.3	45.9	88
Step 3	492	0.31	0.0028	27.0	16.9	89.6	7.7	43.8	178

Table 20: Emission results at the optimal point and corresponding target values under the low load condition

	CO_2	NO_X	Soot	HC	CO
	g/kW-hr				
Target	537	0.32	0.0080	17.3	11.7
Optimal Point	492	0.31	0.0028	27.0	16.7

6.1.3. **Optimization Process under the High Engine Load Condition**

Table 21 presents the factor level settings and corresponding response values of the factor screening experiments for the 10 bar IMEP condition. The design was the same as in the 4.5 bar IMEP condition. The regression coefficients and P values of the 8 factors are given in Table 22. It can be seen that the effects of Dwell, Inj1Fr, P_{rail}, T_{int} and EGR on the response were significant at this condition.

Table 21: Factor level settings and response values of the factor screening design under the high load condition

Test Order	Dwell	SOIC2	Inj1Fr	FEF	P_{rail}	T_{int}	P_{int}	EGR	Response
1	0	0	0	0	0	0	0	0	176
2	-1	1	-1	1	1	-1	1	-1	52
3	-1	-1	-1	-1	-1	-1	-1	-1	11
4	-1	-1	1	1	1	1	-1	-1	119
5	-1	1	-1	-1	1	1	-1	1	39
6	1	1	-1	-1	-1	-1	1	1	50
7	1	1	1	1	1	1	1	1	328
8	1	-1	1	-1	-1	1	-1	1	149
9	1	-1	-1	1	1	-1	-1	1	335
10	0	0	0	0	0	0	0	0	201
11	-1	-1	1	-1	1	-1	1	1	321
12	1	1	-1	1	-1	1	-1	-1	63
13	-1	-1	-1	1	-1	1	1	1	56
14	-1	1	1	-1	-1	1	1	-1	70
15	-1	1	1	1	-1	-1	-1	1	0
16	1	1	1	-1	1	-1	-1	-1	343
17	1	-1	1	1	-1	-1	1	-1	198
18	1	-1	-1	-1	1	1	1	-1	20
19	0	0	0	0	0	0	0	0	179

Table 22: Regression coefficients and P values of the factors from ANOVA of the factor screening results under the high load condition

Term	Regression Coefficient	P Value
Intercept	160.8	—
Dwell	69.6	0.003
SOIC2	12.8	0.504
Inj1Fr	58.6	0.012
FEF	33.6	0.091
P_{rail}	70.6	0.002
T_{int}	-46.4	0.018
P_{int}	-9.9	0.560
EGR	33.4	0.012

Table 23 lists the factor level settings and corresponding response values of the design to fit a first-order model for to the response. Table 24 and Table 25 show ANOVA results of the fitted first-order models with and without TWI terms, respectively. The P values for both models were smaller than 0.05, indicating that a second-order model was needed to better describe the response.

Table 23: Factor level settings and response values of the first-order model design under the high load condition

Test Order	Dwell	Inj1Fr	P_{rail}	T_{int}	EGR	Response
1	0	0	0	0	0	230
2	-1	-1	1	-1	-1	97
3	-1	-1	-1	-1	1	98
4	1	1	1	-1	-1	332
5	0	0	0	0	0	216
6	-1	-1	-1	1	-1	22
7	-1	-1	1	1	1	104
8	1	1	-1	-1	1	303
9	0	0	0	0	0	185
10	1	-1	1	-1	1	245
11	-1	1	-1	-1	-1	186
12	-1	1	1	1	-1	273
13	1	-1	1	1	-1	71
14	0	0	0	0	0	231
15	-1	1	1	-1	1	398
16	1	-1	-1	1	1	97
17	1	1	1	1	1	438
18	0	0	0	0	0	199
19	-1	1	-1	1	1	247
20	1	-1	-1	-1	-1	66
21	1	1	-1	1	-1	157
22	0	0	0	0	0	183

Table 24: ANOVA of the first-order model without TWI under the high load condition

	Degree of Freedom	Sum Square	Mean Square	F value	P Value
First Order Terms	5	213409	42682	21.3	1.5E-06
Residuals	16	32042	2003	—	—
Lack of Fit	11	29570	2688	5.4	0.037
Pure Error	5	2472	494	—	—

Table 25: ANOVA of the first-order model with TWI under the high load condition

	Degree of Freedom	Sum Square	Mean Square	F value	P Value
First Order Terms	5	213409	42682	23.8	6.9E-04
TWI	10	21268	2127	1.2	0.436
Residuals	6	10775	1796	—	—
Lack of Fit	1	8303	8303	16.8	0.009
Pure Error	5	2472	494	—	—

The factor level settings and corresponding response values of the additional axial and center points to build the CCD design is given in Table 26. Table 27 and Table 28 show the regression coefficients and P values of the factors in the second-order models for the response and the five emission terms.

Table 29 and Table 30 present the designed and actual factor level settings and corresponding response values of operating points along the optimization path. The most distinct difference between the designed and actual settings is that the intake air

temperature was higher in the actual experiments than designed values to overcome the large charge cooling and combustion inhibiting effects of hydrous ethanol and hence to maintain stable engine operation. The actual response monotonically increased along the optimization path for four steps and further advance was not feasible due to unstable combustion.

Table 26: Factor level settings and response values of the additional center and axial points of the CCD under the high load condition

Test Order	Dwell	Inj1Fr	P_{rail}	T_{int}	EGR	Response
1	-2	0	0	0	0	70
2	0	0	0	0	0	180
3	0	0	0	0	2	304
4	0	0	0	0	-2	75
5	2	0	0	0	0	291
6	0	0	2	0	0	354
7	0	0	-2	0	0	134
8	0	-2	0	0	0	32
9	0	0	0	-2	0	271
10	0	0	0	2	0	72
11	0	2	0	0	0	421

Table 27: Regression coefficients and P values of the active factors in the second-order models of the response, CO_2 and HC emissions under the high load condition

	Response		CO2		HC	
	Coeff.	P Val.	Coeff.	P Val.	Coeff.	P Val.
Intercept	203.946	4.4E-9	518.456	2.2E-16	19.031	9.8E-12
Dwell	30.257	0.002	1.552	0.172	0.323	0.455
Inj1Fr	96.395	2.5E-8	7.096	2.4E-5	-1.029	0.030
P_{rail}	50.890	2.1E-5	3.059	0.014	-0.935	0.045
T_{int}	-29.726	0.002	-2.699	0.027	-0.868	0.060
EGR	49.342	2.9E-5	2.551	0.034	-0.189	0.660
Dwell:Inj1Fr	-2.047	0.829	-1.694	0.220	-0.733	0.178
Dwell:P_{rail}	9.096	0.346	-0.266	0.843	0.074	0.888
Dwell:T_{int}	-3.137	0.741	0.394	0.769	-0.104	0.842
Dwell:EGR	11.752	0.230	0.133	0.921	0.332	0.530
Inj1Fr:P_{rail}	19.631	0.056	0.844	0.531	-0.710	0.191
Inj1Fr:T_{int}	6.596	0.491	-0.210	0.875	-0.030	0.954
Inj1Fr:EGR	9.443	0.329	0.535	0.690	-0.615	0.253
P_{rail}:T_{int}	-3.543	0.709	-0.297	0.824	-0.174	0.740
P_{rail}:EGR	6.218	0.516	1.766	0.202	0.099	0.850
T_{int}:EGR	0.089	0.993	0.760	0.572	0.110	0.833
$Dwell^2$	-6.783	0.335	-1.839	0.078	-0.270	0.483
$Inj1Fr^2$	4.807	0.490	1.339	0.185	-0.936	0.027
P_{rail}^2	9.078	0.204	0.708	0.471	-0.259	0.501
T_{int}^2	-8.891	0.213	-0.137	0.888	-0.092	0.809
EGR^2	-4.542	0.514	1.180	0.239	-0.261	0.497

Table 28: Regression coefficients and P values of the active factors in the second-order models of CO, NO_X and soot emissions under the high load condition

	CO		NO_X		Soot	
	Coeff.	P Val.	Coeff.	P Val.	Coeff.	P Val.
Intercept	7.471	3.7E-9	0.576	3.0E-7	8.1E-4	9.2E-8
Dwell	0.454	0.123	-0.143	6.4E-4	-6.0E-5	0.152
Inj1Fr	-0.109	0.698	-0.382	3.9E-8	-1.4E-4	0.004
P_{rail}	-0.466	0.114	-0.156	3.2E-4	-1.8E-4	7.5E-4
T_{int}	-0.709	0.024	0.171	1.4E-4	1.2E-4	0.010
EGR	0.561	0.063	-0.210	2.1E-5	-1.1E-4	0.019
Dwell:Inj1Fr	-0.563	0.119	0.086	0.044	2.1E-5	0.677
Dwell:P_{rail}	0.085	0.804	0.035	0.379	1.2E-5	0.811
Dwell:T_{int}	-0.055	0.872	-0.037	0.348	-3.1E-5	0.531
Dwell:EGR	0.237	0.493	0.006	0.869	-7.0E-7	0.989
Inj1Fr:P_{rail}	-0.329	0.345	0.071	0.086	4.9E-5	0.329
Inj1Fr:T_{int}	0.153	0.656	-0.094	0.029	-8.4E-5	0.107
Inj1Fr:EGR	-0.392	0.265	0.109	0.014	6.4E-5	0.211
P_{rail}:T_{int}	-0.129	0.706	-0.026	0.513	-4.5E-5	0.367
P_{rail}:EGR	0.110	0.748	0.055	0.173	4.8E-5	0.336
T_{int}:EGR	0.153	0.656	-0.056	0.172	-2.4E-5	0.627
$Dwell^2$	-0.174	0.490	0.046	0.122	7.5E-5	0.053
$Inj1Fr^2$	-0.440	0.096	0.122	8.9E-4	3.8E-5	0.299
P_{rail}^2	-0.176	0.485	-0.010	0.736	2.7E-6	0.941
T_{int}^2	-0.084	0.737	0.041	0.169	2.8E-5	0.441
EGR^2	-0.214	0.398	0.041	0.171	2.8E-5	0.435

Table 29: Designed factor level settings of the optimization path under the high load condition

Dwell	Inj1Fr	P_{rail}	T_{int}	EGR	Predicted Response
2.11	-2.29	-3.01	-2.99	1.49	122
2.57	-0.36	-0.89	-3.32	2.17	338
2.81	0.60	0.18	-3.48	2.51	607
3.04	1.56	1.24	-3.64	2.84	983

Table 30: Actual factor level settings of the optimization path under the high load condition

Dwell	Inj1Fr	P_{rail}	T_{int}	EGR	Actual Response
2.11	-2.18	-3.01	-2.33	0.95	135
2.57	-0.32	-0.89	-0.11	1.49	311
2.81	0.66	0.18	2.30	1.64	476
3.04	1.68	1.24	5.58	2.07	565

The performance and emissions results of the operating points along the optimization path and at the starting point are shown in Table 31. Table 32 compares the emissions results with the corresponding target values.

Table 31: Performance and emissions of operating points along the canonical path under the high load condition

	CO_2	NO_X	Soot	HC	CO	η_{comb}	CA50	η_i	Response
	g/kW-hr					%	°ATDC	%	—
Starting Point	519	0.56	0.0008	19.0	7.5	89.5	11.8	46.7	207
Stationary Point	516	0.71	0.0021	22.4	11.1	87.7	13.4	47.2	135
Step 1	528	0.16	0.0008	20.0	11.2	88.1	16.1	45.5	311
Step 2	545	0.13	0.0007	13.8	7.5	93.1	16.5	43.7	476
Step 3	546	0.16	0.0010	9.5	4.6	92.3	17.2	45.6	565

Table 32: Emission results at the optimal point and corresponding target values under the high load condition

	CO_2	NO_X	Soot	HC	CO
	g/kW-hr				
Target	537	0.32	0.0080	17.3	11.7
Optimal Point	546	0.16	0.0010	9.5	4.6

6.2. **Results and Discussion**

6.2.1. **Low Engine Load Condition**

From the ANOVA of the factor screening experiments results, SOIC2, Inj1Fr, P_{rail} and P_{int} were identified as the active factors for the 4.5 bar IMEP condition. Figure 14 shows the response values and CO_2 emissions at the starting point and along the

optimization path with respect to the five active factors. It can be seen that the response function monotonically increased along the optimization path. The response value at the stationary point was lower than at the starting point, but it was remarkably higher at the optimal point. CO_2 emissions were mostly constant at the first two steps but slightly increased at the last step. It was hypothesized that this increase was caused by decreased indicated thermal efficiency.

Figure 14: Overall response and CO_2 emissions values at the starting point (hollow square markers) and points along the optimization path (filled circle markers) versus active factors under the low load condition. The horizontal dotted lines denote target emissions values.

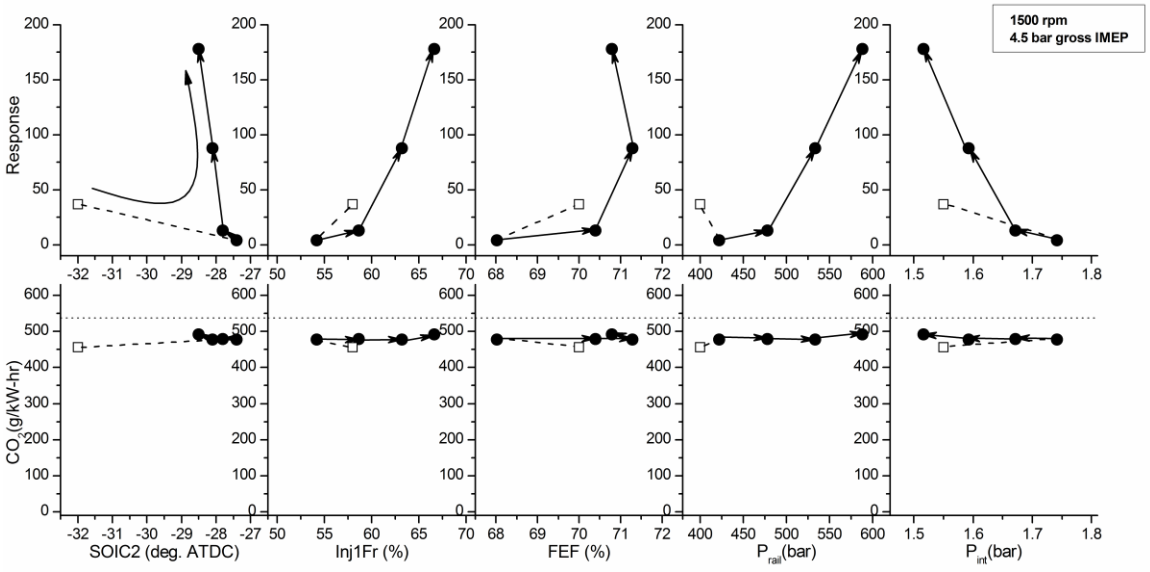

Figure 15 shows the HC and CO emissions at the starting point and along the optimization path versus to the five active factors for the 4.5 bar IMEP condition. The HC emissions monotonically increased along the optimization path, while the CO emissions had an opposite trend. The increase of HC emissions at the first two steps along the optimization path was likely caused by increased FEF, since the ANOVA results in Table 15 show that FEF had the most significant effect on HC emissions among

the five active factors. Figure 16 shows the trend of unburned ethanol compared to the sum of the other HC components emissions measured by the FTIR as a function of FEF. It can be seen that the variation of unburned ethanol emissions closely resembled the trend of HC in Figure 15, and the other HC emissions were mostly constant. These results suggest that unburned ethanol represented the biggest portion of HC emissions and it was more sensitive to variation of operating parameters than other HC species. A greater fraction of ethanol in total fuel input was likely to have caused higher HC emissions since more ethanol fuel stayed in the squish and crevice volumes and was left unburned. At the last step along the optimization path, although FEF was decreased to maintain stable combustion, the HC emissions were still increased. This was likely caused by the fact that the effect of more retarded combustion phasing outweighing the effect of reduced ethanol fuel in squish and crevice volumes. The CO emissions were monotonically decreased along the optimization path. This was possibly due to the decreased intake air pressure that resulted in higher equivalence ratio and thus higher bulk in-cylinder temperature. The ANOVA results in Table 16 show that the effect of P_{int} on CO emissions was the most significant among the five active factors. The HC and CO emissions at the starting point were the highest among all the points shown in Figure 15. In-cylinder pressure analysis revealed that the peak RoHR was lower at the starting point, indicating that the lower in-cylinder temperature might have been the reason for the higher HC and CO emissions.

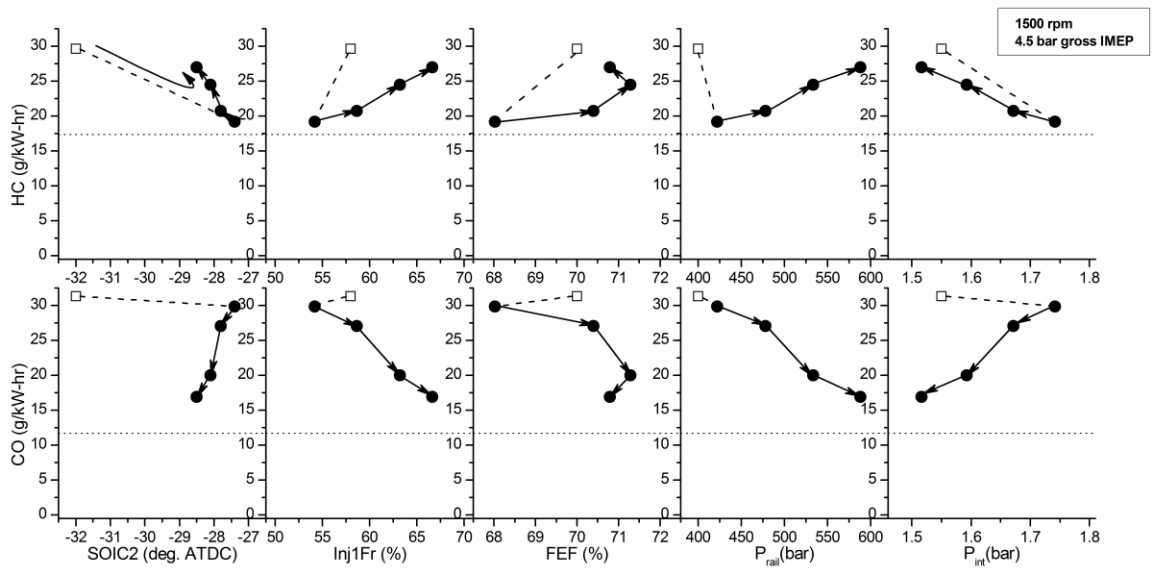

Figure 15: HC and CO emissions values at the starting point (hollow square markers) and points along the optimization path (filled circle markers) versus active factors under the low load condition. The horizontal dotted lines denote target emissions values.

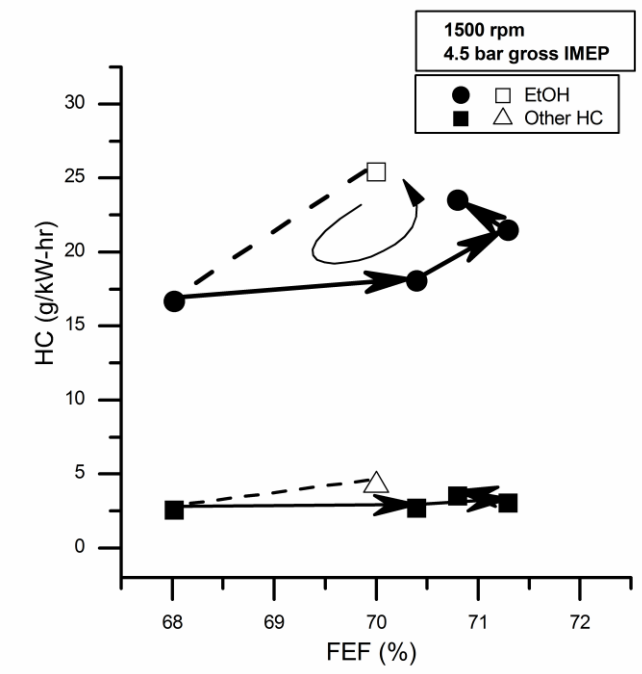

Figure 16: Ethanol and other HC emissions values at the starting point (hollow markers) and points along the optimization path (filled markers) versus FEF under the low load condition.

Figure 17 shows NO_X and soot emissions at the starting point and along the optimization path with respect to the five active factors for the 4.5 bar IMEP condition. NO_X and soot emissions were simultaneously reduced along the optimization path. The ANOVA results in Table 16 show that all the five active factors significantly affected NO_X emissions. With more advanced diesel injection timing, higher fraction of diesel fuel in the first injection event and higher diesel injection pressure, the mixing process of fuel and air was improved, leading to more premixed combustion and lower NO_X emissions. Increasing the fraction of ethanol in the fuel input helped to decrease NO_X emissions in two ways. The first was that with lower fraction of directly injected diesel fuel, the fuel-air charge was more premixed and resulted in fewer stoichiometric zones. The second was that the greater charge-cooling and combustion-inhibiting effects associated with vaporization of a hydrous ethanol resulted in lower in-cylinder temperature and hence lower NO_X emissions. The ANOVA results indicate that the reduction in intake air pressure also had a statistically significant effect on increasing NO_X emissions. The equivalence ratio was increased with reduced intake air pressure, leading to higher peak RoHR that increased the formation rate of NO_X emissions. Therefore, if the intake air pressure had been increased along the optimization path, even lower NO_X emissions might have been generated. The reduction in intake air pressure along the optimization path led to increased NO_X and decreased CO emissions, and the overall effect was higher response values.

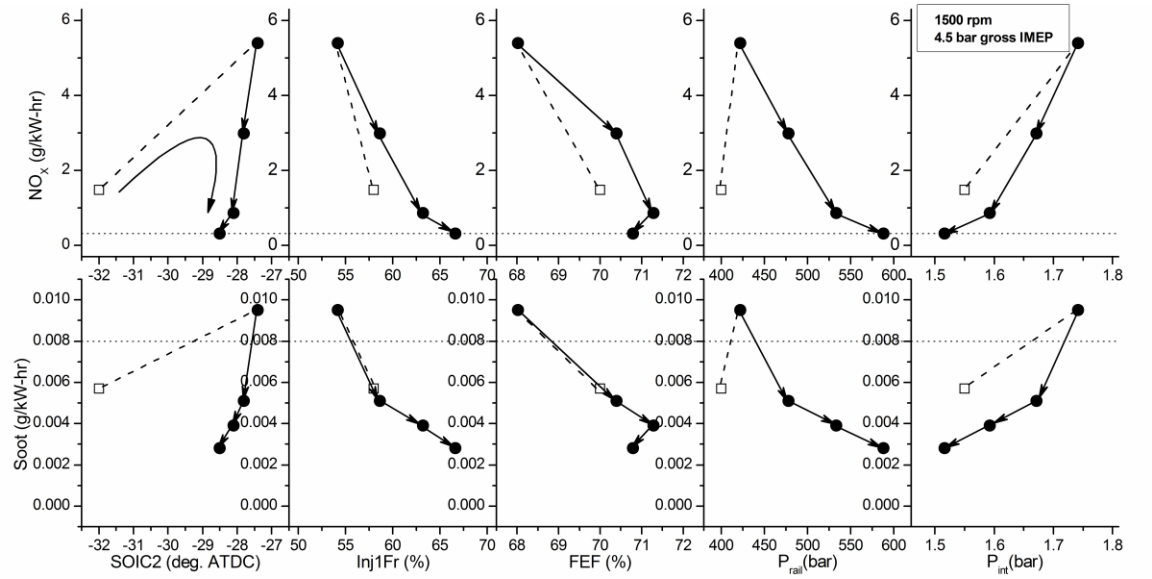

Figure 17: NO_X and soot emissions values at the starting point (hollow square markers) and points along the optimization path (filled circle markers) versus active factors under the low load condition. The horizontal dotted lines denote target emissions values.

The ANOVA results in Table 16 show that P_{rail} and P_{int} were the two factors that significantly impacted soot emissions. Higher diesel fuel rail pressure is well known to reduce soot by improving the mixing of diesel fuel and air. The reason for lower soot emissions at lower intake air pressure might be that the soot oxidation rate was increased to a greater extent due to higher in-cylinder temperature than the increase of the soot formation rate due to higher equivalence ratio. A correlation between NO_X and soot emissions and combustion phasing can also be observed from Figure 17 and Figure 18. With more retarded CA50, the NO_X and soot emissions were lower. The CA50 at the starting point was between those at the beginning and end of the optimization path, and the NO_X and soot emissions at the starting points were also between the values at those two points.

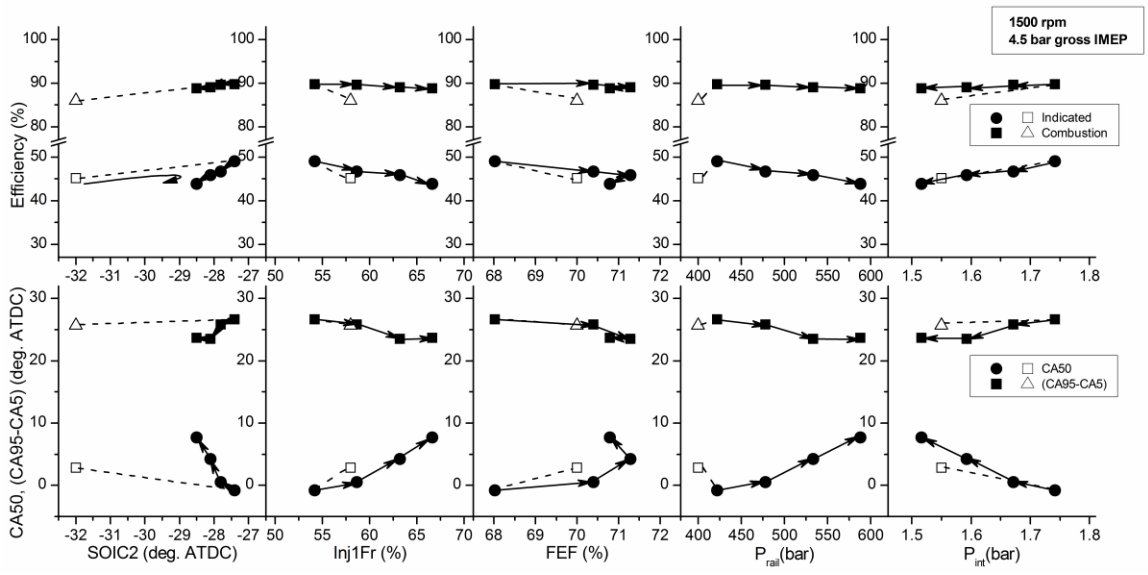

Figure 18: Indicated thermal efficiency, CA50 and combustion duration values at the starting point (hollow square markers) and points along the optimization path (filled circle markers) versus active factors under the low load condition.

Figure 18 shows the indicated thermal efficiency, CA50 and combustion duration at the starting point and along the optimization path with respect to the five active factors for the 4.5 bar IMEP condition. In this study, combustion duration is defined by the difference in CAD between CA5 and CA95. It can be seen that the indicated thermal efficiency was decreased along the optimization path. A previous study by the authors [70] showed that the indicated thermal efficiency was reduced when combustion phasing was more delayed from TDC in RCCI combustion due to lower effective expansion ratio. Along the optimization path, the CA50 was delayed, resulting in a reduction in indicated thermal efficiency. The combustion duration was shortened along the optimization path, indicating more premixed combustion and this possibly explains the increase of HC in Figure 3.

Figure 19 presents the in-cylinder pressure and RoHR curves of the starting points and the points along the optimization paths for the low and high load conditions. For the

low load case, it can be seen that the peak pressure and RoPR were relatively high at the starting point and the stationary point. The RoHR curves exhibited a two-stage heat release event, representing the combustion of the high reactivity diesel fuel in piston bowl followed by the premixed combustion of the remaining well-mixed fuel-air charge. As the optimization process proceeded, the fraction of diesel fuel input was reduced and the mixing of diesel fuel and air was improved due to aforementioned variation of the diesel injection parameters. As a result, the first peak of heat release event was largely diminished and the combustion phasing was delayed with a higher peak of the premixed heat release event, yielding a Gaussian-shaped RoHR curve typically observed in HCCI or RCCI operation [28,65].

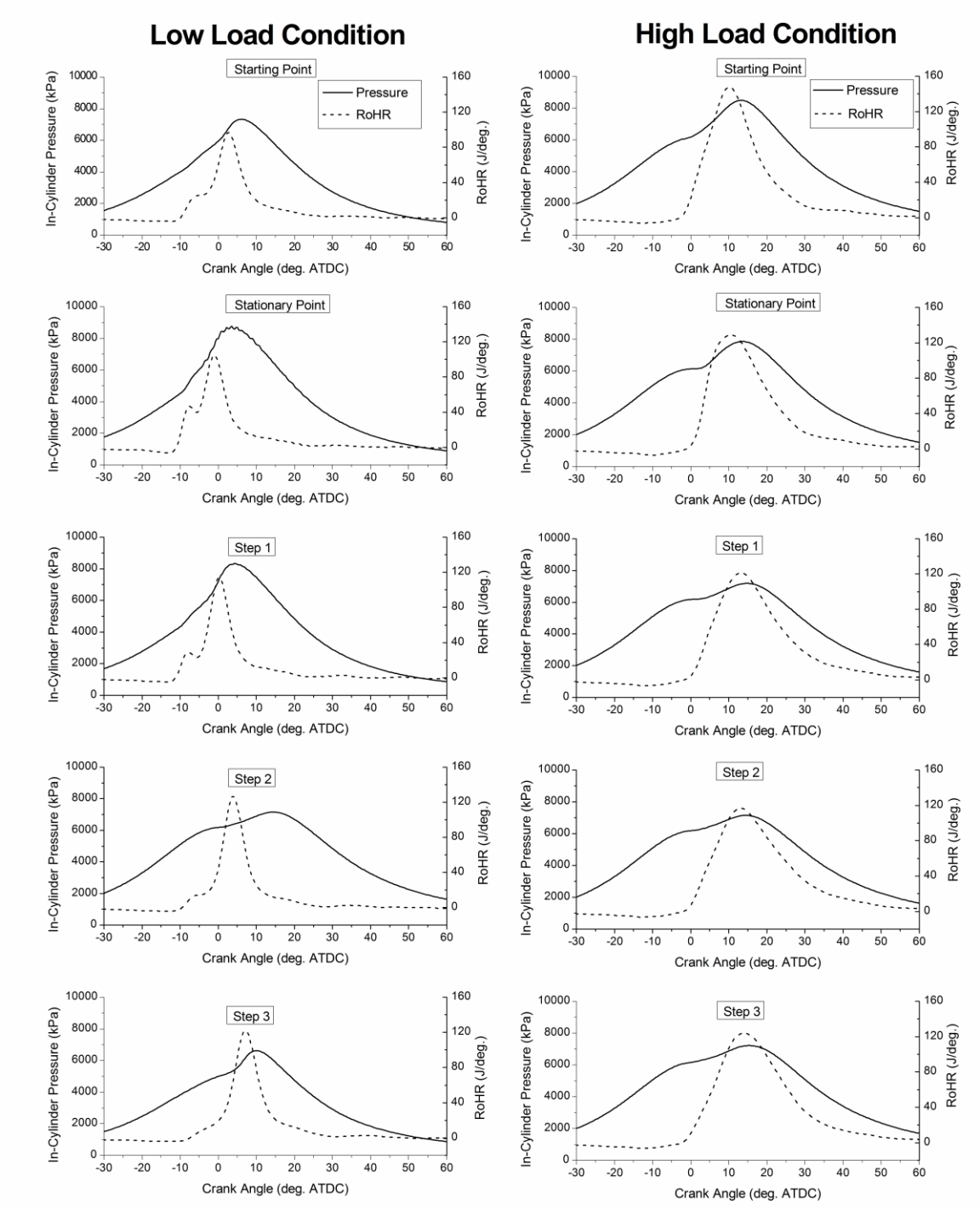

Figure 19: In-cylinder pressure and RoHR traces at the starting points and points along the optimization paths under the low and high load conditions.

6.2.2. **High Engine Load Condition**

The ANOVA results of the factor screening experiments show that Dwell, Inj1Fr, P_{rail}, T_{int} and EGR were the active factors for the 10 bar gross IMEP condition. Figure 20 shows the response values and CO_2 emissions at the starting point and along the optimization path with respect to these factors. Similar to the 4.5 bar gross IMEP condition, the response increased monotonically along the optimization path. The response magnitude was greater than the 4.5 bar gross IMEP condition, indicating better overall emissions response of the RCCI operation at high load conditions. The designed optimization path suggested that the intake air temperature should have been decreased to obtain higher response value. However, if the designed path had been followed, the combustion phasing would have been excessively retarded and stable combustion would not have been possible. Therefore, the intake air temperature was increased along the optimization path to maintain stable combustion in actual experiments. The actual EGR rates were lower than the designed values, and this was also to maintain stable RCCI operation. CO_2 emissions were higher at the optimal point than at the starting point. There are two possible reasons for this increase. Firstly, the indicated thermal efficiency was slightly lower at the optimal point as shown in Figure 23, indicating higher indicated specific fuel consumption and hence total carbon input. Secondly, HC and CO emissions were lower at the optimal point as shown in Figure 21, indicating bigger fraction of CO_2 in the emissions that contains carbon.

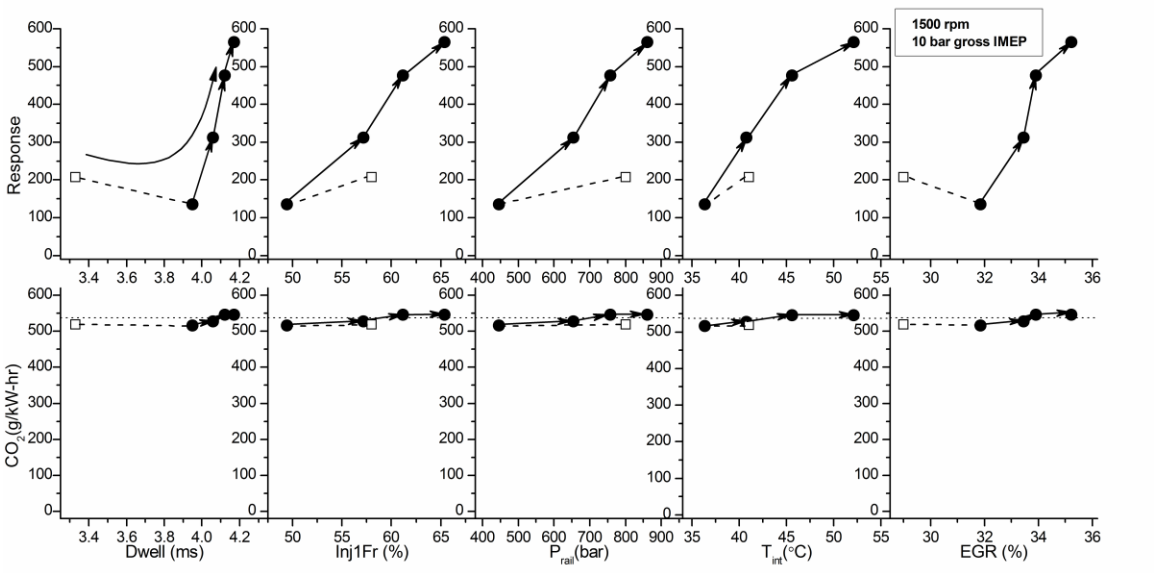

Figure 20: Overall response and CO_2 emissions values at the starting point (hollow square markers) and points along the optimization path (filled circle markers) versus active factors under the high load condition. The horizontal dotted lines denote target emissions values.

Figure 21 shows the HC and CO emissions at the starting point and along the optimization path with respect to the five active factors for the 10 bar gross IMEP condition. The HC emissions monotonically decreased along the optimization path. The ANOVA results in Table 27 show that Inj1Fr and P_{rail} were the two factors that most significantly affected HC emissions. This was possibly due to the fact that more diesel fuel reached the squish area and the overall fuel reactivity was enhanced with increased diesel fuel fraction in the first injection event and diesel rail pressure. CO emissions were nearly constant at the first step, and were decreased at the following two steps along the optimization path. ANOVA results show that T_{int} had the most significant effect on the CO emissions among the five active factors. With increased intake air temperature, CO oxidation rate might have been enhanced due to the higher in-cylinder temperature. It is worth noting that the HC and CO emissions at this condition were remarkably lower than

at the lower load condition, and this might have been due to the higher overall equivalence ratio promoting higher oxidation rates of the unburned species.

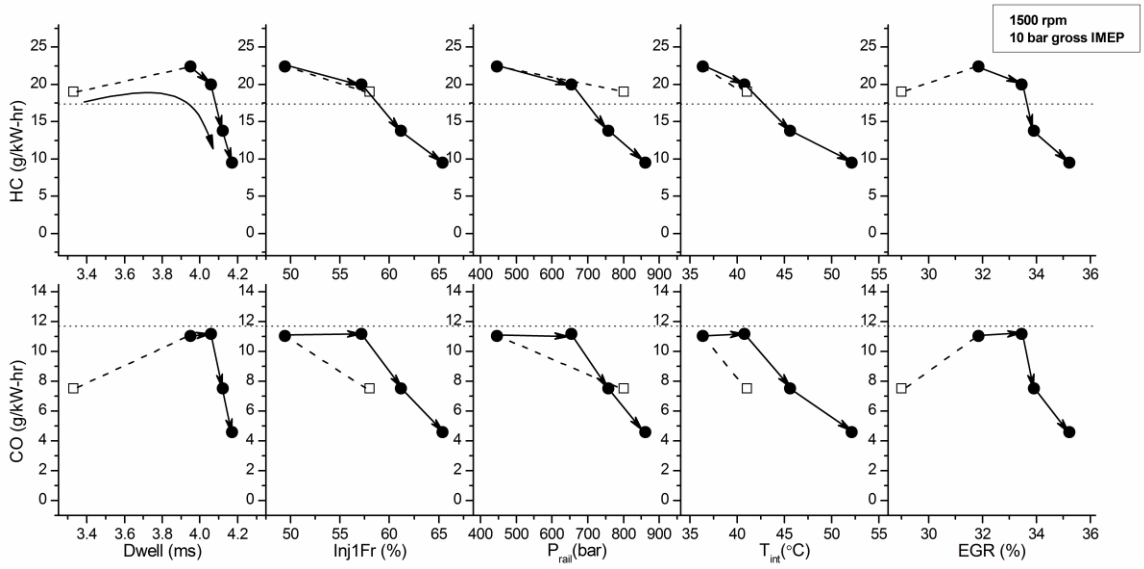

Figure 21: HC and CO emissions values at the starting point (hollow square markers) and points along the optimization path (filled circle markers) versus active factors under the high load condition. The horizontal dotted lines denote target emissions values.

Figure 22 shows the NO_X and soot emissions at the starting point and along the optimization path with respect to the five active factors for the 10 bar gross IMEP condition. The NO_X and soot emissions were simultaneously reduced along the optimization path except at the last step, where an increased occurred. The ANOVA results indicate that all the five active factors significantly impacted NO_X soot emissions. The increase of Dwell, Inj1Fr and P_{rail} improved the mixing process of diesel fuel and air, and thus led to more premixed combustion that produces less NO_X. The increase of EGR rate contributed to lower NO_X emissions by lowering the in-cylinder temperature. Increased intake air temperature along the optimization path should have caused higher NO_X emissions according to the ANOVA results. However, NO_X emissions were

decreased along the optimization path, indicating that intake air temperature was outweighed by the other factors. The soot emissions closely resembled the trend of NO_X emissions, and were shown to be significantly affected by Inj1Fr, P_{rail}, T_{int} and EGR. Although NO_X and soot emissions were increased at the last step, the reduction in HC and CO emissions outweighed this increase and contributed to a higher overall response value. It can be noted that NO_X and emissions at this load were considerably lower than those at the lower load condition, and were well below the target values.

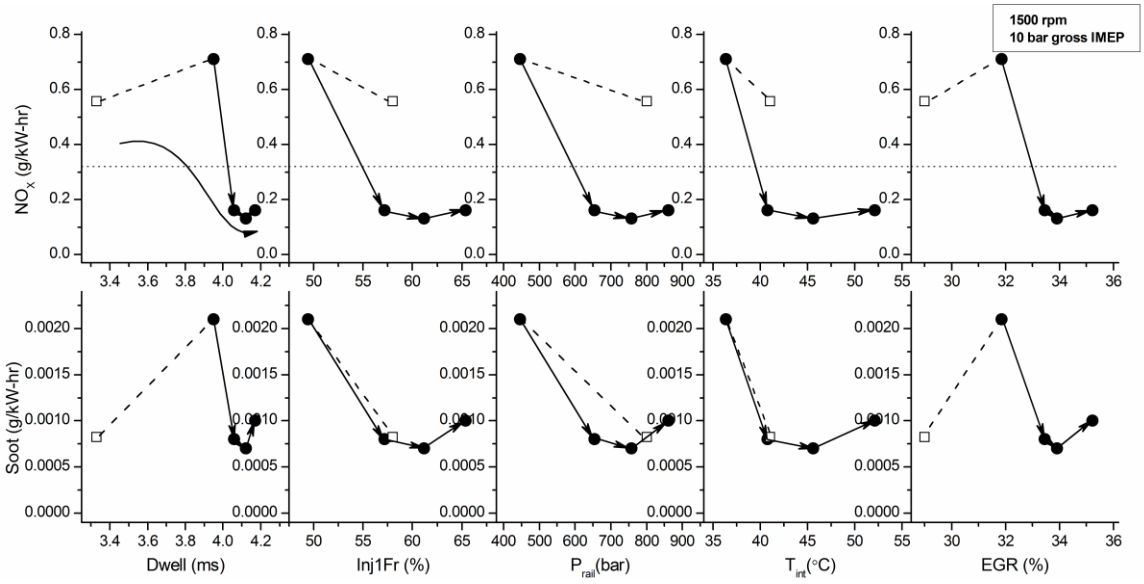

Figure 22: NO_X and soot emissions values at the starting point (hollow square markers) and points along the optimization path (filled circle markers) versus active factors under the high load condition. The horizontal dotted lines denote target emissions values.

Figure 23 shows the indicated thermal efficiency, CA50 and combustion duration at the starting point and along the optimization path with respect to the five active factors for the 10 bar gross IMEP condition. It can be seen that the indicated thermal efficiency was decreased along the optimization path except at the last step, where it was increased. The reduction in the indicated thermal efficiency at the first two steps might have been

due to the delayed combustion phasing, similar to the low load case. The reason for the increase at the last step might have been that the effect of delayed combustion phasing was outweighed by the effect of increased combustion efficiency, as indicated by reduced HC and CO emissions shown in Figure 21.

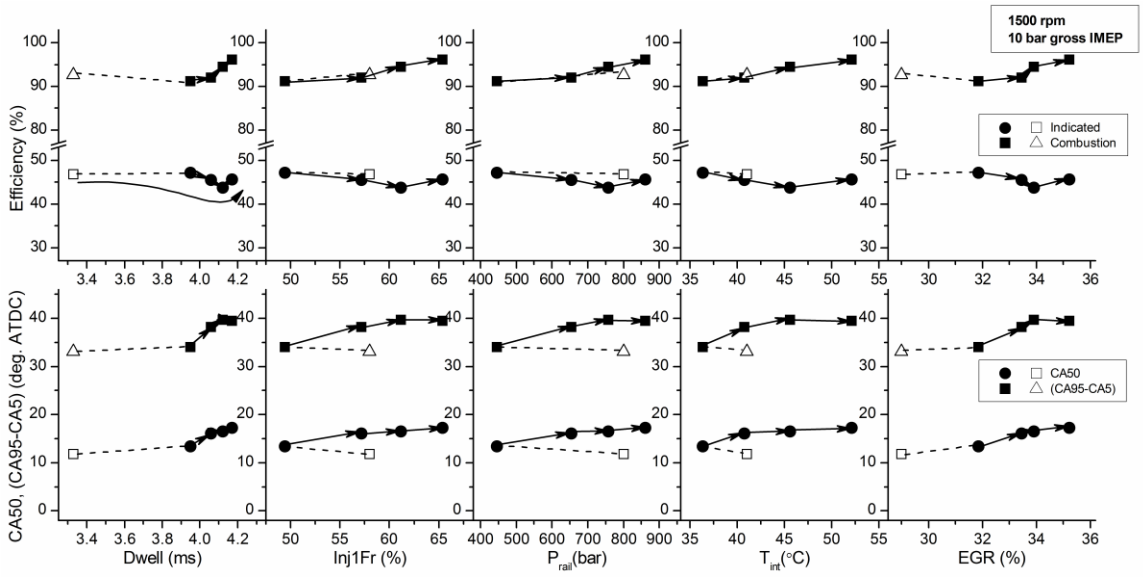

Figure 23: Indicated thermal efficiency, CA50 and combustion duration values at the starting point (hollow square markers) and points along the optimization path (filled circle markers) versus active factors under the high load condition.

Figure 19 gives a comparison of the in-cylinder pressure and RoHR characteristics at the starting points and the points along the optimization paths between the high and low load conditions. One significant difference was the absence of the first peak of diesel fuel combustion at the high load condition. All the operating points exhibited a single-peak RoHR curve with a remarkably longer combustion duration compared to the low load case. Despite the higher fuel input quantity and overall equivalence ratio at the high load condition, the peak RoPR and RoHR were not significantly higher than at the low load condition. This might have been caused by the large charge cooling and combustion inhibiting effects of hydrous ethanol and the use of high EGR rate.

6.3. **Conclusions**

In this study, an operating parameter optimization for RCCI combustion fueled with diesel and hydrous ethanol was conducted using a RSM procedure at two steady state engine load conditions. The overall engine performance and emissions characteristics were significantly improved through the optimization process. At the low load condition, the NO_X and soot emissions were reduced by 79% and 50% compared to the starting point, respectively. At the high load condition, the NO_X and soot emissions were reduced by 72% and 27% compared to the starting point, respectively. The RSM procedure used fractional factorial designs and CCD to identify factors with significant effects, build regression models and generate optimization paths, with less than 60 test points at each load. In contrast, a full two-level factorial design for eight factors alone needs 256 test points.

Complex interactions between active factors in RCCI using hydrous ethanol were also identified in this study. Different operating parameters were shown to have statistically significant impact on the RCCI combustion at different load conditions. For low load RCCI, the fumigant energy fraction significantly impacted HC emissions mainly from unburned ethanol, and the intake air pressure had the most significant effect on CO emissions. At higher load, HC emissions were significantly affected by the fraction of the first diesel injection and diesel rail pressure, and the intake air temperature had the most significant impact on the CO emissions. NO_X emissions were sensitive to all the active factors at both low and high load conditions. Indicated thermal efficiency was sacrificed with the improvement of NO_X and soot emissions due to retarded combustion phasing after the optimization process.

It can be concluded from this study that RSM is an effective tool for elucidating significant factors for reducing emissions, considering complex interactions between numerous parameters in RCCI operation using a reduced number of experimental data points. However, RSM is not physics-based and some operating parameters along the optimization path had to be altered to keep RCCI operation within feasible physical operability regions.

Chapter 7 Characteristics of the Particulate Matter Emissions from Reactivity-Controlled Compression Ignition[4]

The purpose of the work described in this section was to experimentally investigate the dilution sensitivity of PM emissions from RCCI using 150 proof hydrous ethanol and gasoline as the low reactivity fuels by evaluating the effect of the primary dilution ratio and dilution temperature on PM concentration and size distribution.

7.1. **Experimental Procedure**

Table 33 shows the engine operating parameters for the three different engine modes used in the experiments. D-E RCCI mode represents the RCCI operation using hydrous ethanol as the low reactivity fuel, and D-G RCCI represents the operation mode using gasoline as the low reactivity fuel. ULSD was used as the high reactivity fuel for the RCCI modes. For the CDC mode, only ULSD was injected. For the two RCCI modes, the first start of injection command (SOIC1) for diesel fuel was fixed at -58^{o} ATDC with the fraction of total diesel fuel in the first injection fixed at 67%. The second start of injection command (SOIC2) was fixed at -28^{o} ATDC. The fumigant energy fraction (FEF) for the RCCI modes was kept at ~70%. Intake air heating was employed for the RCCI modes, with significantly higher intake air temperature required for the D-E RCCI, due to the large charge cooling and combustion inhibition effects of hydrous ethanol, as discussed in previous studies [45,65].

[4] This chapter is based on paper "Dilution Sensitivity of Particulate Matter Emissions from Reactivity Controlled Compression Ignition Combustion" (Fang et al., 2015), ***Proceedings of 2015 Fall Technical Conference ASME International Combustion Engine Division,*** ICEF2015-1092.

Table 33: Parameters for the investigated engine operating conditions

Mode	D-E RCCI	D-G RCCI	CDC
Fumigant	Hydrous Ethanol	Gasoline	—
Engine Speed (rpm)	1500	1500	1500
IMEP (bar)	4.9	5.3	4.8
EGR (%)	0	0	0
Fumigant Energy Fraction (%)	68	70	0
Intake Temperature (˚C)	111	35	28
Intake Pressure (bar)	1.5	1.3	1.4
Diesel Injection Pressure (bar)	590	590	590
SOIC 1 (˚ATDC)	-58	-58	—
SOIC 2 (˚ATDC)	-28	-28	-9
Fraction of Total Diesel Fuel in 1st Injection (%)	67	67	—
Fuel/Air Equivalence Ratio	0.34	0.39	0.32

Mass concentrations of soot emissions were measured by an AVL Micro-Soot photo-acoustic analyzer. A two-stage micro-dilution system similar to the one developed by Abdul-Khalek [52] was used to simulate the process of exhaust gas mixing with ambient air and cooling. To investigate the effect of dilution conditions on the PM emissions from different combustion modes, two levels of primary dilution temperature and primary

dilution ratio settings were selected. The primary dilution temperature was measured downstream of the primary ejector pump where the exhaust sample and dilution air were well mixed. The low dilution temperature (LDT) and high dilution temperature (HDT) conditions represent the primary dilution temperatures of 25 ˚C and 47 ˚C, respectively. Two orifices of different sizes were used in the primary ejector pump to set the primary dilution ratios. The low dilution ratio (LDR) and high dilution ratio (HDR) conditions represent the primary dilution ratios of 6:1 and 18:1, respectively. The outer wall of the dilution tunnel was water jacketed and held at a constant temperature equal to the primary dilution temperature for each condition. The secondary dilution temperature was kept at 25˚C and dilution ratio was fixed at 14:1 for all the conditions. Table 34 gives the settings of the dilution system at the four different dilution conditions. A TSI Scanning Mobility Particle Sizer (SMPS) was used to measure the PM number concentrations and size distributions downstream of the secondary dilution stage. A sample of diluted exhaust was sent through a catalytic stripper (CS) similar to the device developed by Abdul-Khalek et al. [66] to remove sulfur compounds and soluble organic materials, and a second SMPS was used to acquire the PM measurement downstream of the CS. It has been demonstrated that an operating temperature of 300 ℃ leads to essentially complete removal of volatile sulfate and hydrocarbon particles with the CS [66].

Table 34: Dilution condition settings for the PM sampling system

Condition	LDT/LDR	LDT/HDR	HDT/LDR	HDT/HDR
Primary Dilution Temperature (˚C)	25	25	47	47
Primary Dilution Ratio	6:1	18:1	6:1	18:1
Secondary Dilution Temperature (˚C)	25	25	25	25
Secondary Dilution Ratio	14:1	14:1	14:1	14:1
Tunnel Wall Temperature(˚C)	25	25	47	47

7.2. **Results and Discussion**

In this section, the experimental results are presented and discussed regarding the effect of the primary dilution ratio and temperature on the PM emissions from the three combustion modes. Table 35 shows the gross indicated thermal efficiency and indicated specific CO, HC, NO_X and soot emissions for the three operation modes. It can be seen that the two RCCI modes had roughly the same indicated thermal efficiency, and the CDC mode was the most efficient. The NO_X emissions from the RCCI modes were significantly lower, while the CO and HC emission were remarkably higher compared to the CDC, as has been shown in previous studies [26–30]. The soot emissions sampled with the AVL Micro-Soot analyzer were near the lower detectable measurement limits for all the three operation modes.

Table 35: Indicated thermal efficiency and indicated specific emissions

Mode	$\eta_{i,g}$ (%)	NO_X (g/kW-hr)	CO (g/kW-hr)	HC (g/kW-hr)	Soot (g/kW-hr)
D-E RCCI	45.9	0.26	19.4	18.4	0.003
D-G RCCI	46.2	0.22	15.5	9.9	0.003
CDC	48.0	4.46	7.4	0.1	0.002

Figure 24 and Figure 25 show the dilution ratio corrected total PM number and volume concentrations for the four combinations of dilution ratio and temperature settings, respectively. The number above each column denotes the percentage of the post-CS particle number or volume concentration in the pre-CS total number or volume concentration. For each combustion mode, the LDT&LDR condition gave the highest total particle number and volume concentrations. An increase in either dilution ratio or temperature led to decreased total number and volume concentrations. Particle number and volume concentrations were the minimum under the HDT&HDR condition. PM emissions were more sensitive to change in dilution ratio at lower dilution temperature, and were more sensitive to the change in dilution temperature at lower dilution ratio.

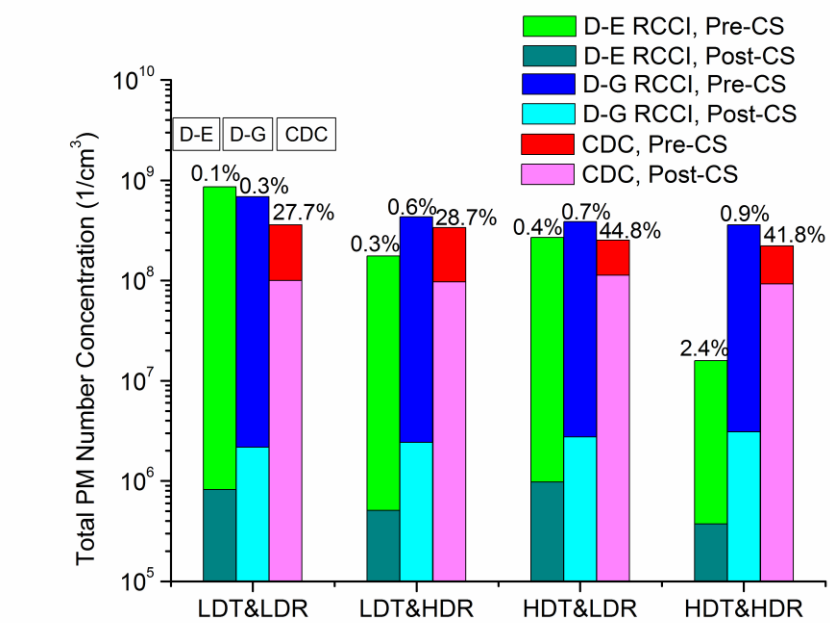

Figure 24: Total PM number concentrations indicating percent solid carbon as determined by pre- and post-CS measurements

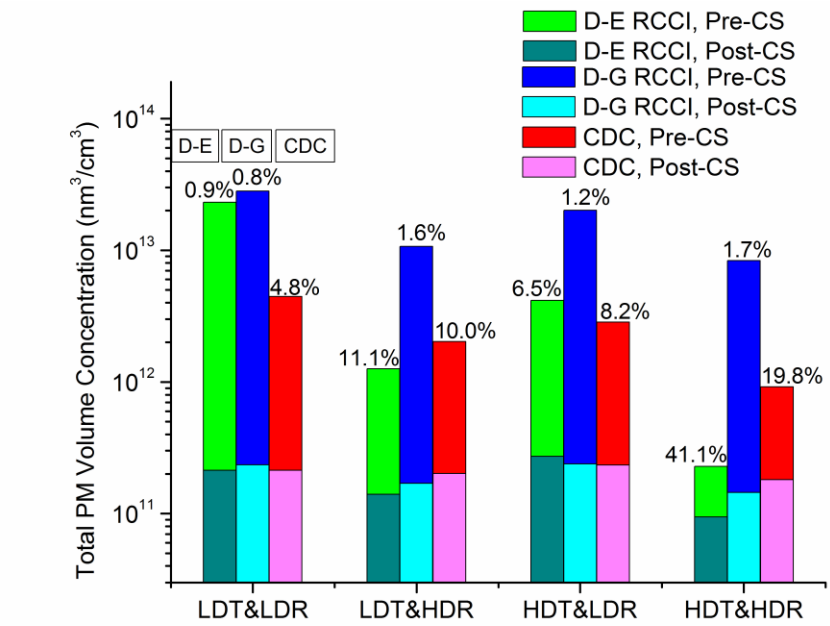

Figure 25: Total PM volume concentrations indicating percent solid carbon as determined by pre- and post-CS measurements

Figure 26, 27, 28 and 29 present PM size distribution curves obtained with the SMPS under the four combinations of dilution ratio and temperature settings. Error bars represent the standard deviation of particle number concentrations calculated from 3 to 5 SMPS samples. Variation of PM concentrations was mostly seen in the nucleation mode, while the accumulation mode particles were relatively consistent under different dilution conditions. Abdul-Khalek et al. [52] presented similar observations in a study on the dilution sensitivity of PM emissions from CDC. It is believed that the reduction in the nucleation mode particles with increased dilution ratio or temperature is due to the decreased vapor pressure in the exhaust samples that slows down the nucleation and growth rates of ultrafine particles. The shape of the post-CS PM size distribution was not significantly influenced by the change of dilution conditions, but the number or volume fraction of solid particles in the total PM concentration was increased as the dilution temperature or dilution ratio was increased.

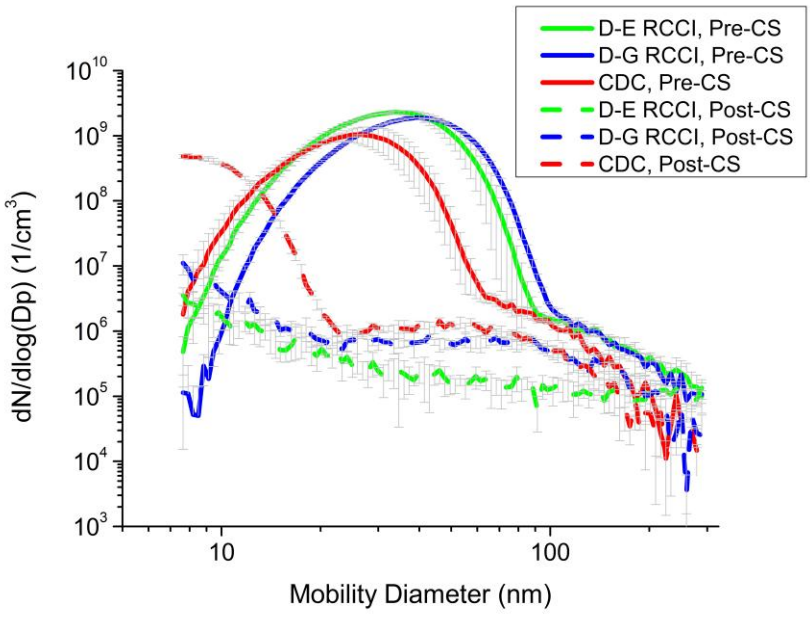

Figure 26: PM size distribution curves under the LDT&LDR condition

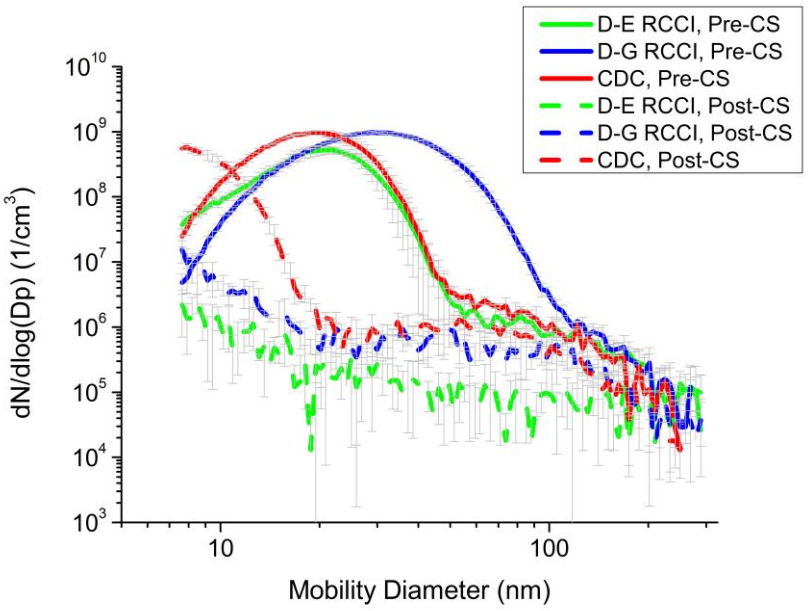

Figure 27: PM size distribution curves under the LDT&HDR condition

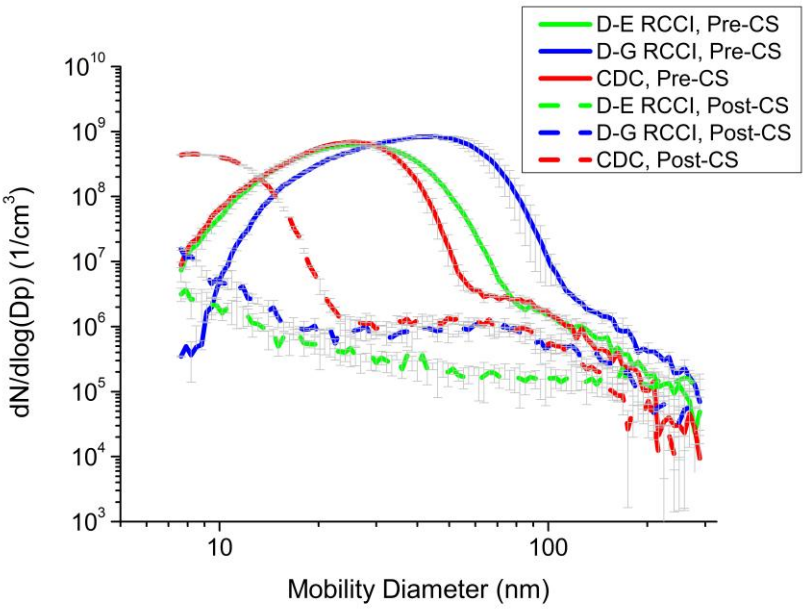

Figure 28: PM size distribution curves under the HDT&LDR condition

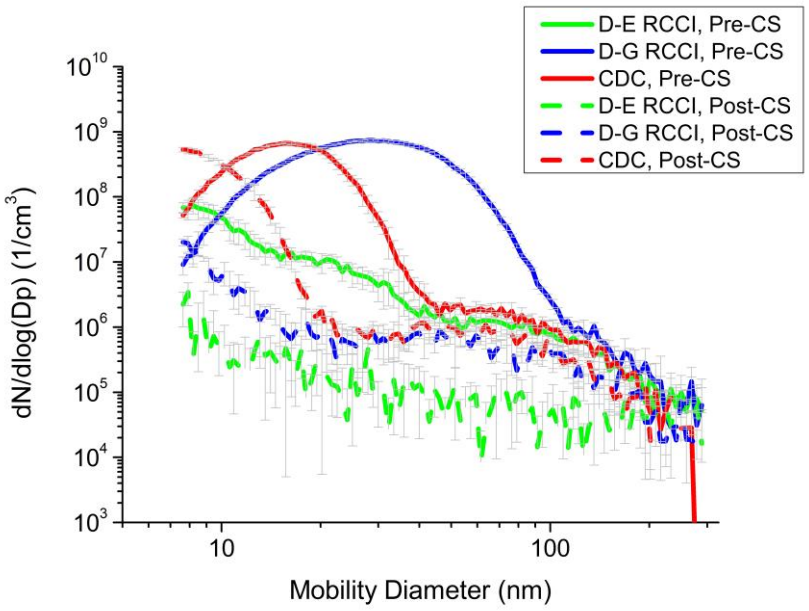

Figure 29: PM size distribution curves under the HDT&HDR condition

Figure 26, 27, 28 and 29 also show that the characteristics of PM emissions from different combustion mode were distinct. The CDC mode had the lowest particle number concentrations under all different dilution conditions. However, the post-CS PM size distribution showed a considerably higher peak of the nucleation mode particles than the RCCI combustion modes. The magnitude of this peak was comparable with that in the pre-CS PM size distribution, but with smaller sizes. The composition of these particles could not be determined from this work but they might have consisted of ash from metallic lubricating oil additives and / or tiny soot particles.

PM emissions from the D-G RCCI mode generally had a higher number of particles with mobility diameters ranging from ~50 to ~100 nm than the other two combustion modes, yielding a smoother transition from the nucleation mode to the accumulation mode. With increased dilution ratio or temperature, the magnitude of the nucleation mode particle concentrations was reduced, but the mobility diameter at the peak was not

significantly changed. Except under the LDT&LDR condition, the total particle number and volume concentrations were the highest among the three combustion modes. The post-CS PM had a remarkably lower number of nucleation particles compared to the CDC mode. The concentration and size of accumulation mode solid particles were comparable with those in the CDC mode.

The PM emissions from the D-E RCCI mode were the most sensitive to changes in dilution ratio or temperature among the three combustion modes. Under the LDT&LDR condition, total particle number concentrations were higher than in the D-G RCCI and CDC modes. Since there were fewer particles with mobility diameter ranging from ~50 to ~100 nm, the total particle volume concentrations were lower than in the D-G RCCI mode. With either increasing dilution ratio or dilution temperature, the nucleation mode peak was reduced and shifted to smaller mobility diameters, leading to significant reduction in total particle number and volume concentrations respectively. Under the HDT&HDR condition, the nucleation mode peak was remarkably diminished, yielding a size distribution curve that gradually descended from the nucleation to the accumulation mode. As a result, the total particle number and volume concentrations were considerably lower than the other two combustion modes. The post-CS PM had lower concentrations of particles over the entire sampling size range compared to the other two combustion modes, and the particles with mobility diameters ranging from ~50 to ~100 nm were largely eliminated for the D-E RCCI mode. The volume percentage of solid particles in the D-E RCCI mode was remarkably increased with the increase of dilution temperature and ratio, from less than 1% under the LDT&LDR condition to over 40% at the HDT&HDR condition. The volume percentage of solid particles in the D-G RCCI mode

was more consistent under different dilution conditions, below 2% for all the four cases. This evidence indicates that the organic materials in the PM resulting from using the hydrous ethanol as the low reactivity fuel were more sensitive to change of dilution condition than those resulting from using gasoline.

Figure 30 shows the in-cylinder pressure and RoHR traces for the three different combustion modes. It can be seen that the two RCCI modes had very similar curves of the in-cylinder pressure and RoHR, except that a low temperature heat release (LTHR) event was observed for the D-G RCCI mode, while the D-E RCCI had a single spike of heat release event. The early-stage LTHR was commonly seen in premixed gasoline fueled LTC strategies [79,80]. The absence of LTHR event in the diesel-hydrous ethanol RCCI mode might have been due to the combustion inhibition effects of hydrous ethanol as discussed in previous studies [65,81]. The injection parameters of diesel fuel delivery were kept the same for the two RCCI modes to minimize the effect of the high reactivity fuel on the PM emissions. Franklin suggested that PM emissions from HCCI engines mostly originate from nucleation of the lighter distillates from the engine lubricating oil and are highly correlated with peak RoHR [54]. Although the heat release curves for the two RCCI cases were well matched, the intake air temperature in the D-E RCCI mode was much higher than that in the D-G RCCI mode and this could lead to different lubricating oil consumption rates. Hence, the differences in the low reactivity fuel properties and lubricating oil consumption rates could contribute to the different PM characteristics seen in the two RCCI modes. Further investigation is needed to characterize the composition of the PM emissions from RCCI combustion and to differentiate the contributions from fuels and lubricating oil.

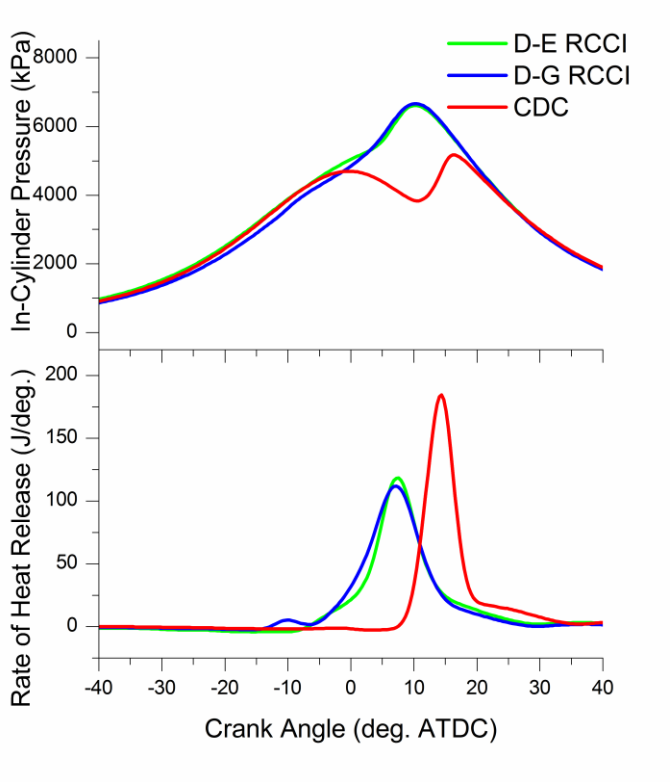

Figure 30: In-cylinder pressure and RoHR traces

7.3. **Conclusions**

In this work, the effect of the engine exhaust dilution conditions on the PM emissions characteristics from three different combustion modes, RCCI fueled with diesel and hydrous ethanol, RCCI fueled with diesel and gasoline, and CDC operation, was experimentally investigated. The engine was operated under the same speed and similar load conditions. PM emissions from the three combustion modes were sampled under four combinations of different dilution temperature and dilution ratio settings.

It can be concluded that both nucleation mode and accumulation mode particles were present in the RCCI exhaust regardless of the dilution conditions, confirming the findings

in previous studies [49,56]. The PM emissions from RCCI combustion were primarily composed of volatile and semi-volatile organic compounds, but a small fraction of solid particles also existed. The semi-volatile fraction in the RCCI PM emissions was up to 99% by volume under low dilution temperature and dilution ratio conditions leading to gas-to-particle conversion upon dilution. This study has found that the low reactivity fuel has an effect on the PM emissions characteristics for RCCI combustion. The PM emissions from hydrous ethanol fueled RCCI had a semi-volatile fraction varying from ~60% to 99% by volume depending on the dilution condition, whereas the semi-volatile fraction in the gasoline fueled RCCI PM emissions were consistently over 98% by volume. The different dilution sensitivity of the semi-volatile fraction of the RCCI PM emissions could be due to the difference in the low reactivity fuel properties or different lubricating oil consumption rates. Future work is needed to investigate the composition of the semi-volatile and non-volatile species from the RCCI PM emissions.

Chapter 8 Summary and Conclusions

Concerns about fossil fuel depletion and environmental degradation have driven internal combustion engine research to focus on improvement of fuel economy and emissions as well as efficient utilization of renewable fuels. RCCI has been shown to be a promising combustion strategy that can be readily implemented on current CI engines with minor modifications of fuel supply system, yielding high thermal efficiency and low NO_X and soot emissions without expensive aftertreatment systems. As an important type of renewable fuel, bio-ethanol has exhibited great potential for automotive use. If hydrous ethanol can be directly used in engines, a large portion of energy for water removal processes will be saved in bio-ethanol production and the bio-ethanol life cycle energy balance and economics will be significantly improved.

This work focuses on combining the RCCI strategy with the utilization of hydrous ethanol. A medium duty Isuzu 4HK1-TC diesel engine was modified to operate in RCCI mode and the performance and emissions were characterized and optimized under different operating conditions.

8.1. **Dual-Fuel Combustion using Different Fumigants**

As preliminary validation and evaluation of the modified diesel engine to operate in diesel-hydrous ethanol RCCI strategy, a set of experiments was conducted to compare the combustion and emissions characteristics of dual-fuel combustion using three different kinds of fumigants, anhydrous ethanol, hydrogen and gasoline, with directly injected diesel fuel as the ignition source. The diesel fuel injection timing was swept over the

widest possible range for each fumigant, and the effect of fumigant energy fraction was investigated in the diesel-gasoline mode.

It was found that very advanced timing led to primarily premixed CI combustion whereas more retarded timing resulted in more traditional fumigation combustion with increased diffusion burning. Peak indicated gross cycle efficiency occurred with advanced diesel injection timing and aligned well with combustion phasing near TDC. A fumigant's propensity for auto-ignition has a discernible effect on ignition delay especially with early diesel injection. For example, ethanol delayed ignition and combustion phasing, severely limited the operable diesel injection timing range and resulted in high unburned ethanol concentration in the exhaust. Hydrogen retarded the ignition but shortened the combustion duration compared with gasoline. Increasing FEF with the same fumigant delayed the ignition timing and combustion phasing as well as increased the combustion duration at early diesel injection timings. The use of hydrogen as the fumigant resulted in very low HC emissions compared with ethanol and gasoline, establishing that they mainly result from incomplete combustion of the fumigated fuel. Hydrogen emissions were independent of diesel injection timing and HC emissions were strongly linked to combustion phasing, giving further indication that squish and crevice flows are responsible for partially burned species from fumigation combustion.

8.2. **Diesel-Hydrous Ethanol RCCI under Different Loads**

To establish baseline settings for further optimization work and a basic understanding of the diesel-hydrous ethanol RCCI combustion on the specific test engine, an experimental investigation was conducted in RCCI mode under various load conditions. Under each load condition, timing and mass fraction of the first diesel injection was held

constant, while timing of the second diesel injection was swept over a range where stable combustion could be maintained. Since hydrous ethanol is highly resistant to auto-ignition and has large heat of vaporization, intake air heating was applied to obtain stable operation of the engine.

It has been shown that 150 proof hydrous ethanol can be used as the low reactivity fuel in RCCI through 8.6 bar IMEP and with ethanol energy fraction up to 75% while achieving simultaneously low levels of NO_X and soot emissions. With increasing engine load, less intake heating is needed and EGR is required to maintain low NO_X emissions. The second diesel injection timing can be adjusted to achieve a maximum in thermal efficiency and minimum in CO and HC emissions while setting a constant first diesel injection. This study in part confirms the feasibility of using hydrous ethanol as the low reactivity fuel in RCCI as was previously suggested in modeling and experimental studies [45,46] and opens the opportunity for further exploration of hydrous ethanol use in diesel engines to improve the renewability of ethanol, increase engine efficiency and reduce harmful engine exhaust emissions.

8.3. **Optimization of Diesel-Hydrous Ethanol RCCI Combustion Using Response Surface Methodology**

Response surface methodology was used to experimentally optimize key engine operating parameters for improvement of performance and emissions under high and low load conditions. Efficient experimental designs were developed that allowed identification of statistically significant operating parameters for optimizing emissions.

Following the optimization path generated by the RSM, NO_X and soot emissions were reduced by 79% and 50% under the low load condition, and by 72% and 27% under

the high load condition, compared to the starting points. Indicated thermal efficiency was compromised along the optimization path due to delayed combustion phasing under both load conditions. The results have also shown that different operating parameters are significant for RCCI emissions at different engine loads. A trade-off between HC and CO emissions was observed under the lower load condition, while HC and CO emissions were both lower after the optimization process under the higher load condition. For low load RCCI, the fumigant energy fraction significantly impacted HC emissions mainly from unburned ethanol, and the intake air pressure had the most significant effect on CO emissions. At higher load, HC emissions were significantly affected by the fraction of the first diesel injection and diesel rail pressure, and the intake air temperature had the most significant impact on the CO emissions. NO_X emissions were sensitive to all the active factors under both low and high load conditions. The RSM procedure used fractional factorial designs and CCD to identify factors with significant effects, build regression models and generate optimization paths, with less than 60 test points at each load. In contrast, a full two-level factorial design for eight factors alone needs 256 test points. Overall, this work shows that RSM can be effectively used to elucidate interactions among multiple engine operating parameters with reduced experimentation to optimize complex dual-fuel RCCI combustion modes. However, RSM is not physics-based and some operating parameters along the optimization path had to be altered to keep RCCI operation within feasible physical operability regions.

8.4. **Characteristics of the Particulate Matter Emissions from Reactivity-Controlled Compression Ignition**

Although soot emissions from RCCI is very low, hydrocarbon emissions are high, potentially resulting in higher than desired total PM mass and number caused by semi-volatile species converting the particle phase upon primary dilution in the exhaust plume. Such high organic fraction PM is known to be highly sensitive to the dilution conditions used when collecting samples on a filter or when measuring particle number using particle sizing instruments. PM emissions from the specific test engine operating in both RCCI and conventional diesel combustion modes were investigated under different dilution conditions. To investigate the effect of the fumigated fuel on the PM emissions, 150 proof hydrous ethanol and gasoline were used as the low reactivity fuels to study the relative contribution of fumigant versus directly injected fuel on the PM emissions. The engine was operated under the same speed and similar load conditions. PM emissions from the three combustion modes were sampled under four combinations of different dilution temperature and dilution ratio settings.

The study has shown that both nucleation mode and accumulation mode particles were present in the RCCI exhaust regardless of the dilution conditions. The PM emissions from RCCI combustion were primarily composed of volatile and semi-volatile organic compounds, but a small fraction of solid carbonaceous particles also existed due to the inhomogeneity of the high reactivity fuel distribution. The semi-volatile fraction in the RCCI PM emissions was up to 99% by volume under low dilution temperature and dilution ratio conditions leading to gas-to-particle conversion upon dilution. This study has found that the low reactivity fuel has a significant effect on the PM emissions

characteristics for RCCI combustion. The PM emissions from hydrous ethanol fueled RCCI had a semi-volatile fraction varying from ~60% to 99% by volume depending on the dilution condition, whereas the semi-volatile fraction in the gasoline fueled RCCI PM emissions were consistently over 98% by volume. The distinct dilution sensitivity of the semi-volatile fraction of the RCCI PM emissions is primarily due to the difference in the low reactivity fuel properties. Future work will focus on determining the composition of the semi-volatile species and characterizing their volatility.

Chapter 9 Suggested Future Work

This work has demonstrated that RCCI combustion using hydrous ethanol as the low reactivity fuel is a feasible approach to achieving simultaneously low NO_X and soot emissions while maintaining diesel-like thermal efficiencies. This approach also reveals a bright prospect of utilizing bio-ethanol without the costly water separation processes. RSM has been shown to be an effective and efficient way to optimize the large number of operating parameters of RCCI operation. Based on the findings of this study, the following recommendations are made for future research on the diesel-hydrous ethanol RCCI operation strategy.

9.1. **Diesel-Hydrous Ethanol RCCI on a Comprehensive Speed and Load Map and Transient Operation Characteristics**

In this study, diesel-hydrous ethanol RCCI operation has proven to be a feasible LTC strategy at a constant speed and under a wide range of load conditions. This finding demonstrates a promising prospect of using diesel-hydrous ethanol RCCI strategy in stationary applications such as power generation and factory machinery, where engines operate in a narrow range of operating conditions. In practical automotive applications, however, engine operates over a comprehensive speed and load map and mostly in a transient manner. Therefore, one of the future research areas is to investigate the diesel-hydrous ethanol RCCI feasibility on a speed and load map that covers the key operating points of the test engine, and to evaluate its transient operation characteristics.

Curran et al. [82] investigated the combustion and emissions characteristics of diesel-gasoline RCCI on a speed and load map of a multi-cylinder light-duty diesel engine.

They demonstrated the feasibility of the RCCI concept over a wide speed and load range. It was found that the thermal efficiency of RCCI was at comparable levels with that of CDC at low engine speeds and loads, and was up to 5% higher than CDC under higher speed and load conditions. NO_X emissions from RCCI were found to be significantly lower than CDC with near-zero Filter Smoke Number (FSN) over the map except for the lowest speed and load conditions. HC and CO emissions from RCCI were shown to be much higher than those from CDC throughout the different operating conditions. Their work has provided guidance to establishing a comprehensive speed and load map for RCCI operation for using hydrous ethanol as the secondary fuel.

In the future research related to the current study, it would be of great interest to conduct RSM optimization under various operating conditions on the basis of a well-established RCCI speed and load baseline map using a multi-cylinder engine. It has been shown from the present study that the RSM model is different as the load condition changes. Hence, it can be expected that great differences will exist among the RSM models for various operating regions. As RSM provides insight into the effect of various operating parameters on combustion and emissions as well as significant time and resource savings in the optimization processes, exercising the RSM optimization as exemplified in the present study in various engine operating regions will give us a more thorough understanding of the RCCI combustion and emissions characteristics. Considering that RSM models are not physics-based, and the model-derived optimal parameter settings are not always within feasible operating regions, it would be highly beneficial to combine RSM with some other engine research tools and techniques such as laser diagnostics, combustion modeling or optical engine technologies to gain a more

comprehensive understanding of the RCCI combustion and emissions mechanisms behind the statistical models.

As the engine fuel economy and emissions in automotive applications are specified and regulated over transient drive-cycles such as the US EPA FTP 75, it is of importance to evaluate the transient performance of RCCI operation using the optimized operating parameters derived from the steady-state optimization processes. Hanson et al. [83] conducted a study on the transient response characteristics of an RCCI engine. They compared the combustion performance and emissions of both closed-loop and open-loop controlled RCCI operation with those of open-loop controlled CDC operation under a step load change from 1 to 4 bar BMEP at a constant speed of 1500 rpm. The results show that transient RCCI operation is feasible and that closed-loop controller gives better HC emissions than open-loop controller. They also demonstrated that the transient RCCI NO and PM emissions are lower while HC emissions are higher as compared to the transient CDC operation. This study sheds some light on the understanding of the RCCI transient operation behaviors. In the future work that relates to the current study, one of the research focuses can be the evaluation of the performance and emissions characteristics of the diesel-hydrous ethanol RCCI combustion over complete transient drive cycles such as the US EPA FTP 75 or HWFET cycles. As differences exist between the transient and steady-state tests, modifications of the engine-dynamometer test cell are necessary such as addition of fast-response emissions analyzers. Further assessment and optimization of the RCCI combustion controller for improved transient performance are of significant research interest as well.

9.2. **Further Investigation on Detailed Chemical Composition of RCCI PM Emissions**

This study has investigated the effect of dilution conditions and fuel properties on the characteristics of the PM emissions from RCCI combustion. Significant differences of the total PM concentrations, solid PM fractions, and the size distributions have been observed when different low-reactivity fuels are used and exhaust samples are collected under different dilution ratios or temperatures. Although soot emissions have been shown to be extremely low for RCCI combustion, a large number of particles primarily composed of semi-volatile materials have been observed. In future work, it would be of great research interest to investigate the chemical compositions of the RCCI PM emissions in order to obtain a better understanding of their impact on the environment and human health.

Schauer et al. [84] conducted a study on the effect of sampling temperature and engine operating conditions on the chemical compositions of PM emissions from gasoline-powered vehicles. They used gas chromatography mass spectrometry (GCMS) to characterize elemental carbon (EC), organic carbon (OC), sulfate ions, nitrate ions, ammonium ions and organic compounds. Differences in the chemical compositions of PM emissions from various test cycles and under different ambient temperatures were demonstrated. Franklin [54] used tandem differential mobility analyzer (TDMA) techniques to characterize the volatility, composition and sources of PM emissions from an ethanol-fueled HCCI engine. It was found that lubricating oil was the primary contributor to HCCI PM emissions. In future research based on the findings of the current study, it would be of interest to explore the detailed chemical composition of RCCI PM

emissions with the use of techniques such as GCMS or TDMA. Similar experimental methods can also be applied such as comparing RCCI operations using different low-reactivity fuels and under various dilution conditions to evaluate the effect of dilution conditions and identify the sources of the RCCI PM emissions. Additionally, conducting detailed measurement and analysis of RCCI PM emissions under various steady-state operating conditions or transient drive cycles will provide a more comprehensive and thorough understanding of the characteristics of RCCI PM emissions.

Bibliography

[1] Caton, J. A., 2011, "Thermodynamic Advantages of Low Temperature Combustion (LTC) Engines Using Low Heat Rejection (LHR) Concepts," SAE Tech. Pap. 2011-01-0312.

[2] Dec, J. E., 2009, "Advanced compression-ignition engines—understanding the in-cylinder processes," Proc. Combust. Inst., **32**(2), pp. 2727–2742.

[3] Christensen, M., Hultqvist, A., and Johansson, B., 1999, "Demonstrating the Multi Fuel Capability of a Homogeneous Charge Compression Ignition Engine with Variable Compression Ratio," SAE Tech. Pap. 1999-01-3679.

[4] Christensen, M., Johansson, B., Amneus, P., and Mauss, F., 1998, "Supercharged homogeneous charge compression ignition," SAE Tech. Pap. 980787, pp. 1129–1144.

[5] Olsson, J., Tunestål, P., and Johansson, B., 2001, "Closed-Loop Control of an HCCI Engine," SAE Tech. Pap. 2001-01-1031.

[6] Martinez-Frias, J., Aceves, S. M., Flowers, D., Smith, J. R., and Dibble, R., 2002, "Thermal Charge Conditioning for Optimal HCCI Engine Operation," J. Energy Resour. Technol., **124**(1), p. 67.

[7] Koopmans, L., and Denbratt, I., 2001, "A four-stroke camless engine, operated in homogeneous charge compression ignition mode with commercial gasoline," SAE Tech. Pap. 2001-01-3610.

[8] Chen, R., and Milovanovic, N., 2002, "A computational study into the effect of exhaust gas recycling on homogeneous charge compression ignition combustion in internal combustion engines fuelled with methane," Int. J. Therm. Sci., **41**(9), pp. 805–813.

[9] Shi, L., Cui, Y., Deng, K., Peng, H., and Chen, Y., 2006, "Study of low emission homogeneous charge compression ignition (HCCI) engine using combined internal and external exhaust gas recirculation (EGR)," Energy, **31**(14), pp. 2665–2676.

[10] Hwang, W., Dec, J. E., and Sjöberg, M., 2007, "Fuel Stratification for Low-Load HCCI Combustion : Performance & Fuel-PLIF Measurements," (724), pp. 776–790.

[11] Dec, J. E., Hwang, W., and Sjöberg, M., 2006, "An Investigation of Thermal Stratification in HCCI Engines Using Chemiluminescence Imaging," SAE Tech. Pap. 2006-01-1518.

[12] Hasegawa, R., and Yanagihara, H., 2003, "HCCI Combustion in DI Diesel Engine," SAE Tech. Pap. 2003-01-0745, pp. 2003–01–0745.

[13] Kimura, S., Aoki, O., Ogawa, H., Muranaka, S., and Enomoto, Y., 1999, "New combustion concept for ultra-clean and high-efficiency small DI diesel engines," SAE Tech. Pap. 1999-01-3681.

[14] Walter, B., and Gatellier, B., 2002, "Development of the High Power NADITM

Concept Using Dual Mode Diesel Combustion to Achieve Zero NOx and Particulate Emissions," SAE Tech. Pap. 2002-01-1744.

[15] Kook, S., Bae, C., Miles, P. C., Choi, D., and Pickett, L. M., 2005, "The Influence of Charge Dilution and Injection Timing on Low-Temperature Diesel Combustion and Emissions," SAE Tech. Pap. 2005-01-3837, (724).

[16] Neely, G. D., Sasaki, S., and Leet, J. A., 2004, "Experimental Investigation of PCCI-DI Combustion on Emissions in a Light-Duty Diesel Engine," SAE Tech. Pap. 2004-01-0121.

[17] Akihama, K., Takatori, Y., Inagaki, K., and Dean, A. M., 2001, "Mechanism of the Smokeless Rich Diesel Combustion by Reducing Temperature," SAE Tech. Pap. 2001-01-0655.

[18] Jacobs, T. J., Knafl, A., Bohac, S. V, and Assanis, D. N., 2006, "The Development of Throttled and Unthrottled PCI Combustion in a Light-Duty Diesel Engine," SAE Tech. Pap. 2006-01-0202.

[19] Iwabuchi, Y., Kawai, K., Shoji, T., and Takeda, Y., 1999, "Trial of New Concept Diesel Combustion System - Premixed Compression-Ignited Combustion," SAE Tech. Pap. 1999-01-0185.

[20] Akagawa, H., Miyamoto, T., Harada, A., Sasaki, S., Shimazaki, N., Hashizume, T., and Tsujimura, K., 1999, "Approaches to Solve Problems of the Premixed Lean Diesel Combustion," SAE Tech. Pap. 1999-01-0183.

[21] Alriksson, M., and Denbratt, I., 2006, "Low Temperature Combustion in a Heavy Duty Diesel Engine Using High Levels of EGR," SAE Tech. Pap. 2006-01-0075.

[22] Inagaki, K., Fuyuto, T., Nishikawa, K., and Nakakita, K., 2006, "Dual-Fuel PCI Combustion Controlled by In-Cylinder Stratification of Ignitability," SAE Tech. Pap. 2006-01-0028.

[23] Olsson, J., Tunestål, P., Haraldsson, G., and Johansson, B., 2001, "A Turbo Charged Dual Fuel HCCI Engine," SAE Tech. Pap. 2001-01-1896.

[24] Kokjohn, S. L., Hanson, R. M., Splitter, D. A., and Reitz, R. D., 2009, "Experiments and Modeling of Dual-Fuel HCCI and PCCI Combustion Using In-Cylinder Fuel Blending," SAE Int. J. Engines, **2**(2), pp. 24–39.

[25] Tomita, E., Kawahara, N., Piao, Z., and Yamaguchi, R., 2013, "Effects of EGR and Early Injection of Diesel Fuel on Combustion Characteristics and Exhaust Emissions in a Methane Dual Fuel Engine," SAE Tech. Pap. 2002-01-2723.

[26] Hanson, R. M., Kokjohn, S. L., Splitter, D. A., and Reitz, R. D., 2010, "An Experimental Investigation of Fuel Reactivity Controlled PCCI Combustion in a Heavy-Duty Engine," SAE Int. J. Engines, **3**(1), pp. 700–716.

[27] Kokjohn, S. L., Hanson, R. M., Splitter, D. A., and Reitz, R. D., 2011, "Fuel Reactivity Controlled Compression Ignition (RCCI) Combustion in Light- and Heavy-Duty Engines," SAE Int. J. Engines, **4**(1), pp. 360–374.

[28] Splitter, D. A., Hanson, R. M., Kokjohn, S. L., and Reitz, R. D., 2011, "Reactivity

Controlled Compression Ignition (RCCI) Heavy-Duty Engine Operation at Mid- and High-Loads with Conventional and Alternative Fuels," SAE Tech. Pap. 2011-01-0363.

[29] Kokjohn, S. L., Hanson, R. M., Splitter, D. A., and Reitz, R. D., 2011, "Fuel reactivity controlled compression ignition (RCCI): a pathway to controlled high-efficiency clean combustion," Int. J. Engine Res., **12**(3), pp. 209–226.

[30] Hanson, R. M., Kokjohn, S. L., Splitter, D. A., and Reitz, R. D., 2011, "Fuel Effects on Reactivity Controlled Compression Ignition (RCCI) Combustion at Low Load," SAE Int. J. Engines, **4**(1), pp. 394–411.

[31] Kokjohn, S. L., and Reitz, R. D., 2009, "A Modeling Study of Charge Preparation and Combustion in an HCCI Engine Using a Variable Pressure Pulse (VPP) Injection System and Optimized PRF Blends," 11th Trienn. Int. Annu. Conf. Liq. At. Spray Syst.

[32] Splitter, D., Kokjohn, S. L., Rein, K., Hanson, R., Sanders, S., and Reitz, R., 2010, "An Optical Investigation of Ignition Processes in Fuel Reactivity Controlled PCCI Combustion," SAE Int. J. Engines, **3**(1), pp. 142–162.

[33] Splitter, D., Hanson, R., Kokjohn, S. L., Wissink, M., and Reitz, R., 2011, "Injection Effects in Low Load RCCI Dual-Fuel Combustion," SAE Tech. Pap. 2011-24-0047.

[34] Walker, N. R., Dempsey, A. B., Andrie, M. J., and Reitz, R. D., 2012, "Experimental Study of Low-Pressure Fueling Under RCCI Engine Operation," Am. 24th Annu. Conf. Liq. At. Spray Syst.

[35] Splitter, D. A., Reitz, R. D., and Hanson, R. M., 2010, "High Efficiency , Low Emissions RCCI Combustion by Use of a Fuel Additive," SAE Int. J. Fuels Lubr, **3**(2), pp. 742–756.

[36] Hanson, R. M., Curran, S. J., Wagner, R. M., and Reitz, R. D., 2013, "Effects of Biofuel Blends on RCCI Combustion in a Light-Duty , Multi-Cylinder Diesel Engine," SAE Int. J. Engines, **6**(1), pp. 488–503.

[37] Nieman, D. E., Dempsey, A. B., and Reitz, R. D., 2012, "Heavy-Duty RCCI Operation Using Natural Gas and Diesel," SAE Tech. Pap. 2012-01-0379.

[38] Matsuoka, S., Ferro, J., and Arruda, P., 2009, "The Brazilian experience of sugarcane ethanol industry," Vitr. Cell. Dev. Biol. - Plant, **45**(3), pp. 372–381.

[39] Flowers, D. L., Aceves, S. M., and Frias, J. M., 2007, "Improving Ethanol Life Cycle Energy Efficiency by Direct Utilization of Wet Ethanol in HCCI Engines," SAE Tech. Pap. 2007-01-1867.

[40] Saffy, H. A., Northrop, W. F., Kittelson, D. B., and Boies, A. M., 2015, "Energy, carbon dioxide and water use implications of hydrous ethanol production," Energy Convers. Manag., **105**, pp. 900–907.

[41] Costa, R. C., and Sodré, J. R., 2010, "Hydrous ethanol vs. gasoline-ethanol blend: Engine performance and emissions," Fuel, **89**(2), pp. 287–293.

[42] Clemente, R. C., Werninghaus, E., Coelho, E. P. D., and Sigaud Ferraz, L. A., 2001, "Development of an Internal Combustion Alcohol Fueled Engine," SAE Tech. Pap. 2001-01-3917.

[43] Chaplin, J., and Janius, R. Bin, 1987, "Ethanol Fumigation of a Compression Ignition Engine Using Advanced Injection of Diesel Fuel," Trans. ASAE, **30**(3), pp. 610–614.

[44] Olson, A., 2010, "The Effect of Ethanol-Water Fumigation on the Performance and Emissions from a Direct-Injection Diesel Engine," Master's Thesis, University of Minnesota.

[45] Dempsey, A. B., Das Adhikary, B., Viswanathan, S., and Reitz, R. D., 2012, "Reactivity Controlled Compression Ignition Using Premixed Hydrated Ethanol and Direct Injection Diesel," J. Eng. Gas Turbines Power, **134**(8), p. 082806.

[46] Dempsey, A. B., Walker, N. R., Splitter, D. A., Wissink, M., and Reitz, R. D., 2012, "Characterization of Reactivity Controlled Compression Ignition (RCCI) Using Premixed Hydrated Ethanol and Direct Injection Diesel in Heavy-Duty and Light-Duty Engines," THIESEL 2012 Conf. Thermo- Fluid Dyn. Process. Direct Inject. Engines.

[47] Kittelson, D. B., 1998, "Engines and Nanoparticles: A Review," J. Aerosol Sci., **29**(5), pp. 575–588.

[48] Kittelson, D. B., Graskow, B. R., Wei, Q., and Brear, F., 1998, "Diesel Exhaust Particle Size: Measurement Issues and Trends," SAE Tech. Pap. 980525.

[49] Prikhodko, V. Y., Curran, S. J., Barone, T. L., Lewis, S. A., Storey, J. M., Cho, K., Wagner, R. M., and Parks, J. E., 2011, "Diesel Oxidation Catalyst Control of Hydrocarbon Aerosols from Reactivity Controlled Compression Ignition Combustion," ASME 2011 Int. Mech. Eng. Congr. Expo. IMECE2011-64147, pp. 273–278.

[50] Kolodziej, C., Wissink, M., Splitter, D., Hanson, R. M., Reitz, R., and Benajes, J., 2013, "Particle Size and Number Emissions from RCCI with Direct Injections of Two Fuels," SAE Tech. Pap. 2013-01-1661.

[51] Storey, J., Curran, S. J., Dempsey, A. B., Lewis, S., Walker, N. R., Reitz, R., and Wright, C., 2014, "The Contribution of Lubricant to the Formation of Particulate Matter with Reactivity Controlled Compression Ignition in Light-Duty Diesel Engines," Emiss. Control Sci. Technol.

[52] Abdul-Khalek, I. S., Kittelson, D. B., and Brear, F., 1999, "The Influence of Dilution Conditions on Diesel Exhaust Particle Size Distribution Measurements," SAE Tech. Pap. 1999-01-1142.

[53] Abdul-khalek, I. S., and Kittelson, D. B., 2000, "Nanoparticle Growth During Dilution and Cooling of Diesel Exhaust : Experimental Investigation and Theoretical Assessment," SAE Tech. Pap. 2000-01-0515.

[54] Franklin, L. M., 2010, "Effects of Homogeneous Charge Compression Ignition (HCCI) Control Strategies on Particulate Emissions of Ethanol Fuel," Doctoral

Dissertation, University of Minnesota.

[55] Montajir, R. M., Kawai, T., Goto, Y., and Odaka, M., 2005, "Thermal Conditioning of Exhaust Gas : Potential for Stabilizing Diesel Nano-Particles," SAE Tech. Pap. 2005-01-0187.

[56] Zhang, Y., Ghandhi, J., and Rothamer, D., 2014, "Comparison of Particulate Size Distributions from Advanced and Conventional Combustion - Part I: CDC, HCCI, and RCCI," SAE Int. J. Engines, **7**(2), pp. 820–834.

[57] Wickman, D. D., Senecal, P. K., and Reitz, R. D., 2001, "Optimization Using Genetic Algorithms and Multi-Dimensional Spray and Combustion Modeling," SAE Tech. Pap. 2001-01-0547.

[58] Hiroyasu, H., Miao, H., Hiroyasu, T., Miki, M., Kamiura, J., and Watanabe, S., 2003, "Genetic Algorithms Optimization of Diesel Engine Emissions and Fuel Efficiency with Air Swirl , EGR , Injection Timing and Multiple Injections," SAE Tech. Pap. 2003-01-1853.

[59] Aldawood, A., Mosbach, S., and Kraft, M., 2012, "HCCI Combustion Control Using Dual-Fuel Approach : Experimental and Modeling Investigations," SAE Tech. Pap. 2012-01-1117.

[60] Montgomery, D. T., 2006, Design and Analysis of Experiments, John Wiley & Sons, Inc.

[61] Montgomery, D. T., and Reitz, R. D., 2000, "Optimization of Heavy-Duty Diesel Engine Operating Parameters Using A Response Surface Method," SAE Tech. Pap. 2000-01-1962.

[62] Lee, T., and Reitz, R. D., 2003, "Response Surface Method Optimization of a High-Speed Direct-Injection Diesel Engine Equipped With a Common Rail Injection System," J. Eng. Gas Turbines Power, **125**(2), pp. 541–546.

[63] Amann, M., and Buckingham, J., 2006, "Evaluation of HCCI Engine Potentials in Comparison to Advanced Gasoline and Diesel Engines," SAE Tech. Pap. 2006-01-3249.

[64] Pandian, M., Sivapirakasam, S. P., and Udayakumar, M., 2011, "Investigation on the effect of injection system parameters on performance and emission characteristics of a twin cylinder compression ignition direct injection engine fuelled with pongamia biodiesel–diesel blend using response surface methodology," Appl. Energy, **88**(8), pp. 2663–2676.

[65] Fang, W., Kittelson, D. B., and Northrop, W. F., 2015, "An Experimental Investigation of Reactivity-Controlled Compression Ignition Combustion in a Single-Cylinder Diesel Engine Using Hydrous Ethanol," J. Energy Resour. Technol., **137**(May), pp. 1–9.

[66] Abdul-khalek, I. S., and Kittelson, D. B., 1995, "Real time measurement of volatile and solid exhaust particles using a catalytic stripper," SAE Tech. Pap. 950236.

[67] Heywood, J. B., 1988, Internal Combustion Engine Fundamentals, McGraw-Hill

Inc.

[68] Kim, A. M., Smith, J. A., Wagler, J. R., and Baldwin, D. D., 2011, "Combustion Characteristics of Producer Gas in the Stationary Gas Engine," ASME 2011 Internal Combustion Engine Division Fall Technical Conference, ASME, pp. 143–150.

[69] Hashimoto, K., 2007, "Effect of Ethanol on the HCCI Combustion," SAE Tech. Pap. 2007-01-2038.

[70] Northrop, W. F., Fang, W., and Huang, B., 2013, "Combustion Phasing Effect on Cycle Efficiency of a Diesel Engine Using Advanced Gasoline Fumigation," J. Eng. Gas Turbines Power, **135**(March), p. 032801.

[71] Guo, H., Hosseini, V., Neill, W. S., Chippior, W. L., and Dumitrescu, C. E., 2011, "An experimental study on the effect of hydrogen enrichment on diesel fueled HCCI combustion," Int. J. Hydrogen Energy, **36**(21), pp. 13820–13830.

[72] Westbrook, C. K., 2000, "Chemical Kinetics of Hydrocarbon Ignition in Practical Combustion Systems," Proc. Combust. Inst., **28**(2), pp. 1563–1577.

[73] Kim, D., Ekoto, I., Colban, W. F., and Miles, P. C., 2008, "In-cylinder CO and UHC Imaging in a Light-Duty Diesel Engine during PPCI Low-Temperature Combustion," SAE Tech. Pap. 2008-01-1602.

[74] Ekoto, I. W., Colban, W. F., Miles, P. C., Park, S., Foster, D. E., and Reitz, R. D., 2009, "Sources of UHC Emissions from a Light-Duty Diesel Engine Operating in a Partially Premixed Combustion Regime," SAE Tech. Pap. 2009-01-1446.

[75] Lachaux, T., and Musculus, M. P. B., 2007, "In-Cylinder Unburned Hydrocarbon Visualization during Low-Temperature Compression-Ignition Engine Combustion using Formaldehyde PLIF," Proc. Combust. Inst., **31**(2), pp. 2921–2929.

[76] Kirchstetter, T. W., Singer, B. C., Harley, R. A., and Kendall, G. R., 1996, "Impact of Oxygenated Gasoline Use on California Light-Duty Vehicle Emissions," **30**(2), pp. 661–670.

[77] Hanson, R. M., Curran, S. J., Wagner, R., Kokjohn, S. L., Splitter, D., and Reitz, R., 2012, "Piston Bowl Optimization for RCCI Combustion in a Light- Duty Multi-Cylinder Engine," pp. 286–299.

[78] Rehnlund, B., Egebäck, K.-E., Rydén, C., and Ahlvik, P., 2007, "Heavy-Duty Ethanol Engines," Final Rep. Lot 2 Bioscopes Proj.

[79] Fang, W., Huang, B., Kittelson, D. B., and Northrop, W. F., 2014, "Dual-Fuel Diesel Engine Combustion with Hydrogen, Gasoline and Ethanol as Fumigants: Effect of Diesel Injection Timing," J. Eng. Gas Turbines Power, **136**(8), p. 081502.

[80] Mehl, M., Pitz, W., Sarathy, M., Yang, Y., and Dec, J. E., 2012, "Detailed Kinetic Modeling of Conventional Gasoline at Highly Boosted Conditions and the Associated Intermediate Temperature Heat Release," SAE Tech. Pap. 2012-01-1109.

[81] Sjoberg, M., and Dec, J. E., 2010, "Ethanol Autoignition Characteristics and HCCI Performance for Wide Ranges of Engine Speed, Load and Boost," SAE Int J Engines, **3**(1), pp. 84–106.

[82] Curran, S. J., Hanson, R. M., Wagner, R., and Reitz, R., 2013, "Efficiency and Emissions Mapping of RCCI in a Light-Duty Diesel Engine," SAE Tech. Pap. 2013-01-0289.

[83] Hanson, R., and Reitz, R. D., 2013, "Transient RCCI Operation in a Light-Duty Multi-Cylinder Engine," SAE Tech. Pap. 2013-24-0050.

[84] Schauer, J. J., Christensen, C. G., Kittelson, D. B., Johnson, J. P., and Watts, W. F., 2008, "Impact of Ambient Temperatures and Driving Conditions on the Chemical Composition of Particulate Matter Emissions from Non-Smoking Gasoline-Powered Motor Vehicles," Aerosol Sci. Technol., **42**(3), pp. 210–223.